UNIVERSIDADE FEDERAL DE SÃO CARLOS
CENTRO DE CIÊNCIAS EXATAS E DE TECNOLOGIA
DEPARTAMENTO DE QUÍMICA
PROGRAMA DE PÓS-GRADUAÇÃO EM QUÍMICA

Compósitos nanoestruturados baseados em polímero condutor/cerâmica como plataforma sensorial para detecção de gás amônia

Rafaela da Silveira Andre*

Tese apresentada como parte dos requisitos para obtenção do título de DOUTOR EM CIÊNCIAS, área de concentração: QUÍMICA.

Orientador: Dr. Luiz Henrique Capparelli Mattoso

***Bolsista: CNPq**

São Carlos, SP

2017

UNIVERSIDADE FEDERAL DE SÃO CARLOS

Centro de Ciências Exatas e de Tecnologia
Programa de Pós-Graduação em Química

Folha de Aprovação

Assinaturas dos membros da comissão examinadora que avaliou e aprovou a Defesa de Tese de Doutorado da candidata Rafaela da Silveira André, realizada em 20/04/2017:

Prof. Dr. Luiz Henrique Capparelli Mattoso
Embrapa

Prof. Dr. Valmor Roberto Mastelaro
IFSC/USP

Prof. Dr. Fernando Josepetti Fonseca
POLI

Prof. Dr. Caio Marcio Paranhos da Silva
UFSCar

Prof. Dr. Waldir Avansi Junior
UFSCar

UNIVERSIDADE FEDERAL DE SÃO CARLOS
CENTRO DE CIÊNCIAS EXATAS E DE TECNOLOGIA
DEPARTAMENTO DE QUÍMICA
PROGRAMA DE PÓS-GRADUAÇÃO EM QUÍMICA

Nanostructured composites based on conducting polymer/ceramic as a sensing platform for ammonia gas monitoring

Rafaela da Silveira Andre*

Thesis presented as part of the requirements to obtain PhD degree in SCIENCES, concentration area: CHEMISTRY.

Advisor: Dr. Luiz Henrique Capparelli Mattoso

***Scholarship: CNPq**

São Carlos, SP
2017

Dedico este trabalho à minha família, em especial à minha mãe Heloisa, que esteve sempre ao meu lado me apoiando física e emocionalmente com muito amor e confiança.

AGRADECIMENTOS

Gostaria de agradecer primeiramente ao Dr. Luiz H. C. Mattoso pela orientação, confiança e suporte.

Ao Dr. Daniel S. Correa por todo aprendizado proporcionado, oportunidades concedidas, colaboração e atenção ao longo destes anos de coorientação.

Agradeço à Drª. Elaine C. Paris pelas contribuições, conselhos e suporte principalmente no início do desenvolvimento deste trabalho.

Aos membros da banca pela disposição e contribuições.

A todos os colaboradores e parceiros dos artigos aqui presentes.

Aos doutores Flávio Makoto Shimizo, Luiza A. Mercante, Adriana Pavinatto e Rafaela Sanfelice por todo apoio, suporte, parceria e amizade.

A todos os colegas de grupo de pesquisa que também contribuíram para a realização deste trabalho.

À Embrapa Instrumentação pela estrutura fornecida para o desenvolvimento deste trabalho. Em especial ao pessoal de suporte à pesquisa, Adriana, Viviane, Silviane, Matteo, Paulinho, Edilson Gabriel e Suzane.

Aos órgãos de fomento (CNPq, CAPES e FAPESP) por todo o suporte financeiro.

Ao Programa de Pós-Graduação em Química da Universidade Federal de São Carlos (PPGQ-UFSCar), por toda a estrutura oferecida.

Gostaria também de agradecer a todos os meus amigos por estarem sempre ao meu lado fazendo a minha vida mais doce.

Em especial, agradeço ao Lucas por seu companheirismo, amor, amizade e apoio incondicional recheados de alegrias e momentos inesquecíveis.

E aos meus pais, Alexandre e Heloisa, gratidão por serem exatamente como são me permitindo chegar até aqui.

RESUMO

COMPÓSITOS NANOESTRUTURADOS BASEADOS EM POLÍMERO CONDUTOR/CERÂMICA COMO PLATAFORMA SENSORIAL PARA DETECÇÃO DE GÁS AMÔNIA. O desenvolvimento de novas plataformas nanoestruturadas para aplicação como sensor de gases tem se intensificado ao longo das últimas décadas. Neste cenário, vale destacar a necessidade do sensoriamento de amônia gasosa encontrada nas câmaras de frango. A amônia, que é produzida pela degradação microbiana do ácido úrico na cama de frango, além de causar significativas perdas econômicas para os criadores de aves, provoca danos à saúde dos trabalhadores. Apesar de estudos encontrados na literatura já reportarem diferentes tipos de sensores químicos de amônia, ainda se faz necessária a optimização destes dispositivos visando melhorar seu desempenho em termos de sensibilidade, limite de detecção (LD) e confiabilidade das medidas. Assim, a presente tese visa contribuir para o desenvolvimento de sensores com alta sensibilidade e baixo LD no monitoramento de amônia, através do estudo de diferentes plataformas nanoestruturadas. Para tal, foram obtidas nanopartículas de óxido de zinco (ZnO) por método hidrotérmico convencional com otimização dos parâmetros de síntese e nanofibras poliméricas produzidas por eletrofiação. As nanoestruturas obtidas foram combinadas para a produção de plataformas hibridas combinando nanopartículas de ZnO com polímeros conjugados. A sensibilidade e o desempenho de tais plataformas foram avaliados frente à diferentes concentrações de amônia visando um melhor entendimento da influência do efeito de heterojunção, entre os materiais, no desempenho das plataformas como sensor de amônia em temperatura ambiente. Tanto as nanopartículas de ZnO quanto as plataformas compósitas desenvolvidas neste trabalho tiveram suas propriedades estruturais, morfológicas e elétricas estudadas de maneira detalhada. Os parâmetros de síntese das nanopartículas bem como os parâmetros de confecção das plataformas foram otimizados em relação às propriedades elétricas e morfológicas visando melhor desempenho do sensor de amônia. Foram realizados testes frente à diferentes concentrações de amônia em atmosfera controlada confirmando o melhor desempenho dos materiais compósitos quando comparados com seus constituintes separadamente. Neste sentido, a influência da composição das plataformas, bem como a sua conformação estrutural foi avaliada para auxiliar no entendimento das propriedades elétricas dos dispositivos obtidos bem como nos possíveis mecanismos de detecção.

ABSTRACT

NANOSTRUCTURED COMPOSITES BASED ON CONDUCTING POLYMER/CERAMIC AS A SENSING PLATFORM FOR AMMONIA GAS MONITORING. The development of novel nanostructured platforms for application as gas sensor has intensified over the last few decades. In this scenario, it is worth mentioning the importance of monitoring ammonia gas in poultry farms. Such environments are rich in ammonia, carbon monoxide, hydrogen sulfide, and organic matter arising from the poultry waste decomposition, which remain in the air as bioaerosol. Ammonia, which is produced by the microbial degradation of uric acid present in the poultry waste, causes significant economic losses to poultry farmers and is harmful to the workers. Although some studies found in the literature present sensors capable to detect low concentrations of ammonia, it is still necessary to optimize these devices in order to improve their performance in terms of the sensitivity, limit of detection (LOD) and reliability. Thus, the present thesis aims to contribute to the development of sensors with high sensitivity and low LOD for detecting ammonia through the study of different nanostructured platforms. Zinc oxide (ZnO) nanoparticles were obtained through the optimization of the synthesis and treatment parameters using conventional hydrothermal method, while polymeric nanofibers were produced by electrospinning technique. Both techniques allowed to produce nanostructured platforms by a combination of ZnO nanoparticles and conjugated polymers in the form of fibers, film and coating architecture. The sensitivity and performance of such platforms were evaluated against different concentrations of ammonia aiming to understand the heterojunction influence among the materials on the performance of the platforms as an ammonia sensor at room temperature. Both the ZnO nanoparticles and the composite platforms developed in this work had their structural, morphological and electrical properties studied in detail. Synthesis parameters as well as the platforms deposition parameters were optimized for attaining superior electrical and morphological properties that improved the sensor performance regarding ammonia detection. Sensing tests were carried out against different concentrations of ammonia under controlled atmosphere confirming the best performance of the composite materials when compared to their constituents separately. In this context, the influence of the platform composition, as well as materials structural conformation were evaluated to help to understand the electrical properties and detection mechanisms.

LIST OF FIGURES

FIGURE 1.1.1: Composite reinforcement types. (Figure available in Eyring et. al.[3]) 2
FIGURE 1.2.1: Scheme of common (nano)composite structures for ceramic materials (a) nanoparticles occupying both inter- and intra-granular positions inside a micronic matrix; (b) elongated nanoreinforcements embedded in a micronic matrix; (c) platelet-like nanoreinforcements embedded in a micronic matrix; (d) containing both rounded and elongated nanoreinforcements, embedded in a micronic matrix; (e) Bi-phasic composite made by two immiscible ultra-fine phases; (f) Multi-phasic composite made by three (or more) immiscible. (Figure available in Palmero et. al. [28]) 3
Figure 1.3.1: Electrospinning fiber formation scheme (Figure adapted from Costa et. al.[50]). 6
Figure 1.3.2: Schematic Layer-by-Layer (LbL) self- assembly technique. (Figure adapted from Correa et. al.[60]) 7
FIGURE 1.4.1: Nanocomposites classification based on their applications. (Figure idealized from Sahay et. al.[72]) 8
Figure 1.4.2: Schematic representation of the p-n energy levels a) before and b) after a heterojunction formation. 11
FIGURE 3.4.1: XRD patterns of ZnO synthetized with (a) PEG 8000, (b) PEG 4000 and (c) PEG 400. (Figure available in Andre, R. S. et. al.[127])22
FIGURE 3.4.2: FEG-SEM images of ZnO synthetized with (a) PEG 8000, (b) PEG 4000 e (c) PEG 400. (d) Histogram of size distribution of ZnO nanoparticles synthetized with PEG 400. (Figure available in Andre, R. S. et. al.[127]) 23
FIGURE 3.4.3: SEM images of (a) PA6/PANI and (b) PA6/PANI_ZnO nanofibers. The inset in panel (b) shows the EDS spectra of PA6/PANI_ZnO. . (Figure available in Andre, R. S. et. al.[127]) 24

FIGURE 3.4.4: TGA curves of ZnO nanoparticles, PA6/PANI nanofibers and PA6/PANI_ZnO nanofibers. (Figure available in Andre, R. S. et. al.[127]) 25
FIGURE 3.4.5: (a) EIS of PA6/PANI_ZnO electrode for different ZnO adsorption times (b) EIS of bare FTO, PA6/PANI and PA6/PANI_ZnO electrodes in 5 mmol L^{-1} $[Fe(CN)_6]^{-3/-4}$ solution with 0.1 mol L^{-1} KCl. The inset in panel b (i) shows the Randle's equivalent circuit model. (Figure available in Andre, R. S. et. al.[127])..... 27
FIGURE 3.4.6: Amperometric current response of PA6/PANI_ZnO electrode in 0.01 molL-1 PBS (pH 7.5) for concentration range 0.5 to 20000 µmolL-1 of Hy. The inset presents the linear relationship between current response and Hy concentrations. (Figure available in Andre, R. S. et. al.[127]) 29
FIGURE 3.4.7: Selectivity amperometric current response of the PA6/PANI_ZnO sensor for Hy (N_2H_4) mixed with interferents in 0.01 mol L^{-1} PBS (pH 7,5). (Figure available in Andre, R. S. et. al.[127])..... 30
FIGURE 4.3.1: Schematic diagram of the experimental setup for NH_3 detection. (Figure available in Andre, R. S. et. al.[174]) 35
FIGURE 4.4.1: Absorption spectra of LbL films (PGPZ2T, PGPZ3T and PGPZ4T). Inset displays the intensity at 840 nm versus the number of deposited tetralayers. (Figure available in Andre, R. S. et. al.[174])..... 36
FIGURE 4.4.2: Raman spectrum of PGPZ4T film. (Figure available in Andre, R. S. et. al.[174]) 36
FIGURE 4.4.3: a) real part of impedance (Z') and b) Nyquist diagram for PGPZ2T, PGPZ3T and PGPZ4T films, c) equivalent circuit model and d) schematic representation of the PANI/GO/PANI/ZnO film deposited onto the IDE. (Figure available in Andre, R. S. et. al.[174])..... 37
FIGURE 4.4.4: AFM 3D images of a) PGPZ2T, b) PGPZ3T and c) PGPZ4T films. (Figure available in Andre, R. S. et. al.[174]) 39

FIGURE 4.4.5: Film roughness (Rrms) calculated using Gwyddion® software for LbL films (PGPZ2T, PGPZ3T and PGPZ4T) before and after exposure to ammonia gas. (Figure available in Andre, R. S. et. al.[174]).. 39
FIGURE 4.4.6: a) Sensor responses at different concentrations of NH3 and b) change in electrical resistance as a function of time upon NH3 exposure of a sensing device with PGPZ3T. (Figure available in Andre, R. S. et. al.[174])..... 41
FIGURE 4.4.7: IDMAP plot obtained with the real component of the impedance data as a function of frequency for PGPZ2T, PGPZ3T and PGPZ4T films. The axes have no labels because what matters in this type of plot is the relative distance between data points. The dashed lines linking data points for each of the sensing units were only included to guide the eyes, and demonstrate the distinction between different NH_3 concentrations. (Figure available in Andre, R. S. et. al.[174]) 42
Figure 5.3.1: X-ray diffraction pattern of the as-prepared ZnO nanofibers. 49
Figure 5.3.2: a) Scanning electron microscopy picture of ZnO nanofibers, b) higher magnification and c) a Histogram of diameter size distribution of ZnONF..... 50
Figure 5.3.3: The high-resolution XPS spectra of a) Zn2p and b) O1s of ZnO_NF. 51
Figure 5.3.4: a) Response-recovery profile of ZnO50/PSS50 device as function of time for NH_3 concentration varying from 10 to 100 ppm and b) Sensing response as function of NH_3 concentration for ZnO50/PSS50 and PZnO devices. 52
Figure 5.3.5: Selectivity performance for 50 ppm of NO_2, NH_3 and CO for ZnO50/PSS50 and PZnO devices. 54

Figure 5.3.6: FTIR spectra of a) glass microfiber paper (GFP), b) GFP@PANI, c) GFP@PANI/PSS, d) GFP@PSS/PANI and e) GFP@PSS, respectively. 55
Figure 5.3.7: Scanning electron microscopy images of a) GFP substrate and b) GFP@PSS/PANI device. The inset represents i) real device picture and ii) real device mechanical flexibility..... 55
Figure 5.3.8: Dynamic response of a) GF@PSS/PANI, b) GFP@PANI/PSS and c) GFP@PANI. The inset shows the I-V curves of different device performed in ambient air conditions. 56
Figure 5.3.9: Gas sensor a) response for different concentrations of NH_3 gas and b) selectivity test for ammonia sensing towards NO_2 and CO gas. 58
Figure A.1: a) Capacitance and b) Resistance variation versus frequency for all three platforms. 76
Figure A.2 a) Real part of dielectric properties and b) tangent loss for all three platforms. 76
Figure A.3: Nyquist plots of a) PGPZ2T, b) PGPZ3T and PGPZ4T when exposed in several concentrations of NH_3. 77
Figure A.4: Impedance spectra of a) PGPZ2T, b) PGPZ3T and c) PGPZ4T film when exposed in several concentrations of NH_3. 78
Figure A.5: Resistance variation of a) PGPZ2T, b) PGPZ3T and c) PGPZ4T film when exposed in several concentrations of NH_3. 79

Table list

TABLE 3.1: Comparison of Linear range and Detection limit between hydrazine sensors based in similar ZnO structures. ……. 29

TABLE 4.1: Parameters of the equivalent circuit used to fit the impedance data with ZView® software (Scribner Associates Inc.). ……38

TABLE 4.2: Comparison of sensor performance for detecting NH_3, where lists are given of the material used in the sensing device, detection limit (DL), response time (RTime), percentage of response. The values quoted for PANI/GO/PANI/ZnO correspond to PGPZ3T. 43

PUBLICATIONS

1. Andre, R. S.; Shimizu, F. M.; Miyazaki, C. M.; Riul, A.; Manzani, D.; Ribeiro, S. J. L.; Oliveira, O. N.; Mattoso, L. H. C.; Correa, D. S. Hybrid Layer-by-Layer (LbL) Films of Polyaniline, Graphene Oxide and Zinc Oxide to Detect Ammonia. *Sensors Actuators B Chem.* **2017**, *238*, 795–801.
2. Andre, R. S.; Pavinatto, A.; Mercante, L. a.; Paris, E. C.; Mattoso, L. H. C.; Correa, D. S. Improving the Electrochemical Properties of Polyamide 6/polyaniline Electrospun Nanofibers by Surface Modification with ZnO Nanoparticles. *RSC Adv.* **2015**, *5* (90), 73875–73881.

OTHER PUBLICATIONS

1. ANDRÉ, Rafaela. S.; ZANETTI, S.M.; VARELA, J.A.; LONGO, Elson Synthesis by a chemical method and characterization of $CaZrO_3$ powders: Potential application as humidity sensors. *Ceram. Int*. **2014**, 40, 16627-16634.
2. André, R.S.; Paris, E.C.; Gurgel, M.F.C.; Rosa, I.L.V.; Paiva Santos, C.O.; Li, M.S.; Varela, J.A.; Longo, E. Structural evolution of Eudoped hydroxyapatite nanorods monitored by photoluminescence emission. *J. Alloys Compd*. **2012**, 531, 50-54.
3. ANDRÉ, RAFAELA S.; ZAMPERINI, CAMILA A.; MIMA, EWERTON G.; LONGO, VALÉRIA M.; ALBUQUERQUE, ANDERSON R.; SAMBRANO, JÚLIO R.; MACHADO, ANA L.; VERGANI, CARLOS E.; HERNANDES, ANTONIO C.; VARELA, JOSÉ A.; LONGO, E. Antimicrobial activity of TiO_2:Ag nanocrystalline heterostructures: Experimental and theoretical insights. *Chemical Physics*. **2015**, 459, 87-95.
4. ZAMPERINI, C. A.; ANDRÉ, R. S.; LONGO, V. M.; MIMA, E. G.; VERGANI, C. E.; MACHADO, A. L.; VARELA, J. A.; Longo, E. Antifungal Applications of Ag Decorated Hydroxyapatite Nanoparticles. *Journal of Nanomaterials* (Print). **2013**, 2013, 1-9.
5. ROSA, I. L. V.; OLIVEIRA, M.C.; ASSIS, M.; FERRER, M.; ANDRÉ, Rafaela. S.; LONGO, E.; Gurgel, M.F.C. A theoretical investigation of the structural and electronic properties of orthorhombic $CaZrO_3$. *Ceram. Int.* **2015**, 41, 3069-3074.
6. MAZZO, TATIANA MARTELLI; MENDONÇA DA ROCHA OLIVEIRA, LUCAS; MACARIO, LEILANE ROBERTA; AVANSI, WALDIR; SILVEIRA ANDRÉ, RAFAELA DA; VIANA ROSA, IEDA LUCIA; VARELA, JOSÉ ARANA; LONGO, ELSON; Photoluminescence properties of $CaTiO_3$:Eu^{3+} nanophosphor obtained by the polymeric precursor method. *Mater. Chem. Phys*. **2014**, 145, 141-150.
7. LONGO, VALÉRIA MORAES; DE FOGGI, CAMILA C.; FERRER, MATEUS MENEGHETTI; GOUVEIA, AMANDA F.; ANDRÉ, RAFAELA S.; AVANSI, WALDIR; VERGANI, CARLOS E.; MACHADO, ANA L.; ANDRÉS, JUAN; CAVALCANTE, LAÉCIO SANTOS; HERNANDES, ANTONIO; LONGO, ELSON; Potentiated Electron Transference in αAg_2WO_4 Microcrystals with Ag Nanofilaments as Microbial Agent. *J. Phys. Chem.* A. **2014,** *118* (31), 5769–577.

Summary

AGRADECIMENTOS v
RESUMO vi
ABSTRACT vii
LIST OF FIGURES viii
Table list xii
PUBLICATIONS xiii
1. Introduction 1
1.1 Composite Materials 1
1.2. Nanocomposites 2
1.3. Nanocomposite fabrication techniques 4
1.4. Nanocomposite application 8
1.5. The ammonia gas problem 12
2. Goals and Overview 14
3. Polymeric nanofibers decorated with inorganic nanoparticles* 16
3.1. Abstract 17
3.2. Introduction 17
3.3. Materials and Methods 19
3.4. Results and Discussions 21
3.5. Conclusions 30
4. Organic/inorganic Layer-by-Layer platform deposition* 31
4.1. Abstract 32
4.2. Introduction 32
4.3. Experimental 33
4.4. Results and discussion 35
4.5. Conclusions 44
5. Ceramic nanofibers and polymeric coated paper – Additional Studies* 45
5.1. Introduction 46
5.2. Experimental 46
5.3. Results and discussion 49
5.4. Conclusions 59

6. General Conclusions and Future perspectives 60
7. References 61
Appendix A 76
Appendix B 80

1. Introduction

1.1 Composite Materials

The first composite materials obtained by men date back to ancient Egypt and were related to straw and mud combination to obtain bricks[1] with good compressive strength (mud property) and good tensile strength (straw property). In the following centuries, civil construction advanced the use of concrete, also classified as composite material[2], as an important mark. A composite material is any material made up by two or more constituent materials sharing a clear interface. Usually, the combined materials present very different properties and their combination in one single material will result in a composite with unique properties. The constituent material can be classified as matrix, which is the continuous and often in larger amounts, or as reinforcement, present in lower concentration. The matrix surrounds and supports the reinforcement, which will impose its special properties to enhance the matrix properties. The reinforcement may consist of particles (yielding particle reinforced composite), fibers and whiskers and fabrics (yielding fiber reinforced composite) as represented in Fig. 1.1.1. Fiber reinforcement may yet consist of continuous and aligned fibers, discontinuous and aligned or discontinuous and randomly oriented fibers[3]. The synergy between matrix and reinforcement will produce unprecedented properties when compared to the raw materials[4].

The careful choice of the matrix and reinforcement materials will drive the synergistic effect on the composite material guiding the resulting properties to meet the right requirements for a specific application. Usually, the type of matrix material is used to classify the composite. Metal matrix composites (MMCs) and ceramic matrix composites (CMCs) are classified as inorganic composite combined with ceramic reinforcement[5–9]. Composites based on polymer matrix (PMCs) and reinforcements, which provides high strength and stiffness, are classified as organic composites, and according with their mechanical properties level they are divided in reinforced plastics or advanced composites[10–12]. Originally, the main applications of composite materials were based on the improvement of the mechanical properties. Fiberglass can be mentioned as the first revolutionary modern composite material followed by carbon fiber materials, which is lighter and stronger than the first one[3,13] and widely employed in

airplane structure and sports equipment[14]. The new generation of composite materials is based on carbon nanotubes, which are even lighter and stronger, but still presenting a few drawbacks including the difficulty for dispersion, matrix compatibility and high costs to be employed in industrial scale. The new generation of composite materials extended the application field beyond the mechanical properties through electrical, magnetic and optical properties[15–18]. Known as advanced composites, they are a younger class of materials with properties not only dependent on the matrix and reinforcement constituents, but also on the relative proportion, size of the particle reinforcement and on the nature of the interactions that will lead the interface connections. For instance, sensors, biosensors, catalysts, or even multifunctional and smart materials with superior performance can be obtained using advanced composites[19–23].

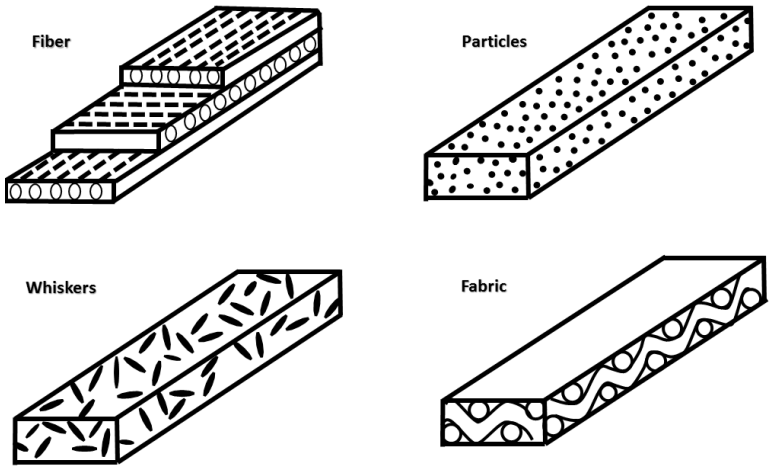

FIGURE 1.1.1: Composite reinforcement types. (Figure available in Eyring et. al.[3])

1.2. Nanocomposites

Advanced composite materials having one of the phases in the nanometric dimension (less than 100 nm), usually working as a reinforcement into the matrix, are classified as nanocomposites. They are also classified according with their matrix constituent, including metal matrix nanocomposites (MMNCs), ceramic matrix nanocomposites (CMNCs) and polymeric matrix nanocomposites (PMNCs). As it has been demonstrated in the literature, nanomaterials present enhanced properties when

compared to the same material in the micro- and macroscale due to the quantum confinement effects and extremely high surface area[24–26]. Therefore, when nanomaterials are employed as a filler material in nanocomposites, the interfacial area or interphase surface area will be proportional to the nanomaterial surface area and the nanocomposite properties ruled by the dominant interactions on the interface[27,28]. For PMNCs, the nanofillers as reinforcement are commonly employed to improve the melt strength and viscosity properties in recycled polymers. When compared to micro sized fillers, a smaller amount of nanofiller is sufficient to achieve excellent properties without reducing the light transmission properties of the polymeric matrix, neither substantially increasing the density and cost of the PMNC[29]. Another goal of PMNCs is the production of fire retardant[30]. The inorganic nanometric reinforcement, especially in exfoliated nanoplatelets shape, can act as a protective barrier and also increase the melting viscosity, enhancing the nanocomposite structural stability at high temperatures[31–33]. In the case of CMNCs with matrix particles in the micron sized scale and reinforcement in the nano sized scale, the nanofiller can occupy both inter- and intra-granular positions and will be able to limit the matrix grain growth, enhancing the hardness and strength properties[34]. When combined in similar volume fractions, matrix and reinforced constituents will form interconnected structures hindering the growth of each other.

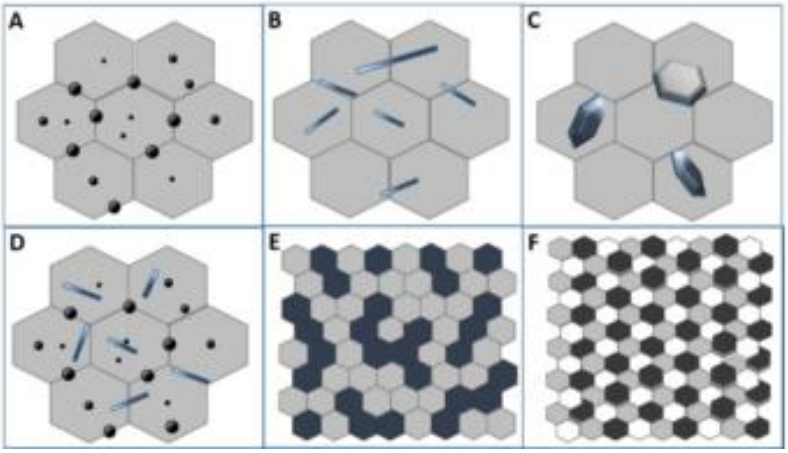

FIGURE 1.2.1: Scheme of common (nano)composite structures for ceramic materials (a) nanoparticles occupying both inter- and intra-granular positions inside a micronic matrix; (b) elongated nanoreinforcements embedded in a micronic matrix; (c) platelet-like nanoreinforcements embedded in a micronic matrix; (d) containing both rounded and elongated nanoreinforcements, embedded in a micronic matrix; (e) Bi-phasic

composite made by two immiscible ultra-fine phases; (f) Multi-phasic composite made by three (or more) immiscible. (Figure available in Palmero et. al. [28])

1.3. Nanocomposite fabrication techniques

Three main methods have been adopted for polymer-based nanocomposites preparation, as follows: i) nanocomposite constituent's solution mixture; ii) polymer melt intercalation and iii) in situ polymerization. A combination of two or more methods may also be useful in the polymer-based nanocomposite fabrication.

In polymer melt intercalation method, the nanometric reinforcement is mixed with the molten polymer. Intercalated or exfoliated nanocomposites are generally obtained if there is a great compatibility between the filler and the matrix within suitable processing conditions[35]. Often a third component must be added to promote better compatibility between the matrix and the reinforcement constituent[36,37]. Nanocomposites production by polymer melt intercalation method has several advantages, such as the relative simplicity of the process, large-scale production and the absence of organic solvents that can be harmful to the environment.

For *in situ* polymerization process, the reinforcement is dispersed in a solution of the polymer monomer. The monomer is expected to penetrate the intermolecular space, causing its delamination. A good affinity between the constituent phases is essential for a homogeneous dispersion of the system. The polymerization process is then started. It is important that the all or part of the polymerization occurs within the filler so the exfoliation takes place by the growth of the polymer chains within the interlamellar space, allowing a greater dispersion of the nanometric reinforcement. This method is very good for core-shell nanocomposite and coated nanomaterials preparation. Since it occurs *in situ*, there is no limitation for the matrix geometry.

Nanocomposite solution mixture method consists on the dispersion of the reinforcement particles in organic solution containing the polymer matrix followed by evaporation of the solvent. It is important to use a solvent with good interaction with the reinforcing nanoparticles to promote the disaggregation, contributing to the homogeneity of the solution, enabling nanocomposites processing. Upon solvent evaporation, the

polymer chains are entrapped between the reinforcing particles forming multilayer structures. The solution mixture process allows the fabrication of different platforms conformed in specific shape, including nanofibers obtained by electrospinning technique and thin films obtained by Layer-by-Layer technique[38–40].

Electrospinning technique

Electrospinning is a fiber fabrication technique capable of producing functional nanofibers for varied applications[41–46], and is usually composed by a high voltage supply, an ejection pump and a syringe as polymeric solution/melted polymer container. In this technique, a droplet of the polymer solution contained in the tip of the spinneret is submitted to a high electrical voltage. In this situation, the drop experiences a repulsive electrostatic force that overcomes the surface tension forces, drawing charged threads from the Taylor cone tip, yielding to the fiber[47] formation. Parameters such as solution viscosity, chains entanglement, electrical conductivity and surface tension directly influence the morphologies and geometry of nanofibers. The solution stretching is affected by parameters including solution viscosity and electrical potential, which should be properly selected allow the production of high quality fibers [48]. The jet region is influenced by bending and whipping instabilities that arise due to the charge-repulsion between the excess of charges present in the jet which favors thinning and elongation of the jet[49]. While the jet travels between the needle and the collector, the solvent evaporates producing nanofibers that are deposited on the collector[50]. The fiber formation, stabilization and collection is represented in Fig. 1.3.1.

Nanofibers mats are very interesting to be used as polymer matrix in composite materials fabrication, since they present a high surface area and nanometric dimensions[51]. Although the most traditional application in composite materials for micro-sized fibers is as structural reinforcement just a few works reported nanofibers as structural reinforcement. Most of researches employing polymeric nanofibers have been devoted to biomedical applications for slow release and cellular scaffold development [52–58]. Another possibility is the incorporation of secondary phases to promotes improved electrical and optical properties providing customized materials according with the necessity[59–62].

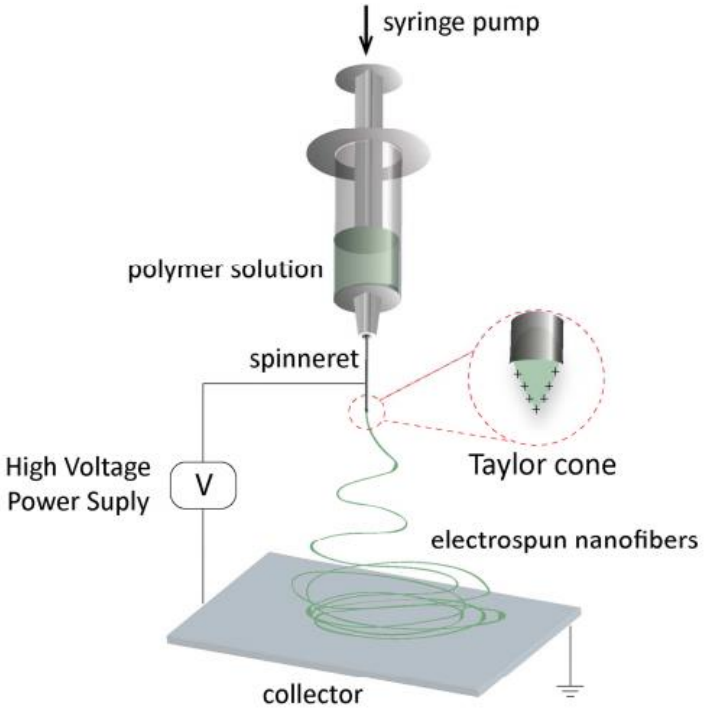

Figure 1.3.1: Electrospinning fiber formation scheme (Figure adapted from Costa et. al.[50]).

Layer-by-Layer (LbL) technique

Another convenient technique for developing nanocomposite based platforms is the Layer-by-Layer (LbL) technique[63]. LbL method is an alternative technique to Langmuir-Blodgett (LB) technique[64] for thin film fabrication and it is based on multilayer adsorption of polyelectrolytes onto a suitable substrate. LbL technique is a technique that requires a simple experimental arrangement with low cost and scaled production. Figure 1.3.2 represents the LbL technique procedure, which consists in alternatively immersing a solid substrate in aqueous solutions of polyanion and polycation. The charge of the first solution must be contrary to the substrate so the electrostatic adsorption can occur. Between each assembly step, the non-adsorbed excess material needs to be removed by a washing step, followed by a drying step. Next, the substrate is then immersed into a solution of opposite charge, resulting in a nanoarchitecture formed by alternate layers of cationic and anionic materials. The repetition of these steps can lead to the formation of multilayer ultrathin films by physical adsorption and, unlike the chemisorption processes, LbL method does not require the formation of

covalent primary chemical bonds. However, the self-assembling technique does not provide the polymer chains with a high degree of organization. Srivastava, S. and Kotov, N. A.[65] presented an overview about efforts to fabricate high-quality nanocomposites based polymeric thin films incorporating inorganic nanomaterials, which LbL films assembly merge the properties of each isolated material resulting in functional films. The authors also highlighted the possibility of manipulating this functionality using inorganic nanomaterials with different geometries such as nanoparticles, nanosheets and nanowires according with the desired property.

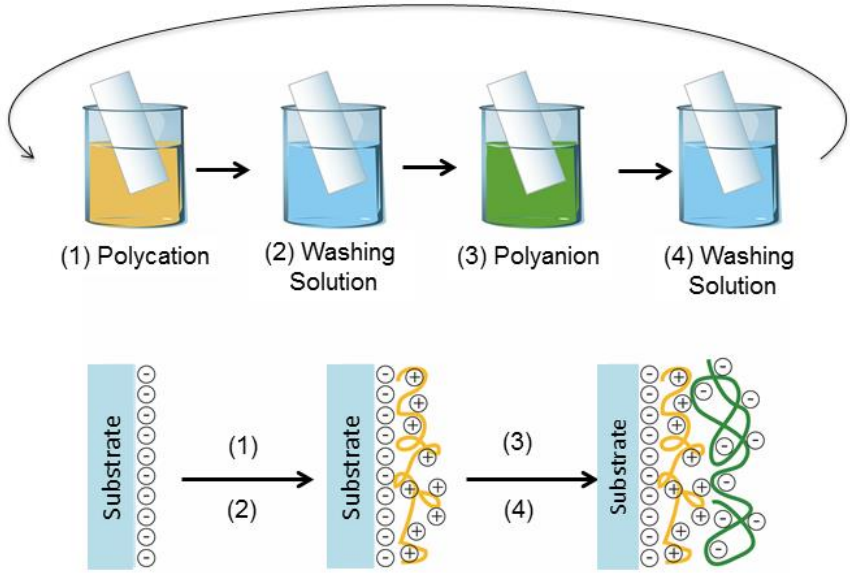

Figure 1.3.2: Schematic Layer-by-Layer (LbL) self- assembly technique. (Figure adapted from Correa et. al.[60])

Finally, for higher quality nanocomposite materials with more attractive properties, two or more methods can be combined. The purpose of combining methods is to take advantage of the individual methods. A good example of combined method for nanocomposites preparation is the fabrication of nanocomposites with high concentration of reinforcement (around 30%) widely used in the plastics industry as color additives. They can be obtained by a combination of solution mixing methods and in situ polymerization. Thus, the ease in prepare exfoliated materials by solution method with the pragmatism and mass production capacity are combined[66]. Another possibility is the use of *in situ* polymerization method being employed for nanofibers mats coating.

A recent work presented by Chen et. al.[67] reported the fabrication of a composite based on polyimide nanofibers membranes as a template to *in situ* polymerization of nanosized polyaniline particles . The as-prepared PANI/PI mats not only presented excellent thermal and mechanical properties but also showed good electrical conductivity, pH sensitivity, and significantly improved electromagnetic impedance when compared with non-coated mats.

1.4. Nanocomposite application

Nanocomposite materials have been employed in a wide range of applications including gas barrier, photovoltaic cells, heat exchangers, optically transparent functional nanocomposite material, filtration systems, medical prostheses, tissue template, drug delivery matrix, optoelectronics, catalysis, and electrical and optical sensor applications[18,68–71] such reported by Sahay et. al.[72] as illustrated in Fig. 1.4.1.

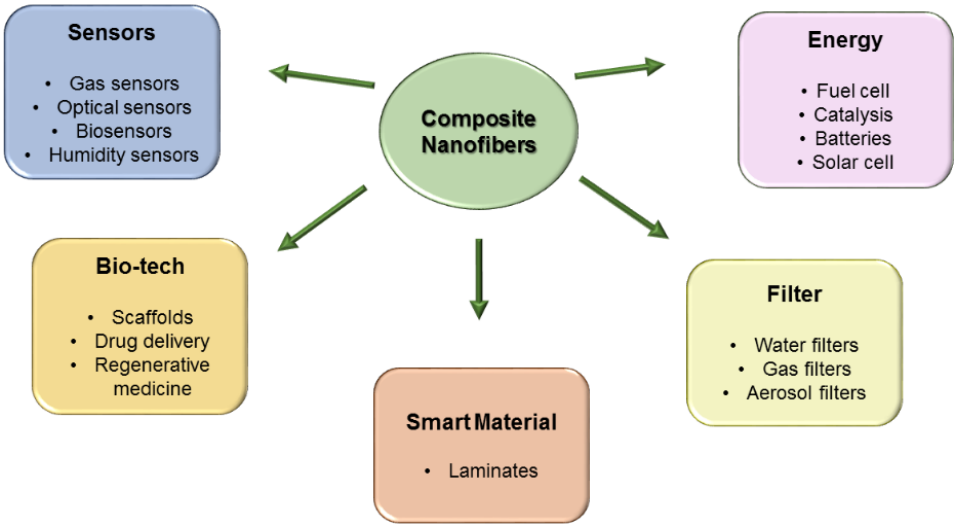

FIGURE 1.4.1: Nanocomposites classification based on their applications. (Figure idealized from Sahay et. al.[72])

Nanocomposites for gas sensing application

In the last few years' great efforts have been made for developing sensitive and selective gas sensors in order to monitor environmental pollution, industrial and public safety and non-invasive diagnosis[20,73–76]. Such sensors are intended to detect low concentrations of gas in the surrounding atmosphere at specific conditions, including under distinct humidity and temperatures levels. Usually, resistive-type metal oxide gas sensors are attractive once they present high sensitivity, low cost and simple operation. However, they present poor selectivity and better performance at high temperatures. Recent studies have reported the improvement of metal oxide gas sensors selectivity using secondary phases to form composite materials[77]. Mirzaei, A. et. al.[78] reported the greater gas sensitivity for Ag/Fe_2O_3 core-shell nanocomposite compared with the pure Fe_2O_3 semiconductor. Ag metallic nanoparticles was used as filling in Fe_2O_3 ceramic matrix. The Fe_2O_3 shell is showed to be thin enough to allow the chemical and electronic sensitization of the Ag nanoparticles when in contact with NO_2 gas. The authors proposed two mechanisms for the nanocomposite sensitivity. In the chemical sensitization (CS) mechanism the metallic nanoparticle catalytically activates the dissociation of gas molecules followed by adsorbing on the nanoparticle surface, capturing conductance band electrons. Another mechanism is the electronic sensitization (ES), where they address the metallic nanoparticle sensitivity to their interaction with the semiconductor matrix. Metallic nanoparticle in oxidized state accept the matrix electrons, inducing to a depletion layer on the interface.

In nanocomposites, the combination of constituents with dissimilar types of conductivity, such as *p*-type and *n*-type materials, sharing interfaces, can equilibrate the Fermi levels to the same energy and form a *p*-*n* heterojunction. In this scenario, the charge transfer is improved and allows the formation of a depletion layer followed by the barrier potential build-up. Several studies have related the nanocomposites enhanced properties and superior functional performance with the presence of *p*-*n* heterojunction. Once the depletion layer is formed, the charge transfer is interrupted by the barrier potential, which requires an extrinsic potential to be re-established. Thus, the production of multifunctional composites depends directly on the understanding of how the nanoscale structure influences the properties of the composite material. Once this knowledge is acquired, the adaptation of the desired composite structures is an additional challenging step in the manufacturing process, which requires innovative

concepts for the stages of production, since the synthesis of nanocomposites until their processing.

As mentioned, composites with dissimilar constituent results in a heterojunction with a depletion layer. Therefore, in composite sensors, the detection process occurs through a synergistic reaction where the analyte reacts with the most readily phase, which in turn may react with the secondary constituent giving an improved response. For instance, Narjinary et. al.[74] reported the fabrication of low-concentration-acetone gas sensor for breath analyses to monitor diabetes. The fabricated nanocomposite platform was obtained using MWCNT as substrate for SnO_2 nanoparticles and presented much better performance than pure SnO_2 with high sensitivity, stability, fast response and good resolution. The better performance was attributed to the heterojunction formation and high surface area, which increases the material adsorption capacity. Conducting polymers also have been used as active layer in gas sensors due to their high sensitivities, good mechanical properties and short response time[79–81]. So, heterostructure based in conducting polymer are also a good choice for gas sensor applications.

A full comprehension on the heterojunction mechanism and how it influences on the sensor activity is of great value for optimized experiments, saving time and lowering costs. A composite formed by the combination of an organic material (p-type) with an inorganic material (n-type) can be treated as a heterostructure with *p-n* heterojunctions. The interaction between both materials and the improved performance of the composite material for sensor applications will be presented for a specific case of a conducting polymer, acting like a p-type material with excess of free positively charge, and an inorganic semiconductor, acting as n-type material with excess of free negative charge. Usually, n-type materials are more used for gas sensing applications than p-type material because n-type material usually show more stability and robustness[82,83]. However, a p-type material can play an important role for gas sensing when combined with a n-type material. When materials with a specific Fermi energy level are in contact, the electrons from higher energy levels tends to flow across the interface to free lower-energy levels, equilibrating the Fermi energy for both materials and consequently forming the depletion layer[84]. After the Fermi levels are equilibrated, a barrier potential is formed due to the band bending caused by the difference in original Fermi energy levels. It is worth to mention that heterojunctions can be classified into three different groups according to the different combinations of conducting band energy and valence

band energy alignment known as straddling heterojunction, staggered heterojunction and broken-gap heterojunction[84]. Figure 1.4.2 present a staggered heterojunction combination and the respective depletion layer formation.

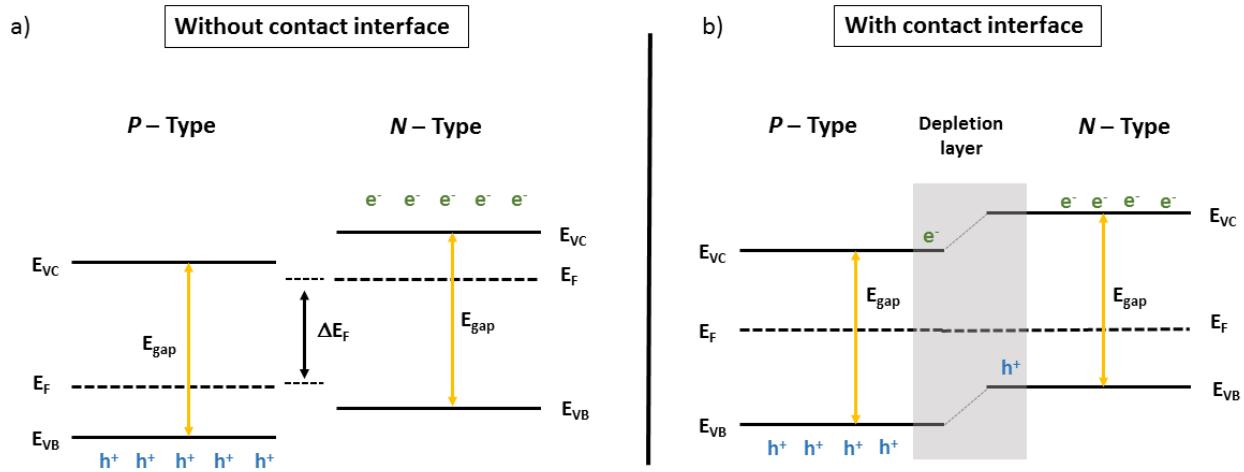

Figure 1.4.2: Schematic representation of the p-n energy levels a) before and b) after a heterojunction formation.

The barrier potential formation will hinder the electron transfer, making necessary to overcome this energy barrier. Considering a hypothetical n-type material in air, the resistance will be higher for the pure material than for the composite material due to the presence of a depletion layer in the last one. The exposure of this composite material to oxidizing and reducing gases will reflect in a resistance variation for higher or lower values according to the availability of free electrons[85,86]. Once the resistance variation can be treated as the sensor response, considering the influence of the secondary composite phase on the initial resistance value, composite materials behavior usually provides better performance and variation for oxidizing gases. Furthermore, the development of nanocomposite materials from two or more constituents should be promising for improvements in gas sensor performance increasing their application in field[82].

1.5. The ammonia gas problem

Brazil has established itself as one of the world's largest food producers, including chicken livestock production. Although this activity generates employment, income and food for the population, there is a strong concern regarding the quality of the environment in poultry farms, especially related to ammonia emissions. In poultry farms, ammonia is formed from the microbial decomposition of uric acid (nitrogen compound) wasted by poultry and its emission is dependent on high temperature, pH variation, humidity, type of material used for bed and its handling[87–91]. Chicken litter is the product resulting from the accumulation of poultry manure, feathers and food wasted on the material used as flooring (rice husks or peanuts, corn cob, wood shavings, paper, etc.). The chicken bed is the only basic byproduct of commercial poultry, that is, it can be marketed for purposes of organic fertilization (natural fertilizer). This material present high levels of nitrogen, phosphorus and potassium and has traditionally been used as a source of nutrients for vegetable crops and in the improvement of soil physical, chemical and biological conditions[92]. However, the ammonia released from the chicken waste affects animal and human health as it is irritant to the mucous membranes of the eyes and respiratory tract, which predisposes the entry of several disease agents[93–95]. High levels of ammonia can be observed at the beginning of breeding in sheds that reuse the bed[92].

The levels of ammonia up to 50 ppm cannot be perceived as harmful, because the human sense of smell does not detect the presence of ammonia at levels below 20 ppm[88,96]. In addition, humans lose their olfactory sensitivity after long or repeated exposures to the same odor. In this way, workers are affected long before the problem can be identified. From 50 to 100 ppm, ammonia can be inhaled without major consequences. From 100 to 200 ppm, ammonia induces drowsiness, salivation and loss of the appetite. In many countries, the ammonia concentration leves are limited to 25 ppm in a period of 8 h / day of work and for short periods of exposure this level increases to 35 ppm[97]. In Sweden, the worker's maximum level allowed is 10 ppm. In Brazil, legislation allows the maximum concentration of 20 ppm in the air, within the industry during the shift of 8h / day of work. For Brazilian conditions of chicken livestock production, a reduction in respiratory capacity in workers from low-mechanized farms it is observed for more than 4 years of activity, where a maximum of 5h / day of exposure limit for activities inside the warehouses is recommended [96]. It is also known that

ammonia formation in aviaries results from the combination of three factors: 1) waste, 2) heat and 3) moisture. Thus, farmers tend to carefully manage chicken litter and ventilation systems in the sheds to reduce the exposure of animals and workers to ammonia gas emissions. Thus, the development of a sensor device that effectively can determine ammonia concentrations is of great importance for improving livestock production and guarantee the workers safety.

2. Goals and Overview

The general goal of this thesis was to develop nanostructured ammonia gas sensors using different platforms based on distinct composite materials (ZnO nanoparticles, graphene oxide, conducting polymers and polyelectrolyte polymer), and to study the adsorption interaction between ammonia gas molecules and the sensing layer material. Since the referred interaction is the key for the development of new ammonia sensor with remarkable sensibility and selectivity aiming environmental safety for humans and animals in critical sites.

Specific goals:

- ✓ Optimization of the synthesis conditions to obtain ZnO as dispersed nanoparticles and ceramic nanofibers;
- ✓ Optimization of the synthesis conditions to obtain Layer-by-Layer and electrospinning platform based on the ZnO nanoparticles, previously obtained and conducting polymers;
- ✓ Investigation of the performance of the ammonia sensors and the sensing mechanism based on the interaction of ammonia molecules with the developed platforms.

Chapters Overview

The main idea of this thesis was to explore the sensing properties of different material combination, as composite materials, in distinct sensing platforms configuration, with the purpose of detecting ammonia in low concentrations. The materials choice for combination was based on the improvement of the charge transfer effect.

Initially, the first platform obtained was based on a fluorine doped tin oxide (FTO) electrode modified with polyamide 6/polyaniline (PA6/PANI) electrospun nanofibers and decorated with ZnO nanoparticles, which was applied as electrochemical sensing device. As a proof of principle, the modified electrode was employed for hydrazine electrochemical detection, once the gas chamber system for ammonia tests was not available at the time of the experiments. Hydrazine (N_2H_4) is a

carcinogenic contaminant with chemical composition very close to ammonia. main results are presented in Chapter I and indicate that the novel sensing platform can be potentially harnessed for electrochemical sensors and biosensors applications.

The second platform was based on the fabrication of Layer-by-Layer architecture composed by polyaniline, graphene oxide and ZnO in tetralayer configuration deposited onto gold interdigitated electrodes. Impedance spectroscopy was employed as sensing technique and useful information was obtained by investigating the charge transfer process on the platform when exposed to ammonia gas. The main results are presented in Chapter II.

A third device was obtained based on ZnO ceramic nanofibers coated with Poly(styrene sulphonic Acid) (PSS) which were deposited on coated in gold interdigitated electrode..

Finally, a fourth platform was obtained based on a glass fiber paper coated with polyaniline layer by *in situ* polymerization, aiming the development of a low cost, flexible and disposable device for ammonia detection in low concentrations at room temperature.

General conclusions are presented in the sequence correlating the obtained results and the sensing properties.

3. Polymeric nanofibers decorated with inorganic nanoparticles*

* The content of this chapter is an adaptation of the article entitled: "**Improving the electrochemical properties of polyamide 6/polyaniline electrospun nanofibers by surface modification with ZnO nanoparticles"** by R. S. Andre, A. Pavinatto, L. A. Mercante, Elaine C. Paris, Luiz H. C. Mattoso and Daniel S. Correa, published in RSC Advances Journal.

Reference: *RSC Adv.* **2015**, *5* (90), 73875-73881.[125]

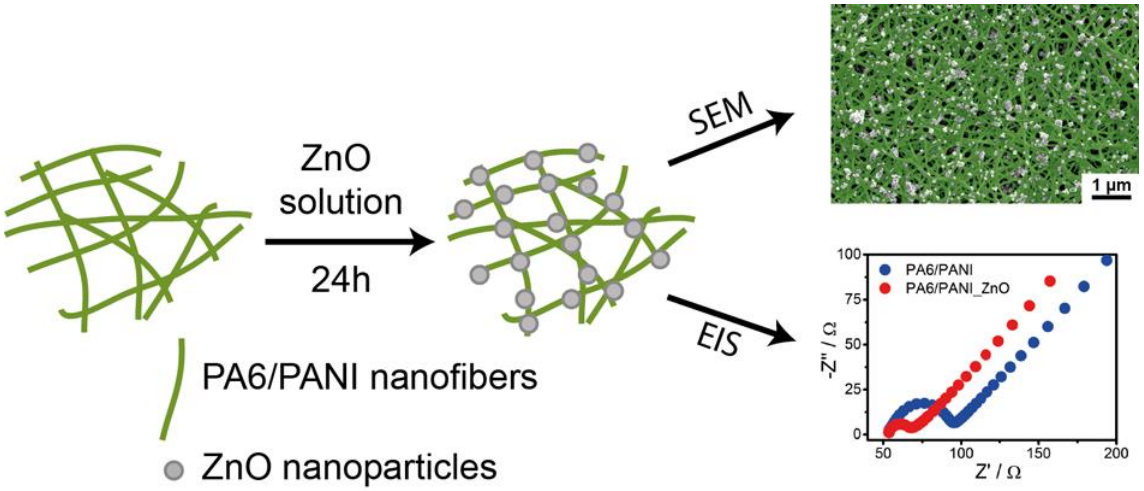

3.1. Abstract

Heterostructured nanomaterials have attracted increasing interest because of their novel and distinct optical and electrical properties, finding applications in devices and chemical sensors. Here we report a new electrochemical platform based on the modification of fluorine doped tin oxide (FTO) electrode with polyamide 6/polyaniline (PA6/PANI) electrospun nanofibers decorated with ZnO nanoparticles. The nanoparticles were synthesized by co-precipitation method, followed by hydrothermal treatment, which route was optimized in order to obtain particles of small average diameter (45 nm). Polymeric nanofibers were obtained by the electrospinning technique and further subjected to the ZnO modification by nanoparticle impregnation. SEM images confirmed the uniform distribution of ZnO nanoparticles adsorbed onto the nanofibers surface, which amount was estimated to be 4% w/w, according to thermal gravimetric analysis (TGA). According to the electrochemical characterization, an improvement in electron transfer kinetic and increase in electroactive area was observed for the ZnO-modified electrode. As a proof of principle, the modified electrode was employed for monitoring hydrazine, and yielded a detection limit of 0.35 μmol L^{-1}. Our results indicate that the novel sensing platform based on the adsorption of ZnO nanoparticles onto the surface of electrospun nanofibers can be potentially harnessed for electrochemical sensors and biosensors applications.

3.2. Introduction

Organic-inorganic hybrid materials have attracted increasing attention due to their potential application in different areas, including optics and electronics.[98,99] In most cases, the combination of organic and inorganic materials can yield a high-performance hybrid material with synergistic behaviors or complementary properties between the polymer and the inorganic component.[100–104] In fact, the combination of polymers and inorganic nanoparticles displays advantageous electrical, optical and mechanical properties, finding applications in opto-electronic devices and also as catalyst, which depends directly on the choice of the organic and inorganic component.[62,105]

A huge variety of polymeric structures could be used for this propose and 1D nanomaterials have been intensively investigated due to their unique properties.[76]

Various techniques have been developed to fabricate 1D nanostructures, including the electrospinning technique, which is a versatile and low-cost method that can produce large specific surface area nanofibers.[44,72] This relatively huge surface area can potentially provide ultra-high sensitivity and fast response time for sensing applications.[61,106–109] In particular, electrospun nanofibers containing conductive polymer such as polyaniline (PANI) have attracted even more interest because of their high conductivity and potential applications in electrochemical devices.[110] In order to improve their properties and to construct multifunctional hybrid nanostructures, more recently considerable efforts have been directed towards attaching metallic and oxide NPs onto electrospun nanofibers.[111,112]

Zinc oxide (ZnO) is a versatile n-type metal oxide semiconductor with a wide band gap (3.36-3.39 eV) at room temperature, and present appealing features such as biocompatibility, nontoxicity and inexpensiveness.[113] It has been extensively used in the fabrication of electronic and optical devices, heterogeneous catalysis and gas sensing[114]. Furthermore, ZnO can be employed to facilitate the charge transfer and enhance the electrochemical activity.[115] Therefore, functionalizing electrospun nanofibers with NPs in order to combine the conductivity of the polymeric phase (PANI) and the high surface area of the nanofibers with the unique properties of ZnO NPs, can become an important strategy for the development of new electrochemical platforms.

In this context, herein we report an effective route to obtain fluorine doped tin oxide (FTO) electrode modified with polyamide 6/polyaniline (PA6/PANI) electrospun nanofibers decorated with ZnO nanoparticles. The hybrid nanomaterial combines the semiconductor properties of ZnO nanoparticles, synthesized by hydrothermal method, the conductive properties of PANI and the mechanical properties of PA6 in the same platform. X-Ray diffraction confirmed the ZnO formation, while the size and shape of nanoparticles were analyzed by field emission scanning electron microscopy (FEG-SEM). The efficient ZnO impregnation on the PA6/PANI nanofibers surface was confirmed by scanning electron microscopy (SEM). Electrochemical measurements were carried out to confirm the improvement in charge transfer efficiency of the PA6/PANI- ZnO modified electrode, enabling futures applications as electrochemical sensor. Electrochemical measurements were carried out to confirm the improvement in charge transfer efficiency of the PA6/PANI–ZnO modified electrode. In order to confirm the potential of this novel platform for sensing applications, we used hydrazine, a carcinogenic contaminant found in trace amounts in the environment, as a model for the

electrochemical measurements. The hydrazine sensor showed a linear range from 0.5 to 5000 mmol L^{-1} and a detection limit of 0.35 mM.

3.3. Materials and Methods

3.3.1. Materials

Polyamide 6 (PA6, M_w = 20 000 g mol^{-1}), polyaniline (PANI, M_w = 20 000 g mol^{-1}), zinc nitrate hexahydrate, Polyethylene glycol (PEG400, M_w = 380-420 g mol^{-1}; PEG 4000, M_w = 3600-4400 g mol^{-1}; PEG8000, M_w = 7000-9000 g mol^{-1}) were all purchased from Sigma-Aldrich. Potassium hydroxide and formic acid were purchased from Synth Chemical (São Paulo, Brazil). The dispersing agent, Liosperse 511, was purchased from Miracema-Nuodex (Campinas, Brazil).

3.3.2. Synthesis of ZnO nanoparticles

ZnO synthesis was carried out by coprecipitation method followed by hydrothermal treatment at 150°C for 1 hour.[116] Initially, zinc nitrate and potassium hydroxide were separately dissolved in deionized water (0,05 mol L^{-1} and 2 mol L^{-1}, respectively) under vigorously stirring. PEG solution (0,1 mol L^{-1}) was added into the zinc nitrate solution for each synthesis and stirred for 30 minutes. Subsequently, potassium hydroxide solution was slowly added until pH 14 was reached. The suspension containing the white solid precipitate was then submitted to the hydrothermal treatment. The suspension was heated up at a rate of 10°C/min under constant pressure (approximately 3.0 bar) until 150°C and maintained at this temperature for 1 hour. Finally, the white solid was washed with deionized water several times until the pH became neutral and then dried in an oven.

3.3.3. Electrospinning of PA6 and PA6/PANI nanofibers

PA6/PANI solution was prepared by dissolving 20% (w/v) PA6 and 1% (w/w) PANI in formic acid and stirred for 5h at room temperature. The electrospun nanofibers were obtained by using an electrospinning apparatus at a feed rate of 0.01 mL h^{-1} and an electric voltage of 25 kV. A working distance of 10 cm was kept between the syringe

and the metallic collector. The inner diameter of the steel needle was 1.2 mm. The produced nanofibers were directly electrospun onto fluorine doped tin oxide (FTO) glass substrates to obtain the modified electrodes. The substrates were attached to the collector at the same position in all experiments with an optimal collection time of 10 min. Control of the experimental conditions was crucial to ensure reproducibility because both the diameter and length of nanofibers depend on the collecting time and other experimental parameters.

3.3.4. Adsorption of ZnO nanoparticles onto the electrospun nanofibers

ZnO nanoparticles (1 mg mL^{-1}) were dispersed in distilled water containing 0.5% (w/w) of Liosperse 511. Ultrasonication at 20 kHz for 5 min was then applied for the dispersion of the nanoparticles. After de dispersion, the electrospun nanofibers were immersed into the ZnO solution, rinsed with distilled water and dried under ambient conditions. Three different adsorption times were tested (12, 24 and 48 h) in order to determine the best electrochemical response.

3.3.5. Physico-chemical Characterization

As-prepared samples of ZnO nanostructures were characterized by X-ray diffraction (XRD) using a Shimadzu, XRD-6000 diffractometer at 30 kV and 30 mA with Cu Kα radiation. Morphology and size characterizations were performed by field emission gun scanning electron microscopy (FEG-SEM) (JEOL, JSM 6510). The morphology of the fibers was evaluated using a scanning electron microscope (SEM, JEOL 6510) operating at 10 kV, and the nanoparticles diameter was estimated by using an image analysis software (Image J, National Institutes of Health, USA). In each experiment, the average nanoparticles diameter and distribution were determined by measuring 100 random particles using representative micrographs. To estimate the amount of ZnO nanoparticles adsorbed onto the nanofiber surface, thermal gravimetric analysis (TGA) was performed using a thermogravimetric analyzer (Q500 TA Instruments) under nitrogen atmosphere, at a flow rate of 20 ml min^{-1}. Samples in platinum pans were scanned from room temperature to 1000°C at a heating rate of 10°C min^{-1}.

3.3.6. Electrochemical Characterization

The electrochemical characterization experiments were carried out using a PGSTAT30 Autolab electrochemical system (Metrohm) controlled with GPES software using a 0.05 mol L^{-1} $[Fe(CN)_6]^{3-/4-}$ containing 0.1 mol L^{-1} KCl. The nanofibers-modified-FTO electrodes were used as working electrodes. A Pt foil and Ag/AgCl (3 mol L^{-1} KCl) electrodes served as the counter and reference electrodes, respectively. Cyclic voltammetry (CV) measurements were performed over a potential range from 0.2 to 0.6 V at a scan rate of 100 mV s^{-1} and electrochemical impedance spectroscopy (EIS) measurements were carried at a potential of 0.3 V over the frequency range from 0.1 Hz to 100 kHz, using an amplitude of 10 mV.

3.4. Results and Discussions

3.4.1. Characterization of ZnO nanoparticles

Different molar weight PEGs were employed to optimize ZnO synthesis in order to obtain nanoparticles with suitable shape and size for impregnation onto the polymeric electrospun nanofibers. The long-range order of ZnO samples was deter- mined by X-rays diffraction. Fig. 3.4.1 shows XRD patterns of ZnO synthetized using (a) PEG 8000, (b) PEG 4000 and (c) PEG 400. All samples present the same diffraction peaks, which are attributed to polycrystalline ZnO. The pattern is typical of the ordered hexagonal wurtzite phase according to JCPDS Card no. 36-1451. Diffraction peaks related to secondary phases were not found, indicating that ZnO without impurities was successfully obtained for the three different molar weight PEGs tested.

As the desired phase of ZnO was successfully obtained for all tested samples, they were analyzed by FEG-SEM to characterize the shape and size of the nanoparticles. Surfactants have been employed to control the shape and size of nanostructures, once features such as hydrophobic chains, headgroups, impurity ions and concentration of surfactants exert direct effects on the nanoparticles properties[117–119].

Using PEGs with high molecular weight (PEG 8000 and PEG 4000), agglomerated nanoparticles with a nearly spherical morphology and polydisperse nature were obtained (see Fig. 3.4.2a and b). In hydrothermal conditions, the solubility of amorphous particles is significantly increased and crystallization can occur concurrently with redissolving and reprecipitation processes.[120,121] After the nucleation process, the increased particle solubility could result in growth of an individual nanostructure aggregation and/or coarsening.[116,122,123] PEG 8000 and PEG 4000 were not very efficient as surfactants, yielding shapeless and large grain originated from random aggregation process between small particles. Thus, our results indicate that the use of PEG surfactant with longer hydrophobic chains leads to nanoparticles with larger sizes.[124] On the other hand, PEG 400 a hydrophobic surfactant with shorter molecular chain, yielded nanoparticles (see Fig. 3.4.2c) of low dispersion with homogeneous distribution and smaller size (44 nm), adjusted by lognormal fit, as shown in histogram of Fig. 3.4.2d, configuring the best- optimized process and the choice for the subsequent studies.

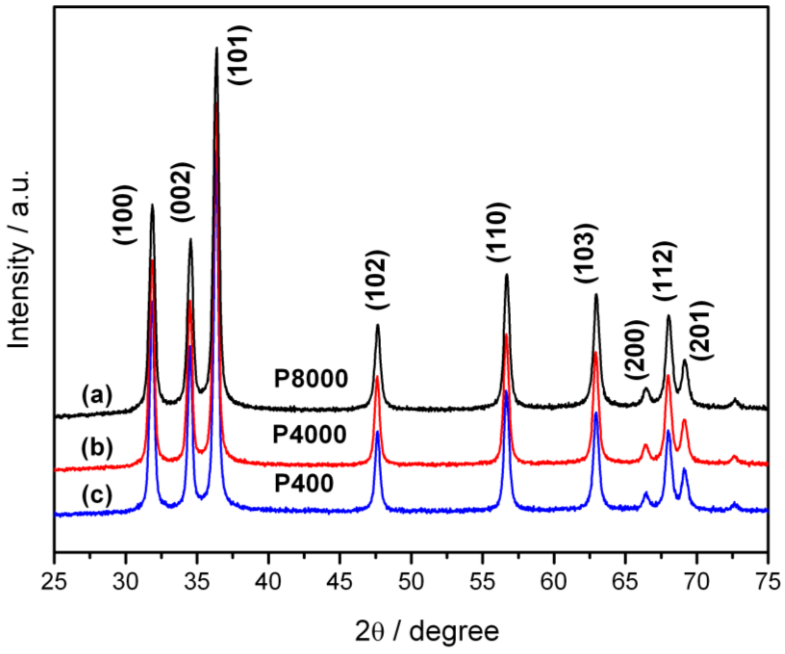

FIGURE 3.4.1: XRD patterns of ZnO synthetized with (a) PEG 8000, (b) PEG 4000 and (c) PEG 400. (Figure available in Andre, R. S. et. al.[125])

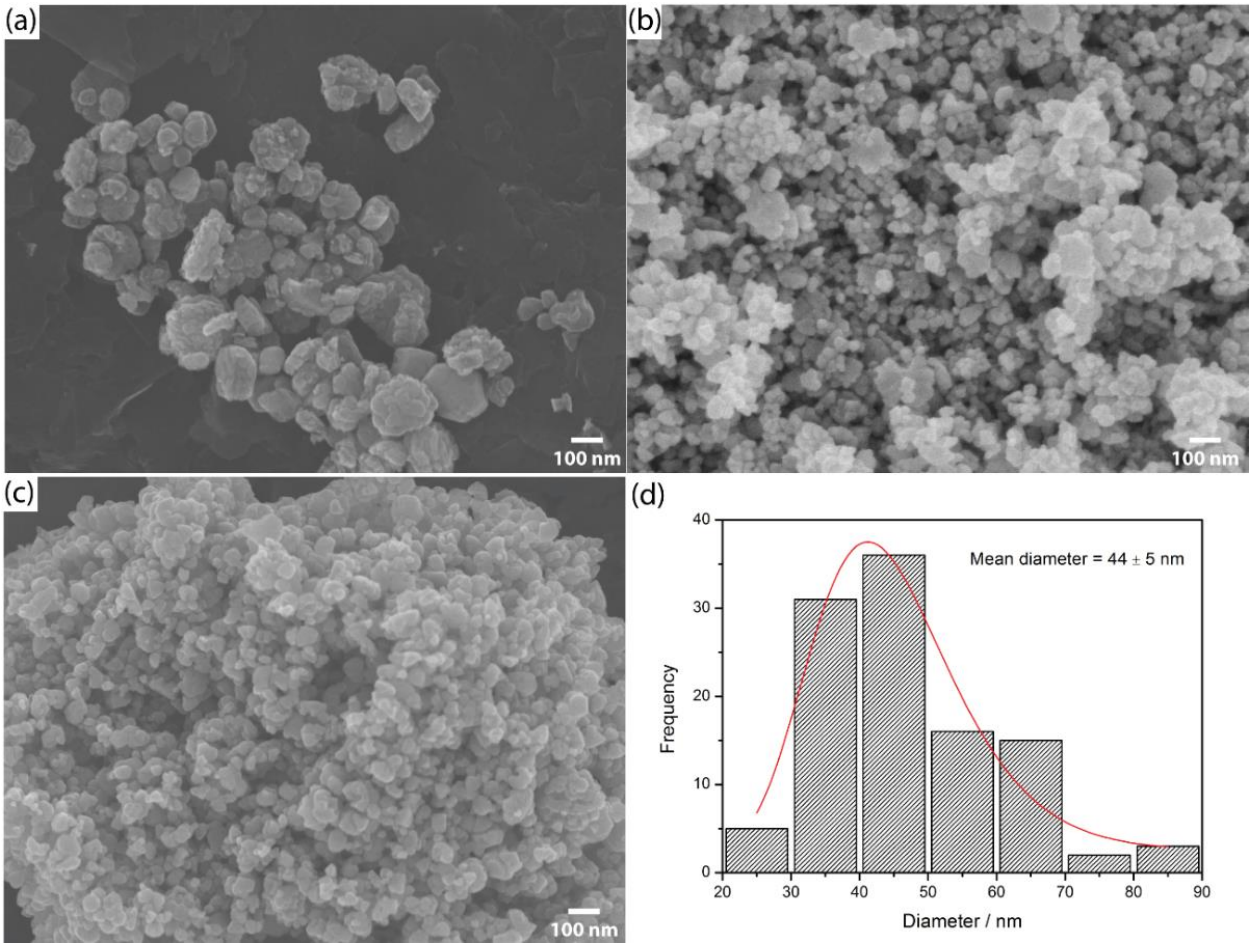

FIGURE 3.4.2: FEG-SEM images of ZnO synthetized with (a) PEG 8000, (b) PEG 4000 e (c) PEG 400. (d) Histogram of size distribution of ZnO nanoparticles synthetized with PEG 400. (Figure available in Andre, R. S. et. al.[125])

3.4.2. Characterization of PA6/PANI nanofibers

To obtain uniform PA6/PANI electrospun nanofibers, the electrospinning parameters were optimized through variation of the flow rate, applied voltage, polymers concentration, and collection distance. Under the improved experimental parameters, smooth and uniform bead-free nanofibers were obtained with a mean diameter of 78 ± 1 nm, as shown in Fig. 3.4.3a.

In order to improve the electrochemical properties of the fabricated nanofibers, a further step was taken aiming at functionalizing them with ZnO nanoparticles. ZnO-containing electrospun polymer nanofibers (PA6/PANI_ZnO) exhibit a huge variety of potential applications, as the composite fibrous mats show flexibility, are freestanding and display hybrid properties determined by the polymer and NPs.[126] The surface of

PA6/PANI nanofibers was efficiently modified with ZnO nanoparticles, as confirmed by the FEG-SEM image in Fig. 3.4.3b and indicates that the coating on the nanofibers surface appears to be uniform. Moreover, the adsorption was strong since the nanoparticles remained on the nanofibers surface even after a washing process, which consisted of repeated submersion in water. This suggests that the ZnO NPs are not simply lying on the nanofiber surface, but instead, they are attached to the PA6/ PANI nanofibers via H-bonding and electrostatic interaction

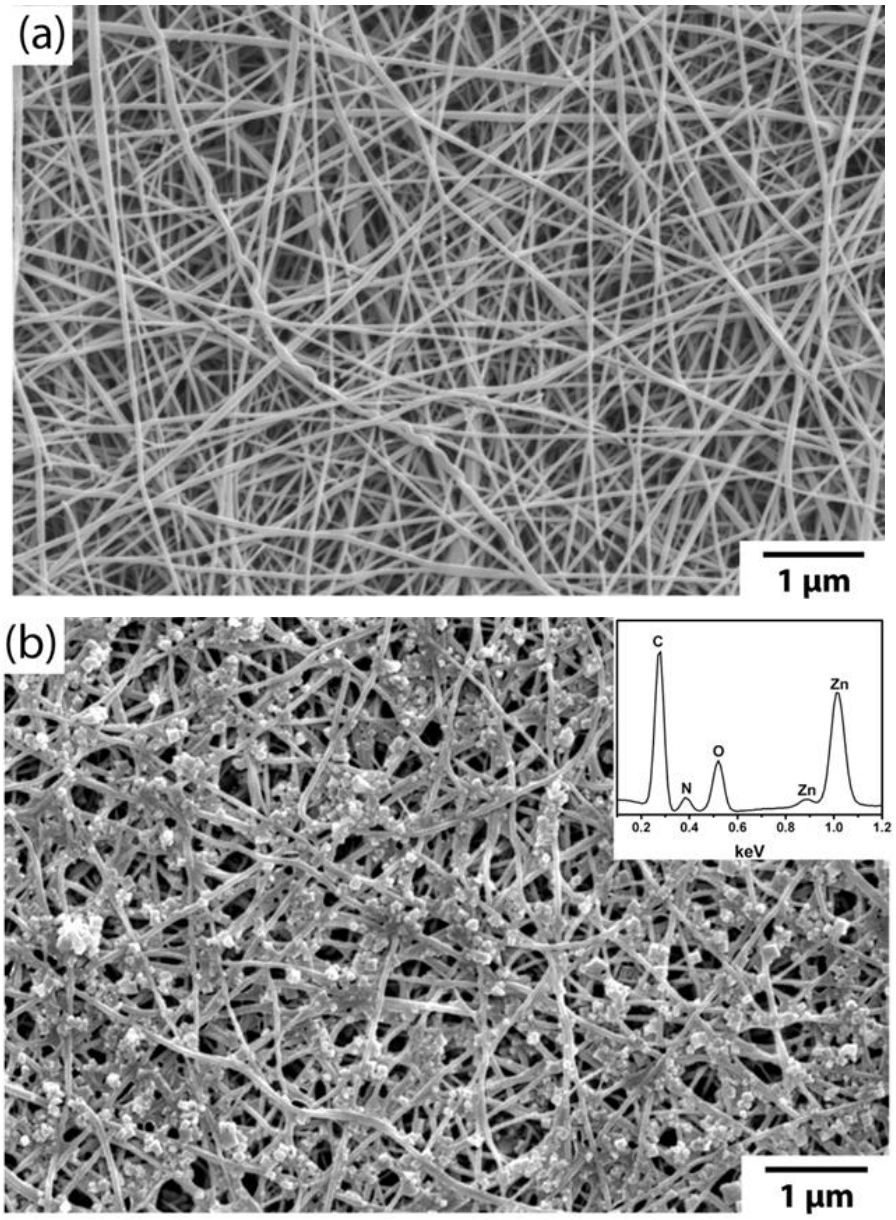

FIGURE 3.4.3: SEM images of (a) PA6/PANI and (b) PA6/PANI_ZnO nanofibers. The inset in panel (b) shows the EDS spectra of PA6/PANI_ZnO. . (Figure available in Andre, R. S. et. al.[125])

The adsorption of ZnO on nanofibers can occur through an interaction between the negatively charged COO– groups from the surfactant Liosperse (based on ammonium polyacrylate) present on the ZnO surface and the positively charged sites from PANI present on the nanofibers.[127] H-bonding may take place between the carboxylic groups (–COOH) of the surfactant and imine nitrogens and/or amine nitrogens of PANI and amide groups from PA6.[128] The Energy Dispersive Spectroscopy (EDS) analysis of the modified PA6/PANI nanofibers was carried out in order to prove the presence of ZnO on the nanofibers surface (inset Fig. 3.4.3b).

The amount of ZnO nanoparticles adsorbed onto the nanofiber surface was determined by thermal gravimetric analysis (TGA). Figure 3.4.4 shows TGA curves of ZnO nanoparticles (solid line), PA6/PANI (dashed line) and PA6/PANI_ZnO (dotted line) nanofibers. Pure ZnO nanoparticles start to degrade only at 860 ºC due its high temperature stability. Both PA6/PANI and PA6/PANI_ZnO exhibit a substantial weight loss, starting at 380 °C and extending up to 470 ºC, resulting in the complete polymer decomposition. Based on the TGA curve for PA6/PANI_ZnO nanofibers is possible to estimate that the mass loading of nanoparticles on the nanofibers surface is around 4 wt.%.

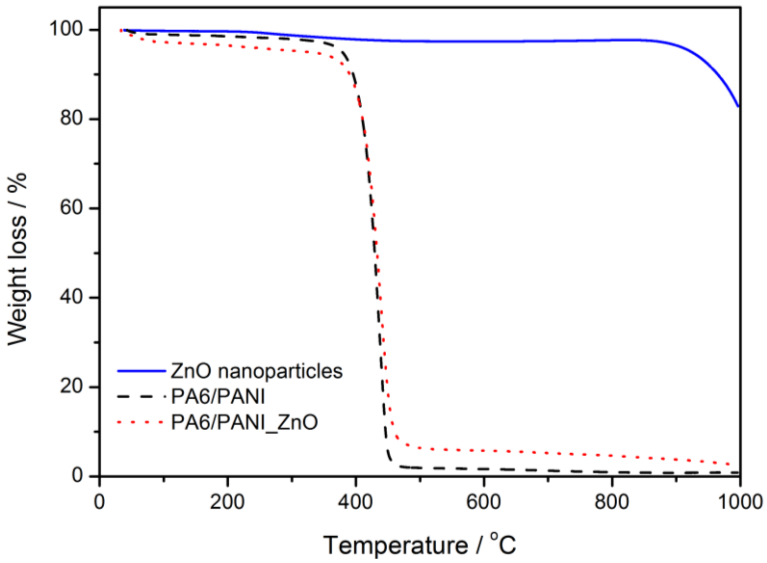

FIGURE 3.4.4: TGA curves of ZnO nanoparticles, PA6/PANI nanofibers and PA6/PANI_ZnO nanofibers. (Figure available in Andre, R. S. et. al.[125])

3.4.3. Electrochemical measurements

ZnO is a metal oxide semiconductor with appealing electrical and optical properties, finding applications in and photovoltaic devices, gas sensing and electrochemical biosensor.[114,129,130] As demonstrated by microscopy analyses, ZnO nanoparticles were successfully adsorbed onto PA6/PANI electrospun nanofibers surface, which suggests a novel and potential platform for sensing application. In order to verify the ZnO influence on the conducting properties of PA6/PANI nanofibers, electrochemical measurements were carried out.

Fig. 3.4.5(a) shows the Nyquist plots for FTO electrode modified with PA6/PANI_ZnO obtained with different ZnO adsorption times. Fig. 3.4.5(b) shows Nyquist plots while (c) displays cyclic voltammograms for bare FTO, and FTO electrodes modified with PA6/PANI and PA6/PANI_ZnO measured in the presence of 5 mmol L^{-1} $[Fe(CN)_6]^{3-/4-}$ in a 0.1 mol L^{-1} KCl solution at a potential of 0.3 V. The Nyquist plots obtained for PA6/ PANI_ZnO modified electrode obtained using different ZnO adsorption times (12, 24 and 48 hours) were interpreted using a Randle's equivalent circuit, shown in inset (i) of Fig. 3.4.5b. The Nyquist plot of EIS includes a linear region at low frequency related to the diffusion-limited process, while the semicircular region at high frequencies is related to the electron-transfer- limited process, where the diameter corresponds to the charge (electron) transfer resistance (R_{ct}).[115] The highest R_{ct} value (41 Ω) was found to ZnO-modified PA6/PANI nanofibers electrode immersed for 12 hours in ZnO solution, while a similar R_{ct} value of nearly 15 Ω was found for electrodes immersed for 24 and 48 hours, respectively. The results suggest that the adsorption of ZnO nanoparticles on the PA6/PANI nanofibers tends to reach the saturation in 24 hours, and therefore this was the time chosen for the electrode immersion.

Fig. 3.4.5b presents Nyquist diagrams for FTO, PA6/PANI and PA6/PANI_ZnO electrodes, whose data were again interpreted using the Randle's equivalent circuit (see inset (i)-Fig. 3.4.5b). The Nyquist diagrams yielded a R_{ct} value of 15 Ω for the PA6/PANI_ZnO electrode, while values of 36 Ω and 39 Ω were found for the bare FTO and PA6/PANI electrodes, respectively. The lowest R_{ct} value for the modified PA6/PANI electrode with ZnO nanoparticles was obtained as a consequence of a faster electron transfer process. Such improvement in charge transfer process occurs thanks to the conducting properties of ZnO nanoparticles.

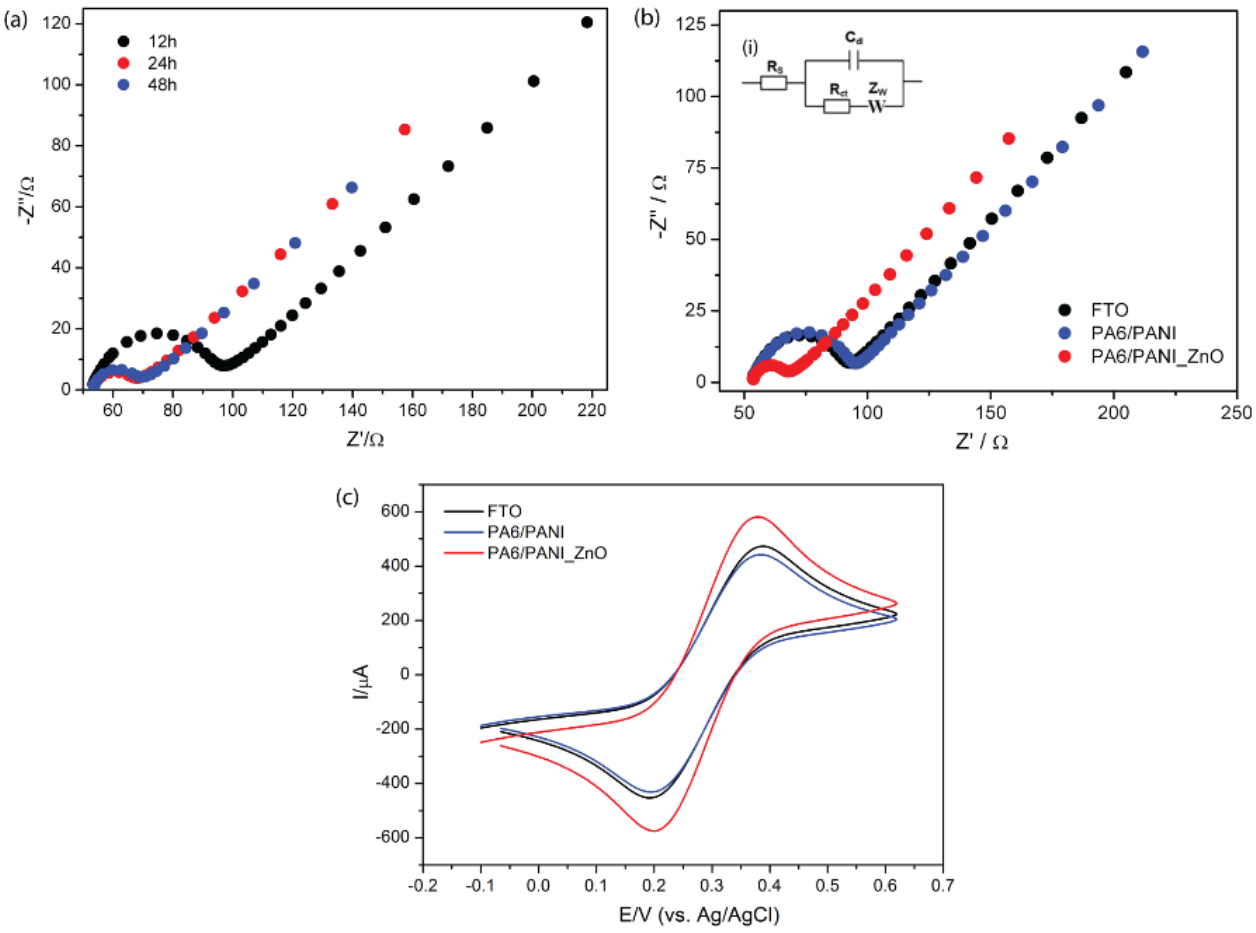

FIGURE 3.4.5: (a) EIS of PA6/PANI_ZnO electrode for different ZnO adsorption times (b) EIS of bare FTO, PA6/PANI and PA6/PANI_ZnO electrodes in 5 mmol L^{-1} $[Fe(CN)_6]^{3/-4}$ solution with 0.1 mol L^{-1} KCl. The inset in panel b (i) shows the Randle's equivalent circuit model. (Figure available in Andre, R. S. et. al.[125])

The voltammograms, displayed in Fig. 3.4.5c, show a quasi-reversible one-electron redox behavior, where I_{pa}/I_{pc} ~1, for all electrodes, with increase in anodic peak current from 479 μA to 585 μA and cathodic peak current from 432 μA to 578 μA, comparing the values for bare FTO and PA6/PANI_ZnO electrode, respectively. Furthermore, the reduction in peak separation (ΔE_p) from 190 mV for bare FTO electrode to 180 mV for PA6/PANI_ZnO modified electrode confirms the faster electron transfer kinetic that is promoted by ZnO nanoparticles. On the other hand, I_{pa}, I_{pc} and ΔE_p values for the PA6/PANI electrode voltammograms was found to be 447 μA, 432 μA and 190 mV, respectively. Furthermore, the electroactive area of the electrodes, i.e. the real area transferring charge to the redox probes, was estimated according to the Randles–Sevcik equation[131] using the cathodic peak current obtained from the

voltammograms. The electroactive areas were calculated to be 0.41, 0.37 and 0.49 cm^2 for FTO, PA6/PANI and PA6/PANI_ZnO electrodes, respectively. The voltammograms show that the PA6/PANI_ZnO modified electrode displayed an increase in the electroactive area, which helps to enhance the electrochemical performance of the electrode. Therefore, both EIS and voltammograms results suggest that modifying electrodes with ZnO nanoparticles/ polymer nanofibers is a suitable strategy for improving charge-transfer process aiming at chemical sensing applications.

3.4.4. *Electrochemical Detection of Hydrazine (N_2H_4)*

In order to prove the potential application of the novel sensing platform, chronoamperometric measurements were employed for hydrazine (Hy) detection. Fig. 3.4.6 shows amperometric response experiments using PA6/PANI_ZnO electrode with successive changes of Hy concentration. The calibration curve was constructed with concentrations ranging from 0.5 to 20 000 μmol L^{-1}, and show a linear range following the equation: I (μA) = 0.027 [Hy] (μmol L^{-1}) - 0.870 (R^2 = 0.994), corresponding to a concentration range from 0.5 to 5000 μmol L^{-1} (inset). The limit of detection (LOD) was estimated to be 0.35 μmol L^{-1}, based on a signal to noise ratio of 3 (S/N = 3). The reproducibility of the PA6/PANI_ZnO electrode was tested by performing repeated experiments with solutions containing 50 μmol L^{-1} of Hy. Good reproducibility was reached for five successive measurements and the relative standard deviation (RSD) was calculated to be 3.5% for a given electrode, while it was found to be 5.5% when three identical electrodes were employed.

The selectivity of PA6/PANI_ZnO electrode for Hy detection was verified by chronoamperometric technique using interfering compounds. The measurements were carried out using 20-fold excess of glucose and 25-fold excess of $CaCl_2$, $Zn(NO_3)_2$ and $Cu(NO_3)_2$ in 100 μmol L^{-1} of Hy solution in 0.01 mol L^{-1} PBS (pH 7.5), which are considered potential interfering compounds for hydrazine detection.[132] The sensing platform proved to be selective for Hy detection, as displayed in Fig. 3.4.7 with no significant interference in current response from the compounds.

Furthermore, the PA6/PANI_ZnO electrode presented a Hy limit of detection (LOD) and linear range of detection compatible to other sensing platforms (based on

electrode modification) recently reported in the literature (Table 3.1). Our results show that the as-prepared platform is suitable for Hy detection even in the presence of distinct interferents, displaying good specificity and low limit of detection, which prompts it as a promising platform for sensor and biosensor design.

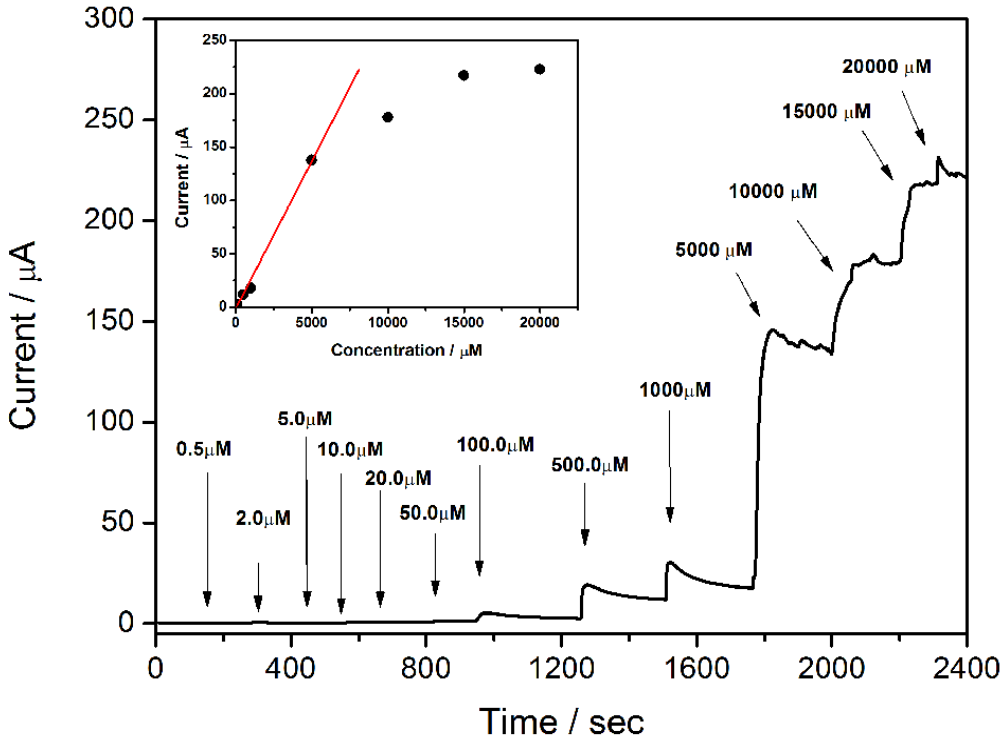

FIGURE 3.4.6: Amperometric current response of PA6/PANI_ZnO electrode in 0.01 molL-1 PBS (pH 7.5) for concentration range 0.5 to 20000 μmolL-1 of Hy. The inset presents the linear relationship between current response and Hy concentrations. (Figure available in Andre, R. S. et. al.[125])

TABLE 3.1: Comparison of Linear range and Detection limit between hydrazine sensors based in similar ZnO structures.

Electrode Modification	Linear Range (μmol L -1)	LOD (μmol L^{-1})	Reference
ZnO Nanoparticles	0.5 - 5000	0.35	This work
ZnO NanoparticlesII	-----	0.147	40
ZnOMicro/nanoarchiteture	0.8 - 200	0.25	41
ZnO NanoFilm	0.5 - 14200	0.5	42
ZnO-RGO	1 - 33500	0.8	39

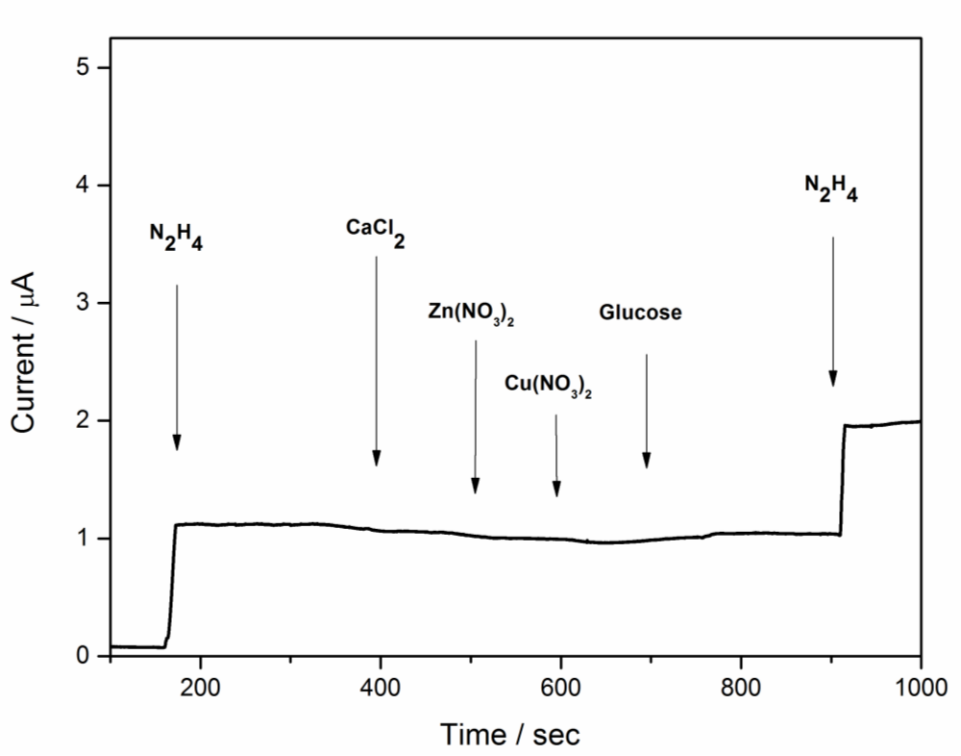

FIGURE 3.4.7: Selectivity amperometric current response of the PA6/PANI_ZnO sensor for Hy (N_2H_4) mixed with interferents in 0.01 mol L^{-1} PBS (pH 7,5). (Figure available in Andre, R. S. et. al.[125])

3.5. Conclusions

A novel electrochemical platform was successfully fabricated by modifying FTO electrodes with PA6/PANI electrospun nanofibers and further decorating them with ZnO nanoparticles. Our results indicated that the ZnO nanoparticles remained strongly attached to the PA6/PANI nanofibers surface *via* H-bonding and electrostatic interaction. Electrochemical measurements revealed improvement in electron transfer kinetic for the ZnO-modified electrode, yielding the lowest R_{ct} value (15 Ω) for the PA6/PANI_ZnO electrode when compared to bare FTO (36 Ω) and PA6/PANI electrodes (39 Ω), which is beneficial for electrochemical application. Additional experiments revealed that the novel platform is suitable for monitoring hydrazine in the presence of interfering compounds with a detection limit of 0.35 μmol L^{-1}. Ultimately, our results indicate that the ZnO decoration of PA6/PANI nanofibers provides a promising platform for designing electrochemical sensors and biosensors.

4. Organic/inorganic Layer-by-Layer platform deposition*

* The content of this chapter is an adaptation of the article entitled: “**Hybrid layer-by-layer (LbL) films of polyaniline, graphene oxide and zinc oxide to detect ammonia”** by Rafaela S. Andrea, Flávio M. Shimizu, Celina M. Miyazakid, Antonio Riul Jr, Danilo Manzani, Sidney J.L. Ribeiro, Osvaldo N. Oliveira Jr, Luiz H.C. Mattosoa and Daniel S. Correa, published in Sensors and Actuators B: Chemical.

Reference: *Sensors and Actuators B*. **2017**, 238, 795–801.[172]

4.1. Abstract

Reliable gas sensors operating at room temperature are in demand for monitoring the environment for hazardous pollutants, such as ammonia (NH_3) gas that may become toxic to humans and animals above a threshold concentration. In this paper, we report on the combination of three materials, namely polyaniline (PANI), graphene oxide (GO) and zinc oxide (ZnO), to produce hybrid layer-by-layer (LbL) films used for sensing NH_3 with impedance spectroscopy measurements. The deposition of tetralayered PANI/GO/PANI/ZnO LbL films was confirmed with UV-vis. absorption and Raman spectroscopies, while atomic force microscopy (AFM) served to investigate film morphology. Exposure of these LbL films to NH_3 caused film roughness to vary, in an effect that depended on the number of tetralayers. Because of synergy in the materials properties, the films with 3 tetralayers were found to be the most adequate for detecting NH_3 in the range from 25 ppm to 500 ppm with a response time of 30s. These figures of merit are adequate for monitoring working environments regarding gas exposure, and highlight the usefulness of the control of film architecture provided by the LbL technique.

4.2. Introduction

Sensitive, reliable gas sensors have great importance in medical applications, air quality supervision and environmental, health and safety monitoring[60,95,133–138]. Ammonia is a colourless gas used in many industries, which may become toxic and affect the health of humans and animals, such as in poultry farms[93,139]. For instance, 100 to 200 ppm of ammonia induce drowsiness, salivation and loss of appetite in humans[140,141]. According to the regulatory agency in Brazil, the ammonia exposure level at working places should not exceed 20 ppm within 48 hours/week[142], while in England the ammonia exposure should not exceed 25 ppm in 8 hours[143]. The human olfactory limit of detection for ammonia is 55 ppm, but loss of sensitivity occurs after long and repeated exposure.[144–146] Therefore, designing robust ammonia sensors with low limits of detection is highly keen to increase safety and health in such environments[147]. The working principle of gas sensors can be based on changes of electrical and optical

properties, with those exploiting electrical signal variations the most used since stable, reproducible sensors can be fabricated[148]. In particular, a myriad of materials can be exploited to achieve such task, including metal oxide semiconductors, conducting polymers, composite materials, carbon nanotubes and their derivatives [136,147,149–153].

In this paper, we report on sensing units made with nanostructured layer-by-layer (LbL) films[63,104,108,154–156] containing the semiconducting polyaniline (PANI), graphene oxide (GO) and zinc oxide (ZnO), all of them already used in sensing applications. The main motivation is rationally combine different materials in a single device originated from a possible synergy of the materials properties. PANI has unique electrical behavior, easy fabrication process and intrinsic redox reaction.[38,157–162] ZnO has remarkable semiconducting properties,[163–166] and GO has a porous structure, high surface area and good gas barrier properties[167–169]. Different LbL film architectures were tested for NH3 sensing using impedance spectroscopy, which were also characterized using UV-vis absorption spectroscopy, scanning electron microscopy, atomic force microscopy and Raman spectroscopy.

4.3. Experimental

4.3.1. Materials

Polyaniline (PANI, Mw = 20000 g.mol^{-1}) was purchased from Sigma-Aldrich. ZnO nanoparticles were synthesized using the coprecipitation method followed by hydrothermal treatment at 150°C for 1 h as described in ref.[125] Graphene oxide (GO) was prepared by typical Hummers' method[170] with a previous preoxidation step[171]. The dispersing agent Liosperse 511 was purchased from Miracema-Nuodex (Campinas, Brazil). Gold interdigitated microelectrodes (IDEs) comprising 50 pairs of digits having 10 µm width and 10 µm apart from each other were fabricated by photolithography at the Brazilian Nanotechnology National Laboratory (LNNano).

4.3.2. Preparation of PANI/GO/PANI/ZnO LbL films

PANI solution (1mg/mL) was prepared by dispersing the emeraldine base in 1 mL of dimethylacetamide (DMAc) under stirring for 12 h. The solution was then filtrated using a filter paper (80g/m^2 and pores with 8µm) purchased from J Prolab. Next, PANI solution was mixed with HCl excess (1:9 v:v) at pH = 3.0. GO was dispersed in the same HCl solution in a concentration of 0.1 $mg.mL^{-1}$ (pH = 3.0). The dispersion of ZnO nanoparticles (1 $mg.mL^{-1}$) was prepared using distilled water and the dispersing agent (0.5% in relation to total volume) (pH = 8.0). Layer-by Layer (LbL) films of PANI/GO/PANI/ZnO were deposited onto quartz plates and IDEs by the sequential alternating immersion into PANI (cationic solution), GO (anionic solution), PANI and ZnO (anionic solution) until the formation of 2, 3 and 4 tetralayers (PGPZ2T, PGPZ3T and PGPZ4T) was achieved.

4.3.3. Multilayer films characterization

The adsorption of LbL multilayers deposited on quartz slides was monitored by UV-vis absorption spectroscopy using a Perkin-Elmer Lambda 25 spectrometer. The morphology of the LbL films was evaluated using a scanning electron microscope (SEM, JEOL 6510) operating at 10 kV. The topography, roughness (root mean square value) and homogeneity of the LbL films were assessed by Atomic Force Microscopy (AFM) using a Dimension V (Veeco) microscope. The Raman spectra of the LbL films were taken at room temperature with a Horiba Jobin-Yvon micro Raman spectrometer model LabRAM-HR equipped with a 632.8 nm laser delivering 30 mW power.

4.3.4. Electrical Measurements

Electrical characterization of the sensing units made with the LbL films deposited on IDEs was performed using an impedance gain phase analyzer (Solartron, model 1260). Data were collected in the frequency range from 1 Hz up to 1 MHz, using an *ac* applied voltage of 25 mV. The sensors were tested for NH_3 detection, in concentrations ranging from 25 ppm up to 500 ppm, in a closed chamber at room temperature (24 ± 2°C) with relative humidity of 65 ± 2% with a dynamic gas flow

system in the homemade setup displayed in Fig. 4.3.1. High purity N_2 was used as carrying gas for NH_3 flux.

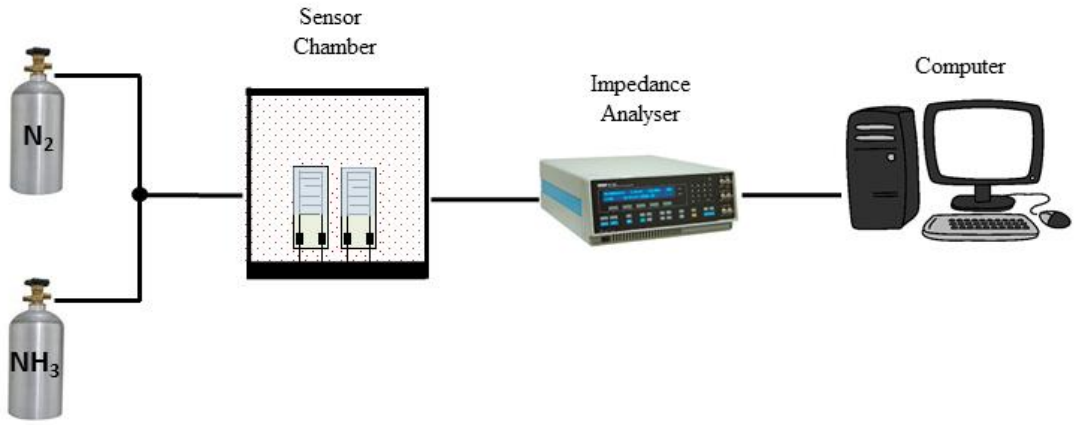

FIGURE 4.3.1: Schematic diagram of the experimental setup for NH_3 detection. (Figure available in Andre, R. S. et. al.[172])

4.4. Results and discussion

Fig. 4.4.1 shows the UV-vis spectra of tetralayered LbL films, with absorption bands at 320 and 840nm, assigned respectively to the π-π* electronic transition of the benzene ring of amine groups and π-π* transition of graphene (at approximately 290 nm)[173], and polaronic band of doped PANI in its conductive emeraldine form[161]. The linear increase in the 840 nm peak intensity with the number of tetralayers reveals that the same amount of material was deposited at each deposition step.

The presence of GO and PANI was inferred in the Raman spectrum in Figure 4.4.2. The bands assigned to GO appear at 1333 cm^{-1} and 1604 cm^{-1}, due to the breathing mode of k-point photons of A_{1g} symmetry and E_{2g} phonon of sp^2 carbon atoms, respectively[173]. The PANI Raman bands appear at 1470 cm^{-1} assigned to C=N stretching vibrations, while the band at 1222 cm^{-1} correspond to C-N stretching in polaronic units and at 1160 cm^{-1} assigned to C-H in plane bending vibrations of benzenoid ring[153]. The ZnO nanoparticles show only one weak Raman band at 416 cm^{-1} assigned to phonons of ZnO compounds with hexagonal structures[168,174].

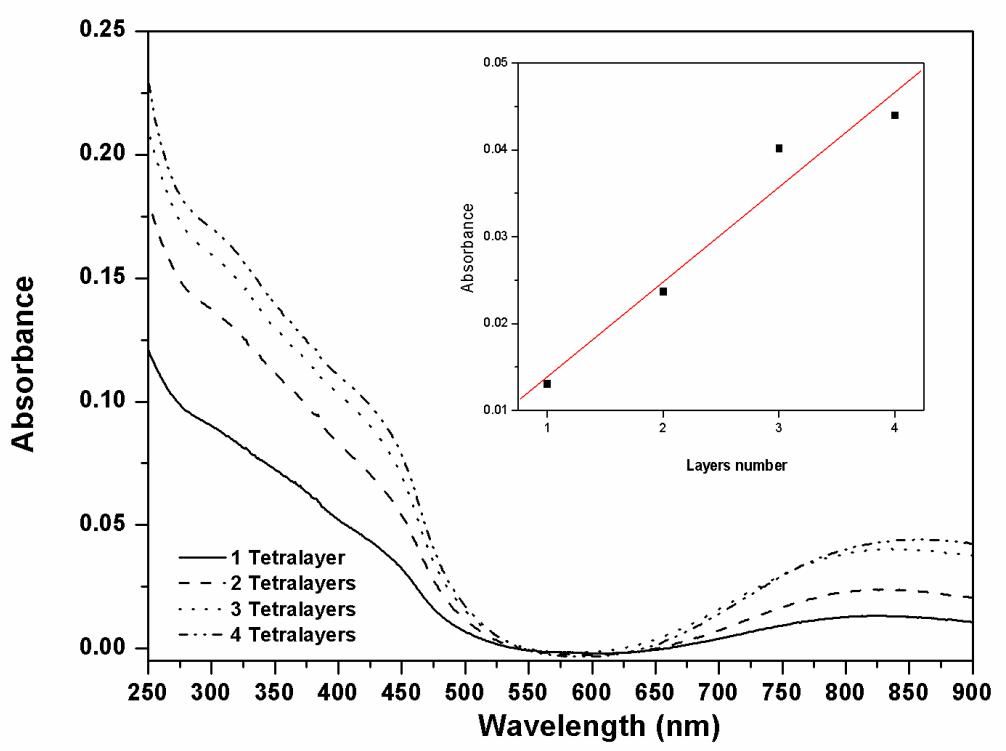

FIGURE 4.4.1: Absorption spectra of LbL films (PGPZ2T, PGPZ3T and PGPZ4T). Inset displays the intensity at 840 nm versus the number of deposited tetralayers. (Figure available in Andre, R. S. et. al.[172])

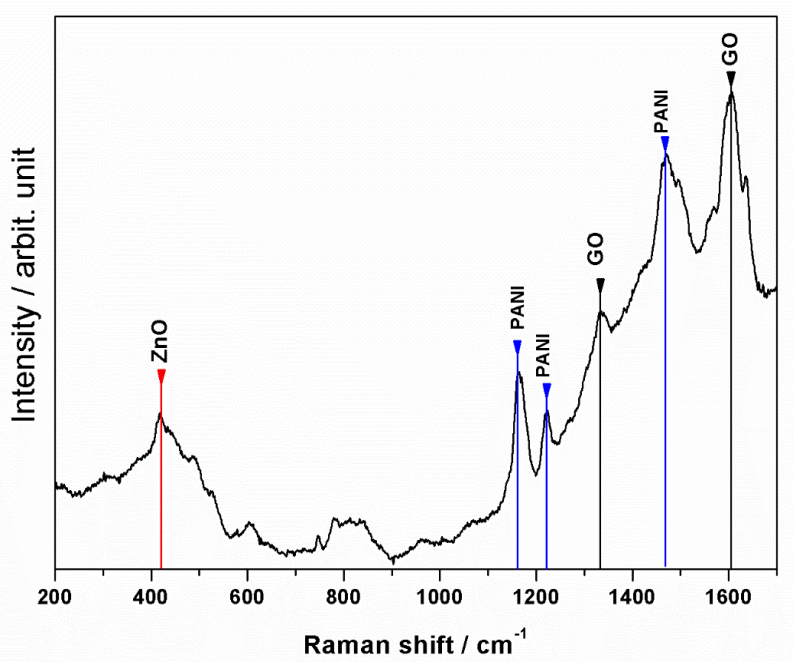

FIGURE 4.4.2: Raman spectrum of PGPZ4T film. (Figure available in Andre, R. S. et. al.[172])

The frequency dependence of the impedance real part (Z') is shown in Figure 4.4a for the three PGPZ LbL films with 2 to 4 tetralayers. The impedance spectra were fitted with an equivalent electrical circuit shown in Figure 4.4c, comprising the resistor R_1 representing the ohmic resistance from the interdigitated electrode (IDE), R_2 for the film resistance and C_1 for the capacitance of charge transfer across the multilayer film, in addition to a phase constant element that was included to improve fitting. The data in the form of Nyquist plots in Figure 4.4.3a for the three films in an inert atmosphere with 65% of humidity were fitted with the parameters in Table 4.1. Both resistances decreased with the number of tetralayers, possibly due to the increase in PANI amount since GO is insulating.

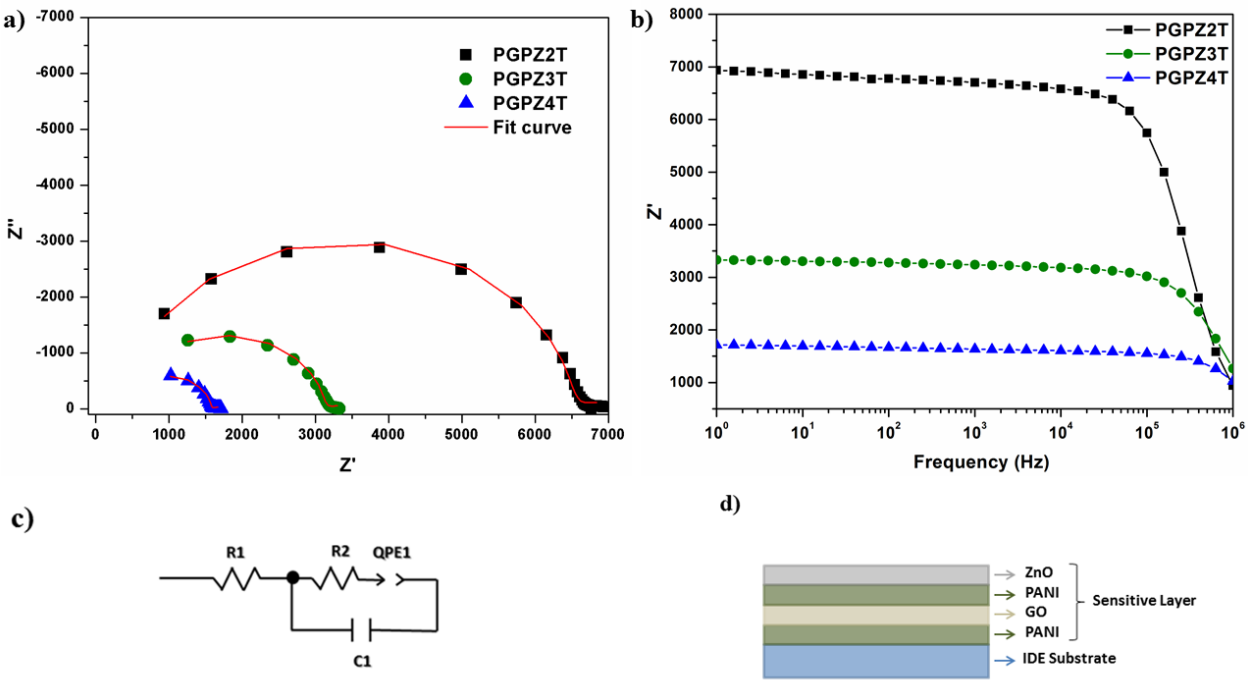

FIGURE 4.4.3: a) real part of impedance (Z') and b) Nyquist diagram for PGPZ2T, PGPZ3T and PGPZ4T films, c) equivalent circuit model and d) schematic representation of the PANI/GO/PANI/ZnO film deposited onto the IDE. (Figure available in Andre, R. S. et. al.[172])

TABLE 4.1: Parameters of the equivalent circuit used to fit the impedance data with ZView® software (Scribner Associates Inc.).

Film	$R_1(\Omega)$	$R_2(\Omega)$	C_1 (F)	QPE_1n
PGPZ2T	437.6	5524	$8.78x10^{-13}$	0.0832
PGPZ3T	460.5	2419	$9.14x10^{-11}$	0.0850
PGPZ4T	387.2	1133	$1.23x10^{-12}$	0.1410

The AFM images in Fig. 4.4.4 evidence two aspects: i) before NH_3 exposure, the film roughness increases with the number of tetralayers deposited from 35 nm (PGPZ2T) up to 52 nm (PGPZ4T); ii) after exposure to the NH_3, the film morphology was clearly affected. Specifically, the thinnest PGPZ2T film was probably deeply penetrated by ammonia, causing both dedoping of PANI and increase in surface roughness. On the other hand, the thicker films with larger amount of PANI had their roughness decreased after ammonia exposure, particularly for the thickest PGPZ4T, whose roughness decreased by ~40%. Significantly, Figure 4.4.5 indicates that the PGPZ3T was only weakly affected by ammonia. It seems therefore that opposite effects to alter film thickness occur for PGPZ3T, which is associated with synergy in the different materials properties. As it will be shown later, such synergy is responsible for the higher sensitivity of PGPZ3T.

The sensor units made of 2, 3 and 4 tetralayers of PANI/GO/PANI/ZnO were tested for detecting ammonia (NH_3) in a relative humidity (RH) set as 65%. The humidity value employed is quite satisfactory, once previous investigations reported in literature [90,175] indicated that the ideal relative humidity in broiler poultry houses should be in the range of 50 and 70%, since lower values can result in a dusty house while higher values could result in wet litter and higher ammonia concentrations.

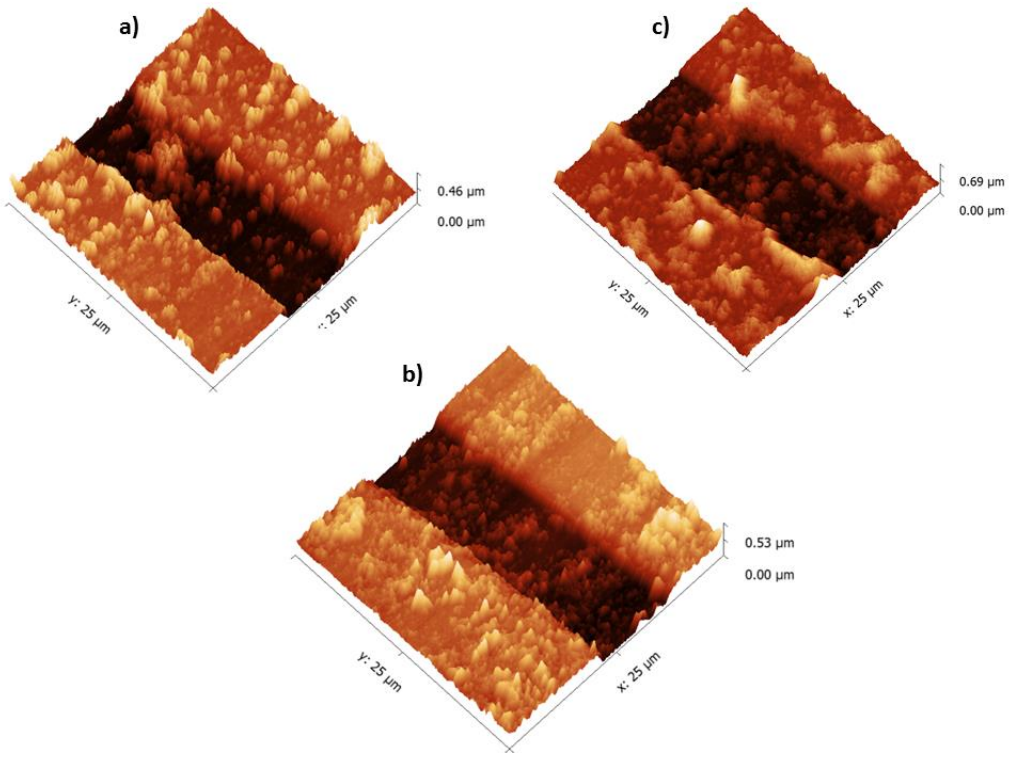

FIGURE 4.4.4: AFM 3D images of a) PGPZ2T, b) PGPZ3T and c) PGPZ4T films. (Figure available in Andre, R. S. et. al.[172])

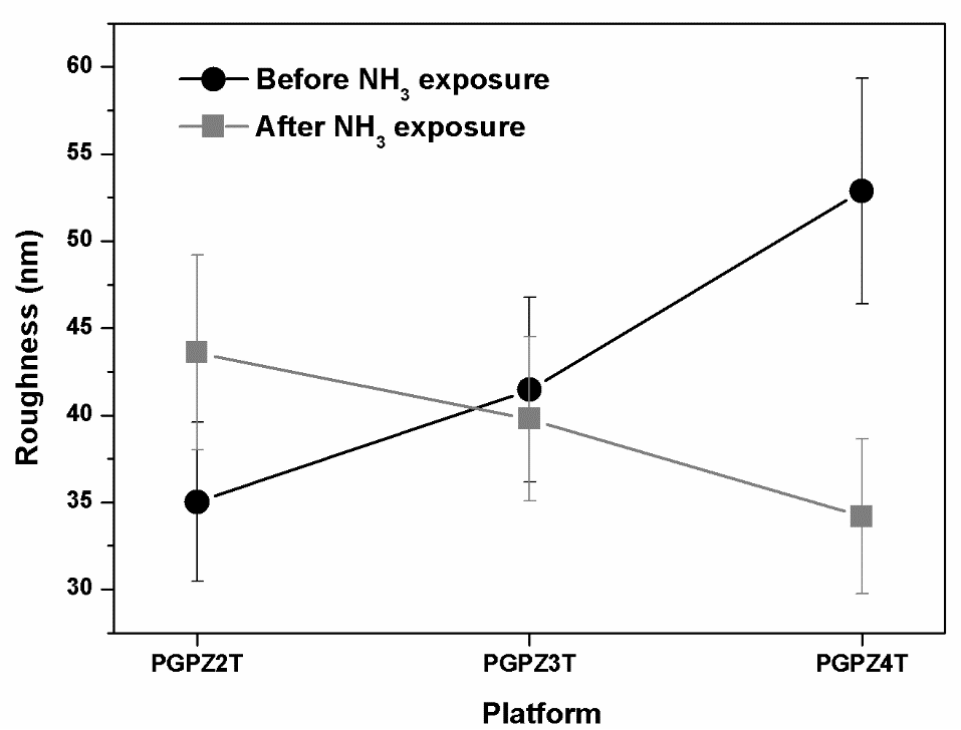

FIGURE 4.4.5: Film roughness (Rrms) calculated using Gwyddion® software for LbL films (PGPZ2T, PGPZ3T and PGPZ4T) before and after exposure to ammonia gas. (Figure available in Andre, R. S. et. al.[172])

The relative response in terms of the impedance ratio (Eq. 4.1) increased with NH_3 concentration up to 500 ppm, as shown in Figure 4.4.6a. PGPZ3T exhibited the most adequate response for all concentrations tested, which may be related to its morphology being less affected by ammonia, according to the AFM results, combined with the moderate resistive response of PANI/GO/PANI/ZnO sensitive layer (Table 4.1). One would expect that the film with larger morphological changes upon NH_3 exposure would yield the highest sensing performance. However, the sensing mechanism appears to depend on a combination of the charge transfer property of each material, since ZnO [147,176–179] is a *n*-type semiconductor and PANI a conductive polymer, both allowing free electrons mobility, hindering the stable double layer formation on the interface, while GO being an insulator provides the stability needed for the charge transfer phenomenon in gas sensor application.

$$\text{Response} = {Z'_{NH_3}}/{Z'_{air}} \qquad \text{Eq. 4.1}$$

It should be noted that for low NH_3 concentrations the sensing units exhibited similar responses, with low error associated to the measurements. That is an important issue to develop sensors able to detect NH_3 below 50 ppm[144–146]. In addition, the larger errors at higher concentrations of NH_3 may be associated with the lower stability of the measuring system, since gas injection can cause small turbulences in the airflow system, as observed in the calibration curve of Fig 4.4.6b. The response time for each NH_3 concentration range was calculated using Eq. 4.2 to fit the calibration curve in Fig. 4.4.6b, leading to values ranging from 10 to 30 s. It is worth mentioning that fitting required the use of two exponential functions in Eq. 4.2, which points to more than one process rulling in the sensing mechanism.

$$R(t) = y_0 + A_1\left(1 - e^{-t/t1}\right) + A_2\left(1 - e^{-t/t2}\right) \qquad \text{Eq. 4.2}$$

R(t) is the resistance as a function of time (t), y_0, A_1 and A_2 are constants, and t_1 and t_2 are the response times.

Response times ranging values from 10 to 30s are suitable for a device operating at room temperature, since NH_3 gas diffusion and sensing usually occur in a time scale shorter than 30 s [149,180].

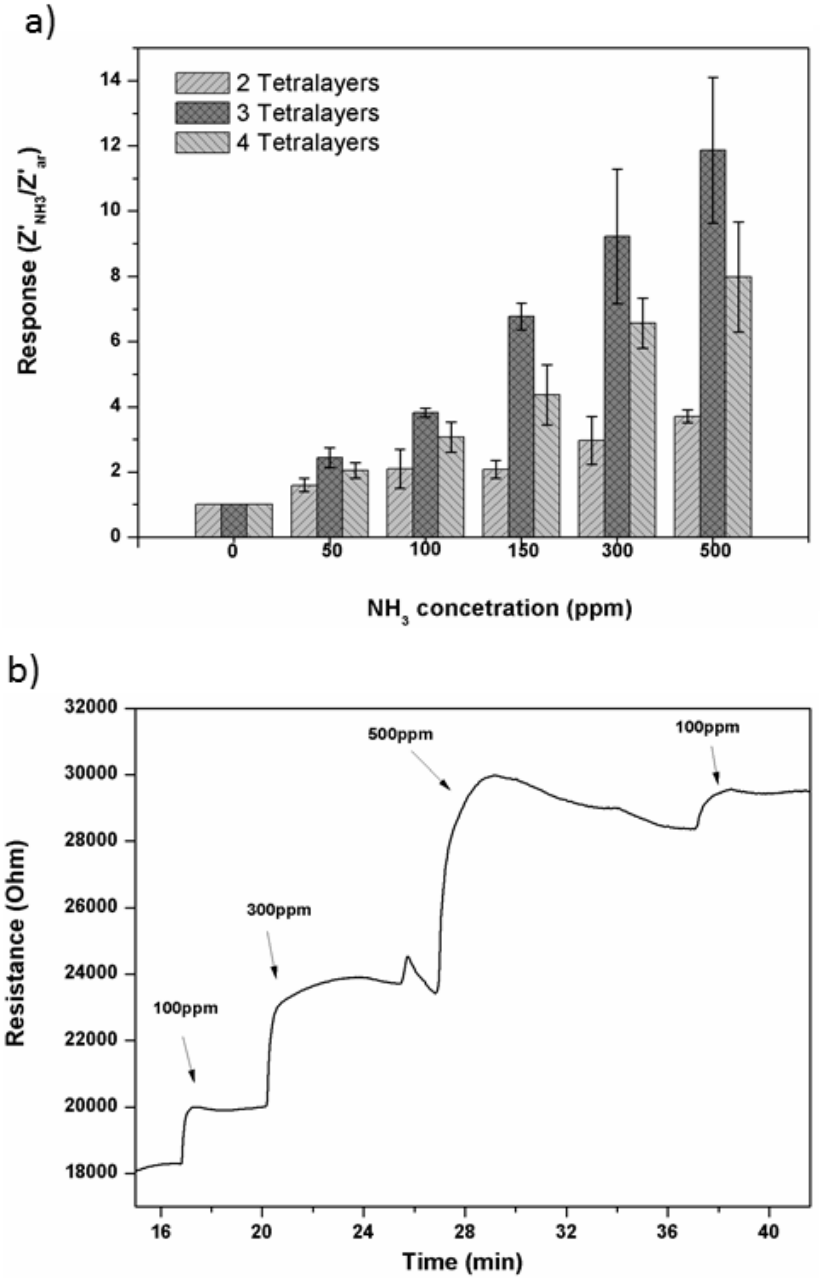

FIGURE 4.4.6: a) Sensor responses at different concentrations of NH3 and b) change in electrical resistance as a function of time upon NH3 exposure of a sensing device with PGPZ3T. (Figure available in Andre, R. S. et. al.[172])

Statistical analysis of the impedance data was carried out using PEx-Sensors software[181–183], implementing multidimensional projection techniques. Here we used IDMAP (Interactive Document Map) with Euclidian distances between the data points and employing real impedance data dimensionally reduced by the Fastmap technique in the frequency range 10^3 - 10^6 Hz. The IDMAP plot in Figure 4.4.7 confirms that all the

three sensors produced were effective to detect ammonia levels from 50 up to 500 ppm, with a combined silhouette coefficient of 0.64 (separate values of 0.60 for PGPZ2T, 0.59 for PGPZ3T and 0.54 for PGPZT4T), calculated according to Paulovich *et. al.*[182] With this quantitative measure of the discriminating power of a sensing device, PGPZ3T and PGPZ2T appear as the most adequate molecular architectures.

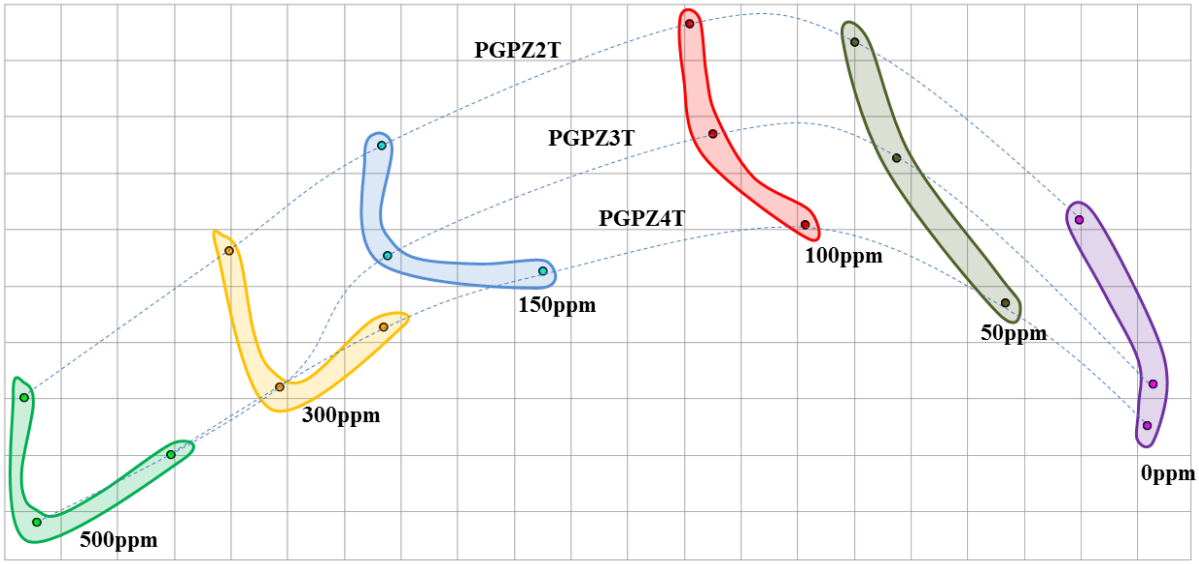

FIGURE 4.4.7: IDMAP plot obtained with the real component of the impedance data as a function of frequency for PGPZ2T, PGPZ3T and PGPZ4T films. The axes have no labels because what matters in this type of plot is the relative distance between data points. The dashed lines linking data points for each of the sensing units were only included to guide the eyes, and demonstrate the distinction between different NH_3 concentrations. (Figure available in Andre, R. S. et. al.[172])

Regarding to distinct ammonia sensors recently published in the literature, Table 4.2 shows that the sensors made with tetralayer LbL films are competitive both in terms of response time and magnitude of the detection. The limit of detection (LOD) was estimated to be 23 ppm, based on a signal to noise ratio of 3 (S/N = 3). Significantly, the figures of merit of the sensors presented here are an adequate choice for target applications, such as monitoring work places for excessive NH_3 exposure. It is worth mentioning that the sensor response remained stable up to 15 days, while a decay of 56% on response signal was observed 30 days later.

TABLE 4.2: Comparison of sensor performance for detecting NH_3, where lists are given of the material used in the sensing device, detection limit (DL), response time (RTime), percentage of response. The values quoted for PANI/GO/PANI/ZnO correspond to PGPZ3T.

Material	Detection Limit	Response Time	Response (%)	Ref
PANI/GO/PANI/ZnO	23 ppm	30s (100ppm)	38.31	This work
PANI/GO	1 ppm	50s (100ppm)	11.33	[149]
TiO_2/PPy/GN	1 ppm	36s (50ppm)	36	[184]
PANI/αFe_2O_3	5 ppm	27s (100ppm)	39	[185]
PPy/SnO_2	257 ppb	259s (5ppm)	30	[186]
PANI/SnO_2	1.8 ppm	34s (100ppm)	29	[187]

Although one would expect that a platform based solely on PANI and ZnO (PANI/ZnO) combination could be adequate for sensing application, once PANI presents high sensibility at room temperature[188] while ceramic materials may provide suitable response time for sensing application[153,189], this was not the case. Subsidiary experiments (not shown) employing solely PANI/ZnO platform (without GO) showed to be sensitive to NH_3 but with an electrical response highly unstable, which is not desirable for gas sensor application. Definitely, the GO addition to the nanostructured platform can improve the sensor response[190]. Furthermore, PANI/GO/PANI/ZnO platform showed not only improved sensitivity to NH_3 but also enhanced stability, reproducibility and fast response. Such behavior can be explained in terms of the electrical properties of the composing material: ZnO is a *n*-type semiconductor, while PANI is a conducting polymer which increases the mobility of free electrons, and impairs the formation of a stable double layer at the electrode interface. The addition of an insulating layer (GO) to the platform tends to decrease the velocity of electrons transport, providing higher stability for the electrical signal of the sensor tested under air

and ammonia atmosphere. Therefore, the results demonstrate the importance of adding GO to the PANI/ZnO platform, exploiting molecular combinations of three distinct materials in the same platform, which allowed the sensor operation at room temperature with fast response and high sensitivity.

4.5. Conclusions

Tetralayered LbL films could be produced with PANI, GO and ZnO, with the presence of all components being confirmed with UV-vis. absorption and Raman spectroscopies. The number of tetralayers for the PANI/GO/PANI/ZnO architecture affected the electrical properties and morphology, according to impedance spectroscopy data and AFM images, respectively. The overall electrical resistance of the film decreased with the number of tetralayers owing to an increased amount of the conducting PANI. In contrast, film roughness increased with the number of tetralayers, as expected for nanostructured films. The roughness dependence, however, was not monotonic when exposure to NH_3 was considered, since roughness decreased for PGPZ2T, increased for PGPZ4T, and remained practically constant for PGPZ3T. This indicates synergy in combining the materials properties, which was indeed confirmed by the higher performance of PGPZ3T for detecting NH_3 in impedance spectroscopy measurements. The metrics of interest of the sensors made with the LbL films for use in monitoring working environments, namely limit of detection, response time and amplitude of response, were all adequate. Therefore, these PANI/GO/PANI/ZnO films can be considered as an alternative platform for room temperature NH_3 sensors in which synergy is achieved upon combining distinct materials.

5. Ceramic nanofibers and polymeric coated paper – Additional Studies*

* The content of this chapter is a compilation of the results obtained during an internship abroad supported by a PDSE-CAPES sponsorship. The project was developed at the University of Connecticut/Department of Chemical and Biomolecular Engineering located in Storrs, CT, United States, under the supervision of Prof. Dr. Yu Lei. A detailed studied of the obtained results is published as:

- Sensitive and Selective NH_3 Monitoring at Room Temperature Using ZnO Ceramic Nanofibers Decorated with Poly(styrene sulfonate).[191]

- A flexible and disposable poly(sodium 4-styrenesulfonate)/polyaniline coated glass microfiber paper for sensitive and selective detection of ammonia at room temperature.[192]

5.1. Introduction

Solid-state sensors emerge as an important candidate for gas and breath sensor, once they are low-cost devices, portable and can be integrated to other devices [193–195] Nanofibers are solid-state nanomaterials with high specific surface area, good flexibility and mechanical resistance, making them suitable candidates for a variety of applications [196–198]. Among nanofibers, metal oxide nanofibers can be conveniently prepared by electrospinning solutions containing a high molecular weight polymer and a metal precursor, followed by heat treatment for crystallization of the metal oxide [199–203]. Several metal oxides such as ZnO, SnO_2, In_2O_3, CuO, TiO_2, CeO_2, with different morphologies have been studied as gas sensors to detect the concentration variation of different gases at room and higher temperatures [204,205].

The goal of this work was to develop and characterize a nanostructured sensor based on ceramic nanofiber, prepared by electrospinning through a solution containing a polymer and a metal precursor, with subsequent calcination step. The performance of the ceramic nanofibers sensor was investigated for ammonia gas, nitric oxide and carbon monoxide. Specifically, ZnO metal oxide nanofibers was employed due to the high sensitivity of this material to ammonia.

Besides the ceramic nanofiber platform, a second platform was obtained with glass fiber based paper (GFP) employed as substrate for *in situ* polyaniline polymerization aiming a low cost, flexible and disposable platform for ammonia detection at room temperature. PSS was combined with PANI in two distinct configurations and compared with pure PANI deposition on GFP substrate.

5.2. Experimental

5.2.1. Materials

Poly(vinyl pyrrolidone) (PVP, Mw= 1,300,000.00 $g.mol^{-1}$), zinc nitrate hexahydrate ($Zn(NO_3)_2 \cdot 6H_2O$), dimethylformamide (DMF) and poly(styrene sulfonic acid) solution 30 wt. % in H_2O (PSS, Mw= 200,000 g/mol)were all purchased from Sigma-Aldrich. Glass microfiber paper (Whatman™ 934-AH™ Glass Microfiber filter) was purchased from GE Healthcare Bio-Sciences Corp. Aniline ($C_6H_5NH_2$, 99.5%) and ammonium persulfate (APS - $(NH_4)_2S_2O_8$, 99.99%) and poly(sodium 4-styrenesulfonate)

(PSS - M_w ~1,000,000) were purchased from Sigma Aldrich. The gas sensing experiments were performed using synthetic dry air, ammonia gas mixture (NH_3, 200 ppm in air), nitrogen dioxide (NO_2, 1000 ppm in N_2), carbon monoxide (CO, 5% in Argon) and high-purity nitrogen (N_2, 99.998%) obtained from Airgas.

5.2.2. Ceramic Nanofibers

The procedure for electrospinning ceramic nanofibers was based on previous works[79,194,206]. $Zn(NO_3)_2.6H_2O$ and PVP (50:50 wt%) were dissolved in 3 mL DMF. The precursor solution was stirred for 6 hours and then transferred to a plastic syringe with a 19-gauge needle for the electrospinning process. Electrospinning parameters were set as 20 kV for applied voltage, a flow rate of 0.3 mL h^{-1} over 15 cm of collecting distance. The collected nanofibers were submitted to a heat treatment in a muffle furnace at 500°C during 3 h for the PVP matrix removal and formation of ZnO in crystalline phase (ZnO_NF).

Three different concentrations of ZnO_NF suspensions were prepared dispersing the ZnO_NF in PSS aqueous solutions (ZnO/PSS). The concentrations were determined by weight percentage for ZnO:PSS as 94:6, 75:25 and 50:50, being the final concentration for each suspension as 5 mg mL^{-1}. A ZnO_NF aqueous suspension (5 mg mL^{-1}) without PSS was also prepared for comparative purpose. The suspensions were sonicated for 30 minutes and then dropped in an interdigitated electrode (IDE) composing the sensor device. The volume of suspension added in each IDE was of 2 μL.

5.2.3. Polymeric coated paper

The flexible devices were fabricated through an *in situ* polymerization process in GFP substrate. Three solutions were prepared based on aniline, APS and PSS with concentration of 0,04 mol L^{-1}, 0,05 mol L^{-1} and 0,1 mol L^{-1}, respectively. Then the solutions were added separately on the GFP substrate in different sequences to compare the sensibility to ammonia gas. The first device (GFP@PANI) was obtained by APS addition as oxidant agent for *in situ* polymerization followed by aniline coating. *In situ* polymerization was observed by the color change from colorless to green. The second (GFP@PANI/PSS) was obtained as the first one with an additional step of PSS

drop coating. Finally, the third device (GFP@PSS/PANI) was obtained by PSS drop coating on GFP substrate followed by APS and aniline drop coating in sequence. Solution volume was fixed in 50 μL for all solutions additions. The devices were left to dry in ambient conditions for 12 hours. Carbon tape was used as contact channels with 4 mm of distance between then.

5.2.4. Physico-chemical Characterization

5.2.4.1. Ceramic nanofiber

Structural crystalline phase composition for ZnO nanofibers was characterized by X-ray diffraction (XRD) using an Oxford diffraction Xcalibur TM PX Ultra with ONYX detector. Morphology and size of the electrospun nanofibers after calcination were observed through scanning electrons microscopy (SEM) analyses carried out in a JEOL 6335F field-emission scanning electron microscope. The nanofibers and nanoparticles diameters were estimated by using an image analysis software (Image J, National Institutes of Health, USA). For further study the chemical composition and surface characteristics of the obtained ceramic nanofibers X-ray photoelectron spectroscopy (XPS) was carried out with a PHI multiprobe using Mg as the exciting source.

5.2.4.2. Polymeric coated paper

In order to confirm the successfully PANI polymerization and PSS adsorption into the substrate surface, Fourier Transform Infrared (FTIR) spectra were recorded with a Nicolet Magna-IR 560 spectrometer. The surface homogeneity and polymer distribution into to the GFP were characterized through scanning electron microscopy (SEM) analyses carried out in a JEOL 6335F field-emission scanning electron microscope.

5.2.5. Sensing tests

All devices obtained were tested for several concentrations of NH_3 gas in a tube chamber connected to a CHI 660D electrochemical analyzer (CH Instruments Inc., USA). The current output was optimized and fixed at 5 V DC bias for continuously measurement of the ZnO_PSS platform and 1 V DC bias for GFP coated platforms.

The performance of the devices as ammonia gas sensor at room temperature (25°C) was evaluated by measuring the current change upon exposure to different concentrations of NH_3 in a dynamic gas flow system and synthetic air was used as carrier gas. The gas flow rate was set as 3 L min^{-1} for the carrying synthetic air and gas mixtures (NH_3/synthetic air) and regulated by a computer-controlled gas mixing system (S-4000, Environics Inc., USA). Prior to the measurement, the carrying gas was purged for 20 minutes in order to obtain a stable baseline.

5.3. Results and discussion

5.3.1. Ceramic Nanofibers

Long range order of the calcinated ceramic fibers was evaluated by powder X-ray diffractometry (XRD) and characterized as pure ZnO by hexagonal wurtzite phase diffraction pattern (JCPDS 36-1451), confirming the successfully elimination of the polymeric matrix and crystallization of the ceramic phase.

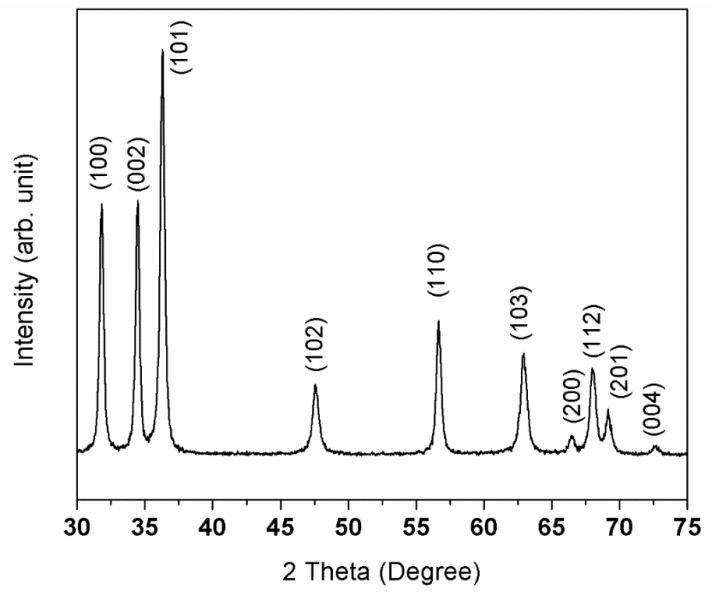

Figure 5.3.1: X-ray diffraction pattern of the as-prepared ZnO nanofibers. (Figure available in Andre, R. S. et. al.[191])

The ceramic nanofibers morphology was investigated by SEM. As it is possible to observe in Fig. 5.3.1 a) the nanofibers are presented as interconnected spherical nanoparticles in an oriented attachment process. Fig 5.3.1 b) obtained with higher magnification shows the nanoparticles organization in nanofibers orientations. It is also possible to observe the coalescence of the nanoparticles forming an interconnected chain, occasioned by the thermal treatment. The nanofiber structure presents a mean diameter of 215 nm (Fig. 5.3.1 b) while the nanoparticles presents a mean diameter of 75 nm.

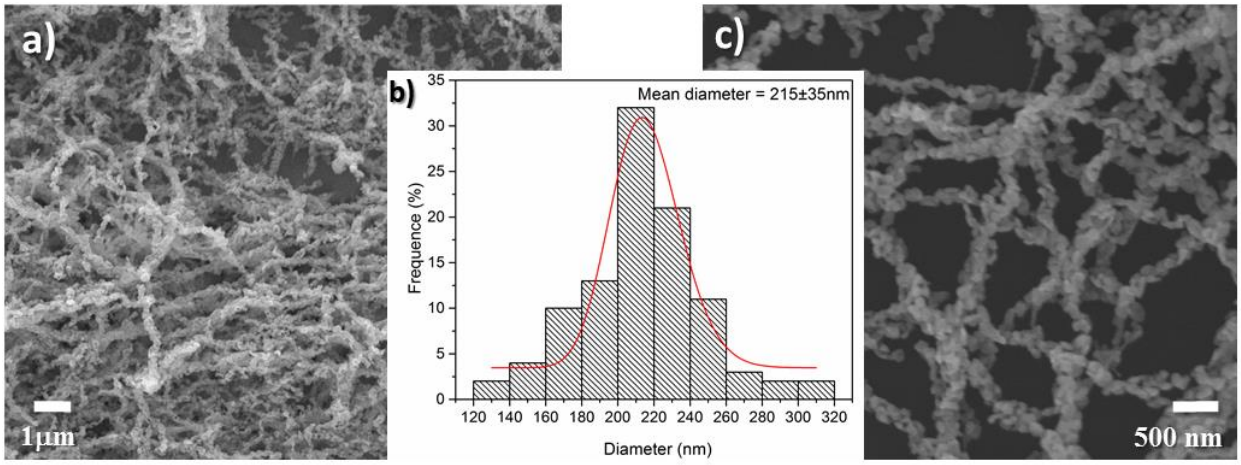

Figure 5.3.2: a) Scanning electron microscopy picture of ZnO nanofibers, b) higher magnification and c) a Histogram of diameter size distribution of ZnONF. (Figure available in Andre, R. S. et. al. [191])

The ZnO_NF composition and chemical bond configuration were studied through X-ray photoelectron spectroscopy (XPS). The XPS data was corrected with respect to the standard peak of C1s at 284.6 eV, regarding to the high chemical purity of the ZnO_NF sample, once it presents only Zn and O in the constitution. Figure 5.3.2 a) presents Zn2p spectra with two peaks at 1042.08 eV and 1019.08 eV of $Zn2p_{1/2}$ and $Zn2p_{3/2}$, respectively, indicating that all Zn ions in the sample are in Zn^{2+} oxidation state and correspond to a 2p binding energy of Zn (II) ions [207,208] . The 23 eV of distance between these two peaks agrees with the splitting energy reported in the literature for ZnO[208]. The O1s spectrum also shows its characteristics binding energy, and tree distinct oxygen species could be well distinguished for the O1s state. The main peak at 528.95 eV correspond to the ions in the ZnO crystal lattice (O_A), while the peak at

530.98 eV can be assigned to oxygen vacancies in the crystal lattices (O_B). The peak at 532.61 eV can be ascribed to oxygen adsorbed in the ZnO surface mainly as hydroxide (-OH), but also as $–CO_3$, H_2O, and O_2 species [209,210].

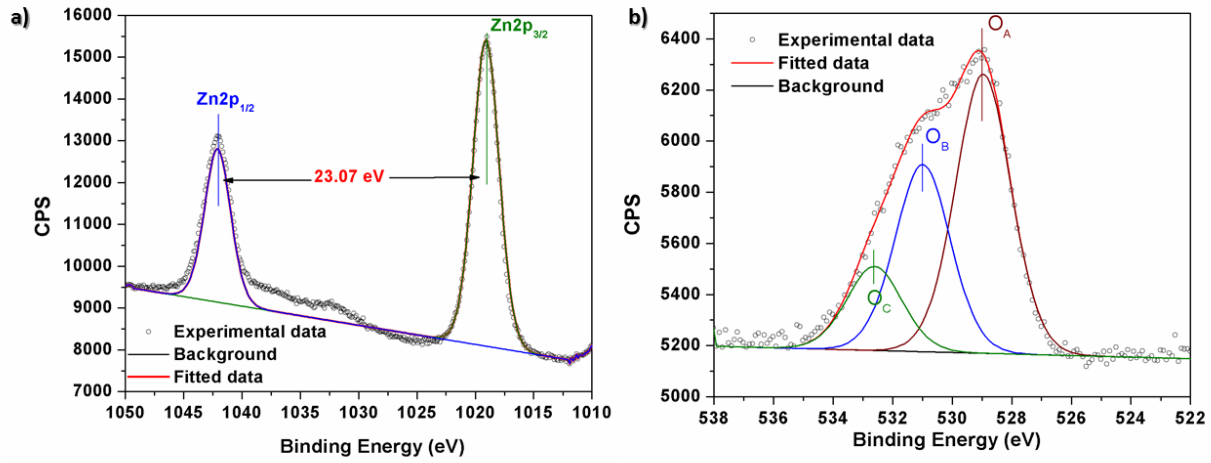

Figure 5.3.3: The high-resolution XPS spectra of a) Zn2p and b) O1s of ZnO_NF. (Figure available in Andre, R. S. et. al. [191])

The as prepared devices (ZnO94/PSS6; ZnO25/PSS75 and ZnO50/PSS50) were tested for ammonia (NH_3) sensitivity at room temperature. A device with pure ZnO nanofibers without PSS (PZnO) was prepared and also tested for NH_3 sensitivity for comparative purposes. The sensitive NH_3 test was carried out for all devices mentioned for 100 ppm of NH_3 at room temperature. The sensor response showed to be proportional to the PSS concentration.

For all the NH_3 sensing cycle experiment, the sensor was exposed to NH_3 for 4 minutes followed by synthetic air for 6 minutes to recover the sensor. The current in the sensor was continuously measured during the gas flow cycles. The electric resistance of the sensor was calculated by applying Ohm's Law ($R = V/I$) and the resistance variation observed could be directly related to the ammonia concentration and normalized as

$$\Delta R\ (\%) = (R_0 - R)/R_0\ x\ 100 \qquad \text{Eq. 5.1}$$

where R_0 is the electrical resistance of the sensor in synthetic air and R_g is the measured resistance in NH_3. Therefore, the resistance normalization corresponds to the NH_3 sensing performance of the sensor.

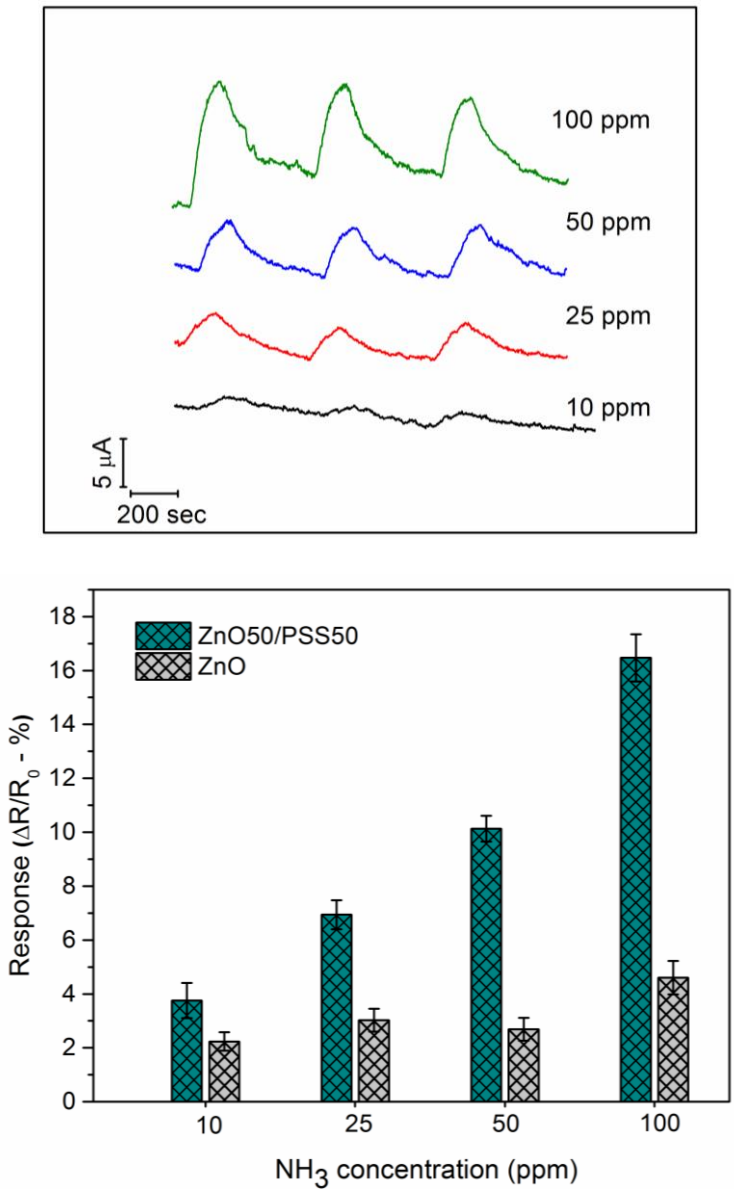

Figure 5.3.4: a) Response-recovery profile of ZnO50/PSS50 device as function of time for NH_3 concentration varying from 10 to 100 ppm and b) Sensing response as function of NH_3 concentration for ZnO50/PSS50 and PZnO devices. (Figure available in Andre, R. S. et. al. [191])

Fig. 5.3.4 a) presents the current-recovery profile of ZnO50/PSS50 to various NH_3 vapor concentrations in air as function of time. Figure 5.3.4 a) shows that NH_3 gas flow causes a current increase typical of a n-type semiconductor sensing mechanism. Fig. 5.3.4 b) shows the sensing response for different concentrations of NH_3 for PZnO and ZnO50/PSS50. As can be observed, the ZnO50/PSS50 presents much better sensing performance than PZnO, even for lower concentrations as 10 ppm. The better performance can be related with the PSS presence. PSS is a well-known polyelectrolyte, where ionic groups present in the polymeric chain enable/increase the charge mobility. Therefore, PSS act improving the NH_3 adsorption capability as well as the sensing performance along with an improvement on the charge mobility between the ZnO ceramic nanofibers and the substrate [211]

The ZnO50/PSS50 sensor response presented a liner range for NH_3 concentrations varying from 10 up to 100 ppm (Fig 5.3.4 b) with R square of 0.9807. The limit of detection (LOD) was determined as 3.22 ppm considering signal to noise ratio as 3 (S/N=3), which is considerably lower than 25 ppm, recommended limit for long period of exposure for human and animal[142,143]. The detection limit also indicates that the platform developed here presents an outstanding performance compared with further works from the literature with a LOD of a NH_3 concentration between 5 and 10 ppm for pure ceramic nanoparticles platform also operating at room temperature [212,213].

The ZnO50/PSS50 and PZnO selectivity were also investigated (see Fig. 5.3.5). The devices were tested for 50 ppm of NO_2 and CO, since the ammonia detection was carried out in synthetic air presence and once NO_2 and CO are potential interfering compounds for ammonia detection in indoor environment in poultry farms [94,138]. It is possible to observe that the use of PSS improved the selectivity against NO_2 when compared to pure ZnO.

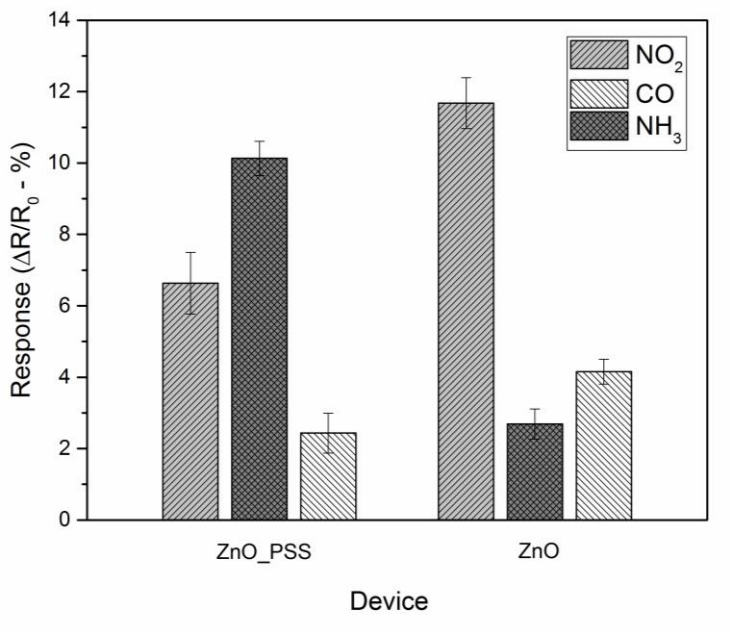

Figure 5.3.5: Selectivity performance for 50 ppm of NO_2, NH_3 and CO for ZnO50/PSS50 and PZnO devices. (Figure available in Andre, R. S. et. al.[191])

5.3.2. Polymeric coated paper

Polyaniline coated glass fiber paper was produced as described in experimental section and combined with PSS layer. Recent studies have reported the development of gas sensors using PSS in the composition and related better reversibility due to its presence[214–216]. Therefore, PSS was combined as a coating layer on and under the PANI layer for different unit devices. The device with PSS coating on PANI layer was obtained to evaluate the PSS influence in the sensibility. A change color was observed from colorless to green for all three devices, indicating the successful aniline polymerization. The formation of PANI on substrate was further confirmed by the FTIR spectra (Figure 5.3.6, traces b-d). The vibrational modes related to PANI were observed for GFP@PANI, GFP@PANI/PSS, and GFP@PSS/PANI. The peak at 1487 cm^{-1} is ascribed to the stretching vibration of C=C benzenoid rings and the peak at 1128 cm^{-1} to the stretching vibration of C=C quinonoid ring while the peak at 1011 cm^{-1} is assigned to in-plane benzene ring bending vibration[217]. The PSS coating layer on the substrate was also confirmed by FTIR spectra (Figure 5.3.6, traces d-e) where PSS vibrational modes were observed for GFP@PANI/PSS and GFP@PSS/PANI at 1184 cm^{-1}

corresponding to asymmetric stretching of SO_3^- group[218]. As a comparison, a sample of GFP coated with pure PSS (Figure 5.3.6, trace e) was also presented.

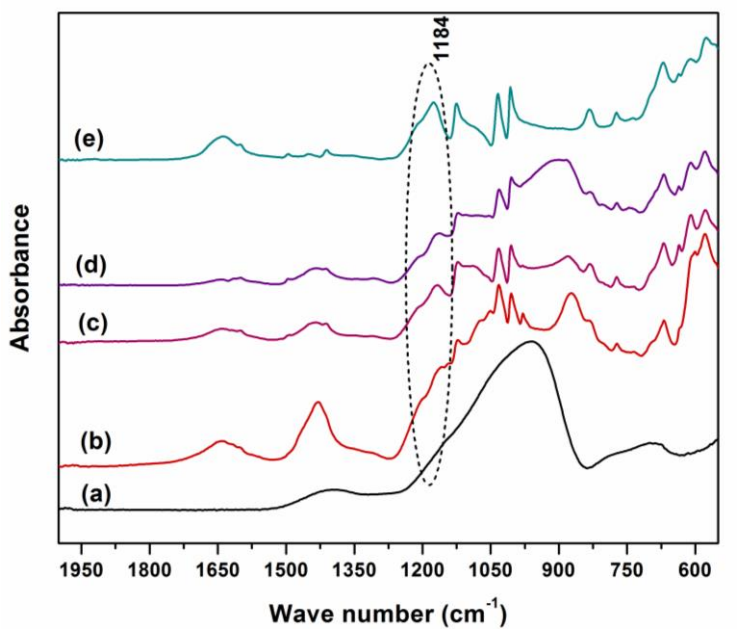

Figure 5.3.6: FTIR spectra of a) glass microfiber paper (GFP), b) GFP@PANI, c) GFP@PANI/PSS, d) GFP@PSS/PANI and e) GFP@PSS, respectively. (Figure available in Andre, R. S. et. al.[192])

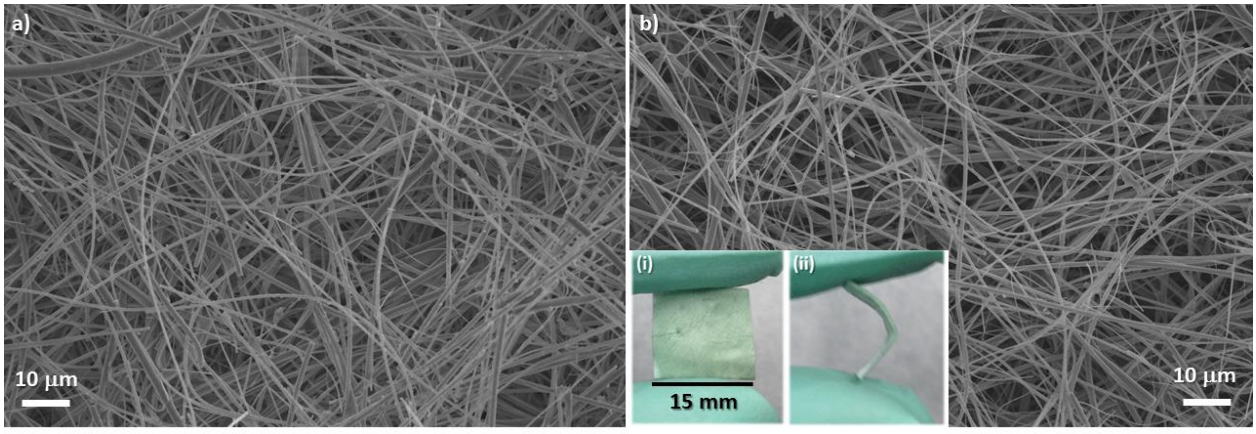

Figure 5.3.7: Scanning electron microscopy images of a) GFP substrate and b) GFP@PSS/PANI device. The inset represents i) real device picture and ii) real device mechanical flexibility. (Figure available in Andre, R. S. et. al.[192])

Figure 5.3.7 present SEM images for a) GFP paper and b) GFP@PSS/PANI, showing the fiber structure and high surface area, which it is very important for gas detection applications, once the gas can flow and diffuse into the fiber matrix. In addition, no continuous film formation was observed on the paper fiber substrate, indicating a homogenous coating on fibers. The inset (i) brings a real device photography representing the green color provide by PANI and inset (ii) demonstrates the device mechanical flexibility.

Once the devices presented satisfactory morphology, the study moved on to their electrical properties. At first, cyclic voltammetry curves were obtained for all devices in atmospheric air (Fig 5.3.8 - inset), confirming the conductivity property and its magnitude. The devices were exposed to 100 ppm of ammonia gas with synthetic air as carrying gas at room temperature. Ammonia flow was turned on and off (cycle on-off) three times.

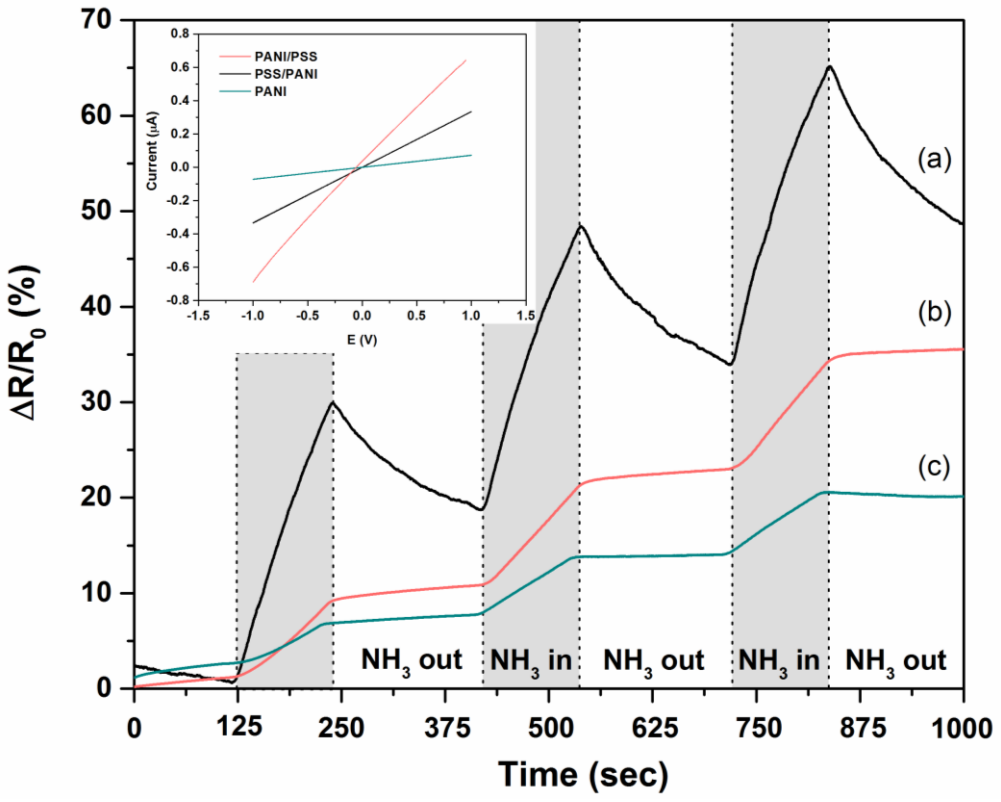

Figure 5.3.8: Dynamic response of a) GF@PSS/PANI, b) GFP@PANI/PSS and c) GFP@PANI. The inset shows the I-V curves of different device performed in ambient air conditions. (Figure available in Andre, R. S. et. al.[192])

In order to optimize the fabrication sequence of PSS and PANI, the as-prepared devices (GFP@PANI, GFP@PANI/PSS, and GFP@PSS/PANI) were tested for ammonia (NH_3) sensitivity at room temperature, upon exposure to 100 ppm of NH_3. As it is possible to observe GFP@PANI device presented very low response to NH_3 with very poor reversibility. Meanwhile the GFP@PANI/PSS showed an increased response at first but possesses poor reversibility. Whereas, the GFP@PSS/PANI device presented obvious and constant signals with reasonable reversibility. Therefore, the flexible and disposable ammonia sensor based on GFP@PSS/PANI is used for subsequent experiments.

Therefore, the GFP@PSS/PANI device was tested for ammonia detection through sensing tests varying ammonia concentration. The tests were carried out at room temperature. Sensing property was recorded as real-time dynamic curves as a function of time. The sensing properties, like current/resistance variation, showed to be dependent on ammonia concentration, presenting a larger variation for higher concentrations. Figure 5.3.9. shows the calibration curve of GFP@PSS/PANI device as a function of NH_3 concentrations ranging from 10 ppm to 100 ppm at room temperature. The response showed a good reproducibility for three “on-off” cycles of the same concentration of NH_3. The normalized resistance of GFP@PSS/PANI device shows a 29% change upon exposure to 10 ppm NH_3. At a cut-off signal-to-noise ratio of 3, the detection limit was estimated to be 125 ppb NH_3, which is significantly lower than the recommended threshold limit value of 25 ppm for human exposure[219,220] and better than or at least on par with most of reported values based on conducting polymers or metal oxides[221–226]. The good performance and fast response can be attributed to the highly porous structure and ultrathin PSS/PANI-coating layer on glass microfiber paper, in which porous structure allows the free access of NH_3 molecules to sensing material while ultrathin PSS/PANI layer greatly reduces the diffusion resistance. It is worthy to note that the NH_3-induced PSS/PANI composite resistance increase shows reasonably good recovery at high NH_3 concentrations, but in practical terms, low reversible at low NH_3 concentration, even though a longer recovery time was used. This incomplete reversibility in low NH_3 concentration range does not pose a problem in our system

since the GFP@PSS/PANI films are accessed in a cost-effective manner such that they could be used as disposable sensor strips[227].

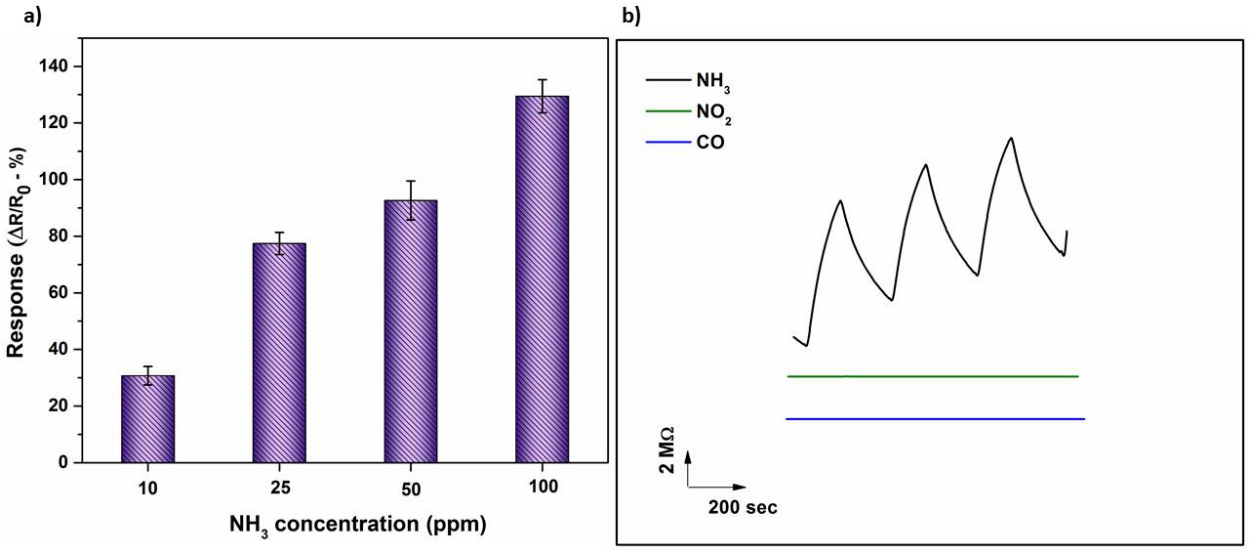

Figure 5.3.9: Gas sensor a) response for different concentrations of NH_3 gas and b) selectivity test for ammonia sensing towards NO_2 and CO gas. (Figure available in Andre, R. S. et. al.[192])

The selectivity of the GFP@PSS/PANI was also investigated and the corresponding results were presented in Figure 5.3.9b. The sensor device was tested against 50 ppm of NO_2 and CO, which are potential interferents in ammonia detection in indoor environment at poultry farms [94,138]. The sensor exposure periodically to 50 ppm of NH_3 result in prominent and repeatable resistance change of the sensor device though a slight baseline drift, which may be attributed to the incomplete recovery of the sensing material after its interaction with NH_3. As a comparison, the sensor response to the same concentration of NO_2 and CO is completely negligible, indicating the excellent selectivity of the flexible GFP@PSS/PANI sensing materials.

5.4. Conclusions

In summary, two different ammonia sensors were successfully obtained. Ammonia sensing tests for ZnO50/PSS50 device showed great sensitivity for concentration varying from 10 ppm to 100 ppm and a LOD of 3.2 ppm at room temperature. ZnO50/PSS50 presented great selectivity for NH_3 detection in presence of potential interfering as NO_2 and CO.

A flexible and disposable device for ammonia gas detection was also successfully obtained and tested. The GFP@PSS/PANI showed to be a promising platform for ammonia detection in low concentrations at room temperature with the advantage of been flexible, disposable and low cost. The detection limit found was of 125 ppb while the response for a concentration as low as 10 ppm was of 29%.

6. General Conclusions and Future perspectives

In the present thesis, it was possible to demonstrate the importance of the combining distinct materials to produce nanocomposites aiming at designing chemical and electrochemical sensors with superior performances. According with the results presented here and based on the proposed goals it is possible to conclude that the selectivity will be determined by the charge transfer, which is dependent on the analyte free electrons capability. For polyaniline, the sensing mechanism is due to the deprotonation process when *n*-type analytes are adsorbed. The interplay with the distinct materials properties can lead to a better performance for sensor devices even separated or in composite combination. Additionally, a few remarks deserve to be highlighted:

- Electrochemical measurements revealed improvement in electron transfer kinetic for the electrode modified with polymeric nanofibers decorated with ZnO nanoparticles, yielding the lowest R_{ct} values, which is advantageous for electrochemical detection application. Additional experiments revealed the sensitivity for nitrogen species even in the presence of interfering compounds;
- The materials properties synergy was indeed confirmed by the higher performance of the tetralayer platform PGPZ3T for detecting NH_3 in impedance spectroscopy measurements;
- A first-hand ZnO/PSS material combination was developed and explored in the affording a promising device for ammonia detection at room temperature;
- The GFP@PSS/PANI was chosen as a promising platform for ammonia detection in low concentration at room temperature with the advantage of been flexible, disposable and low cost. The PSS/PANI combination in the specific configuration was great in promoting an outstanding alternative for low concentrations ammonia sensor.

In terms of future work, such platforms can be integrated with portable and lab-on-a chip platforms for simultaneous measurements and remote system operation to monitor food quality and safety. Flexible substrates will be better exploited aiming one-use disposable devices for integrated systems.

7. References

(1) Nicholson, P. T.; Shaw, I. Ancient Egyptian Materials and Technology. **2000**.

(2) Voglis, N.; Kakali, G.; Chaniotakis, E.; Tsivilis, S. Portland-Limestone Cements. Their Properties and Hydration Compared to Those of Other Composite Cements. *Cem. Concr. Compos.* **2005**, *27* (2), 191–196.

(3) Eyring, G. *Advanced Materials by Design*, OTA-E-351.; Office of Technology Assessment, U. C., Ed.; Office, U.S. Government Printing: Washington, DC, 1988.

(4) Szeluga, U.; Kumanek, B.; Trzebicka, B. Synergy in Hybrid Polymer/nanocarbon Composites. A Review. *Compos. Part A Appl. Sci. Manuf.* **2015**, *73*, 204–231.

(5) Niihara, K. Development of High Performance Ceramic Base Nanocomposites. *Met. Powder Rep.* **1999**, *54* (3), 37.

(6) Hassan, S. F.; Gupta, M. Development of High Performance Magnesium Nano-Composites Using Nano-Al2O3 as Reinforcement. *Mater. Sci. Eng. A* **2005**, *392* (1–2), 163–168.

(7) Lü, L.; Lai, M. .; Liang, W. Magnesium Nanocomposite via Mechanochemical Milling. *Compos. Sci. Technol.* **2004**, *64* (13–14), 2009–2014.

(8) Stolyarov, V. V.; Zhu, Y. .; Lowe, T. .; Islamgaliev, R. .; Valiev, R. . Processing Nanocrystalline Ti and Its Nanocomposites from Micrometer-Sized Ti Powder Using High Pressure Torsion. *Mater. Sci. Eng. A* **2000**, *282* (1–2), 78–85.

(9) Curtin, W. A. Theory of Mechanical Properties of Ceramic-Matrix Composites. *J. Am. Ceram. Soc.* **1991**, *74* (11), 2837–2845.

(10) Suvorova, Y. V.; Alekseeva, S. I.; Fronya, M. a.; Viktorova, I. V. Investigations of Physical and Mechanical Properties of Polymeric Nanocomposites (Review). *Inorg. Mater.* **2013**, *49* (15), 1357–1368.

(11) Mostafa, N. H.; Ismarrubie, Z.; Sapuan, S.; Sultan, M. Fibre Prestressed Polymer-Matrix Composites: A Review. *J. Compos. Mater.* **2017**, *51* (1), 39–66.

(12) Leao, M. a.; Aquino, E. M. F.; Tino, S. R. L.; Fontes, R. S. Licuri Fibers: Alternative Reinforcement to Polymeric Composites. *J. Reinf. Plast. Compos.* **2011**, *30* (6), 516–523.

(13) Zhong, Y.; Tran, L. Q. N.; Kureemun, U.; Lee, H. P. Prediction of the Mechanical Behavior of Flax Polypropylene Composites Based on Multi-Scale Finite Element Analysis. *J. Mater. Sci.* **2017**, *52* (9), 4957–4967.

(14) Kadla, J. .; Kubo, S.; Venditti, R. .; Gilbert, R. .; Compere, A. .; Griffith, W. Lignin-Based Carbon Fibers for Composite Fiber Applications. *Carbon N. Y.* **2002**, *40* (15), 2913–2920.

(15) Dong, J.; Xu, Z.; Kuznicki, S. M. Magnetic Multi-Functional Nano Composites for Environmental Applications. *Adv. Funct. Mater.* **2009**, *19* (8), 1268–1275.

(16) Jeon, I.-Y.; Baek, J.-B. Nanocomposites Derived from Polymers and Inorganic Nanoparticles. *Materials (Basel).* **2010**, *3* (6), 3654–3674.

(17) Singh, N. B.; Agarwal, S. Nanocomposites: An Overview. *Emerg. Mater. Res.* **2016**, *5* (1), 5–43.

(18) Shrivastava, S.; Jadon, N.; Jain, R. Next-Generation Polymer Nanocomposite-Based Electrochemical Sensors and Biosensors: A Review. *TrAC Trends Anal. Chem.* **2016**, *82*, 55–67.

(19) Gibson, R. F. A Review of Recent Research on Mechanics of Multifunctional Composite Materials and Structures. *Compos. Struct.* **2010**, *92* (12), 2793–2810.

(20) Duncan, T. V. Applications of Nanotechnology in Food Packaging and Food Safety: Barrier Materials, Antimicrobials and Sensors. *J. Colloid Interface Sci.* **2011**, *363* (1), 1–24.

(21) Liu, Y. Y.; Wang, X. Y.; Cao, Y.; Chen, X. D.; Xie, S. F.; Zheng, X. J.; Zeng, H. D. A Flexible Blue Light-Emitting Diode Based on ZnO Nanowire/Polyaniline Heterojunctions. *J. Nanomater.* **2013**, *2013*, 1–4.

(22) Cai, S.; Liang, G.; Zhang, P.; Chen, H.; Zhang, S.; Liu, B.; Kong, J. A Miniature Chip for Protein Detection Based on Magnetic Relaxation Switches. *Biosens. Bioelectron.* **2011**, *26* (5), 2258–2263.

(23) Arantes, T. M.; Sala, R. L.; Leite, E. R.; Longo, E.; Camargo, E. R. Comparison of the Nanoparticles Performance in the Photocatalytic Degradation of a Styrene-Butadiene Rubber Nanocomposite. *J. Appl. Polym. Sci.* **2013**, *128* (4), 2368–2374.

(24) Dowling, A.; Clift, R.; Grobert, N.; Hutton, D.; Oliver, R.; O'neill, O.; Pethica, J.; Pidgeon, N.; Porritt, J.; Ryan, J.; Et Al. *Nanoscience and Nanotechnologies: Opportunities and Uncertainties*; The Royal Society & The Royal Academy of Engineering, 2004.

(25) Borrelli, N. F.; Hall, D. W.; Holland, H. J.; Smith, D. W. Quantum Confinement Effects of Semiconducting Microcrystallites in Glass. *J. Appl. Phys.* **1987**, *61* (12), 5399–5409.

(26) Rama Krishna, M. V.; Friesner, R. A. Quantum Confinement Effects in Semiconductor Clusters. *J. Chem. Phys.* **1991**, *95* (11), 8309–8322.

(27) Saheb, N.; Qadir, N.; Siddiqui, M.; Arif, A.; Akhtar, S.; Al-Aqeeli, N. Characterization of Nanoreinforcement Dispersion in Inorganic Nanocomposites: A Review. *Materials (Basel).* **2014**, *7* (6), 4148–4181.

(28) Palmero, P. Structural Ceramic Nanocomposites: A Review of Properties and Powders' Synthesis Methods. *Nanomaterials* **2015**, *5* (2), 656–696.

(29) Zare, Y. Recent Progress on Preparation and Properties of Nanocomposites from Recycled Polymers: A Review. *Waste Manag.* **2013**, *33* (3), 598–604.

(30) Idumah, C. I.; Hassan, A.; Affam, A. C. A Review of Recent Developments in Flammability of Polymer Nanocomposites. *Rev. Chem. Eng.* **2015**, *31* (2), 149–177.

(31) Paul, D. R.; Robeson, L. M. Polymer Nanotechnology: Nanocomposites. *Polymer (Guildf).* **2008**, *49* (15), 3187–3204.

(32) Dittrich, B.; Wartig, K.-A.; Hofmann, D.; Mülhaupt, R.; Schartel, B. Flame Retardancy through Carbon Nanomaterials: Carbon Black, Multiwall Nanotubes, Expanded Graphite, Multi-Layer Graphene and Graphene in Polypropylene. *Polym. Degrad. Stab.* **2013**, *98* (8), 1495–1505.

(33) Hemmati, M.; Rahimi, G. H.; Kaganj, A. B.; Sepehri, S.; Rashidi, A. M. Rheological and Mechanical Characterization of Multi-Walled Carbon

Nanotubes/Polypropylene Nanocomposites. *J. Macromol. Sci. Part B* **2008**, *47* (6), 1176–1187.

(34) Faber, K. T. CERAMIC COMPOSITE INTERFACES:Properties and Design. *Annu. Rev. Mater. Sci.* **1997**, *27* (1), 499–524.

(35) Vaia, R. a.; Jandt, K. D.; Kramer, E. J.; Giannelis, E. P. Kinetics of Polymer Melt Intercalation. *Macromolecules* **1995**, *28* (24), 8080–8085.

(36) Vaia, R. a; Giannelis, E. P. Polymer Melt Intercalation in Organically-Modified Layered Silicates: Model Predictions and Experiment. *Macromolecules* **1997**, *30* (25), 8000–8009.

(37) Vaia, R. A.; Giannelis, E. P. Lattice Model of Polymer Melt Intercalation in Organically-Modified Layered Silicates. *Macromolecules* **1997**, *30* (25), 7990–7999.

(38) Zhang, Y.; Rutledge, G. C. Electrical Conductivity of Electrospun Polyaniline and Polyaniline-Blend Fibers and Mats. *Macromolecules* **2012**, *45* (10), 4238–4246.

(39) Jin, Y.; Fang, M.; Jia, M. In Situ One-Pot Synthesis of Graphene–polyaniline Nanofiber Composite for High-Performance Electrochemical Capacitors. *Appl. Surf. Sci.* **2014**, *308*, 333–340.

(40) Pawar, S. G.; Patil, S. L.; Chougule, M. A.; Raut, B. T.; Godase, P. R.; Mulik, R. N.; Sen, S.; Patil, V. B. New Method for Fabrication of CSA Doped PANi- TiO2 Thin-Film Ammonia Sensor. *IEEE Sens. J.* **2011**, *11* (11), 2980–2985.

(41) Xia, Y.; Zhu, H. Polyaniline Nanofiber-Reinforced Conducting Hydrogel with Unique pH-Sensitivity. *Soft Matter* **2011**, *7* (19), 9388.

(42) Mondal, B.; Basumatari, B.; Das, J.; Roychaudhury, C.; Saha, H.; Mukherjee, N. ZnO–SnO2 Based Composite Type Gas Sensor for Selective Hydrogen Sensing. *Sensors Actuators B Chem.* **2014**, *194*, 389–396.

(43) Lv, Y.-Y.; Wu, J.; Xu, Z.-K. Colorimetric and Fluorescent Sensor Constructing from the Nanofibrous Membrane of Porphyrinated Polyimide for the Detection of Hydrogen Chloride Gas. *Sensors Actuators B Chem.* **2010**, *148* (1), 233–239.

(44) Wu, J.; Wang, N.; Zhao, Y.; Jiang, L. Electrospinning of Multilevel Structured Functional Micro-/nanofibers and Their Applications. *J. Mater. Chem. A* **2013**, *1* (25), 7290.

(45) Rodríguez-Tobías, H.; Morales, G.; Ledezma, A.; Romero, J.; Grande, D. Novel Antibacterial Electrospun Mats Based on Poly(d,l-Lactide) Nanofibers and Zinc Oxide Nanoparticles. *J. Mater. Sci.* **2014**, *49* (24), 8373–8385.

(46) Bagheri, H.; Aghakhani, A. Polyaniline-Nylon-6 Electrospun Nanofibers for Headspace Adsorptive Microextraction. *Anal. Chim. Acta* **2012**, *713*, 63–69.

(47) Taylor, G. Electrically Driven Jets. *Proc. R. Soc. A Math. Phys. Eng. Sci.* **1969**, *313* (1515), 453–475.

(48) Costa, R. G. F.; Oliveira, J. E. De; Paula, G. F. De; Picciani, P. H. de S.; Medeiros, E. S. De; Ribeiro, C.; Mattoso, L. H. C. Eletrofiação de Polímeros Em Solução: Parte I: Fundamentação TeÃ³rica. *Polímeros* **2012**, *22* (2), 170–177.

(49) Baji, A.; Mai, Y.-W.; Wong, S.-C.; Abtahi, M.; Chen, P. Electrospinning of Polymer Nanofibers: Effects on Oriented Morphology, Structures and Tensile Properties. *Compos. Sci. Technol.* **2010**, *70* (5), 703–718.

(50) Mercante, L. A.; Scagion, V. P.; Migliorini, F. L.; Mattoso, L. H. C. C.; Correa, D. S. Electrospinning-Based (Bio)sensors for Food and Agricultural Applications: A Review. *TrAC Trends Anal. Chem.* **2017**, *91*, 91–103.

(51) Huang, Z. M.; Zhang, Y. Z.; Kotaki, M.; Ramakrishna, S. A Review on Polymer Nanofibers by Electrospinning and Their Applications in Nanocomposites. *Compos. Sci. Technol.* **2003**, *63* (15), 2223–2253.

(52) Khadka, D. B.; Haynie, D. T. Protein- and Peptide-Based Electrospun Nanofibers in Medical Biomaterials. *Nanomedicine Nanotechnology, Biol. Med.* **2012**, *8* (8), 1242–1262.

(53) Gunn, J.; Zhang, M. Polyblend Nanofibers for Biomedical Applications: Perspectives and Challenges. *Trends Biotechnol.* **2010**, *28* (4), 189–197.

(54) Hassiba, A. J.; El Zowalaty, M. E.; Nasrallah, G. K.; Webster, T. J.; Luyt, A. S.; Abdullah, A. M.; Elzatahry, A. A. Review of Recent Research on Biomedical Applications of Electrospun Polymer Nanofibers for Improved Wound Healing. *Nanomedicine* **2016**, *11* (6), 715–737.

(55) He, W.; Yong, T.; Teo, W. E.; Ma, Z.; Ramakrishna, S. Fabrication and Endothelialization of Collagen-Blended Biodegradable Polymer Nanofibers: Potential Vascular Graft for Blood Vessel Tissue Engineering. *Tissue Eng.* **2005**, *11* (9–10), 1574–1588.

(56) Yoo, H. S.; Kim, T. G.; Park, T. G. Surface-Functionalized Electrospun Nanofibers for Tissue Engineering and Drug Delivery. *Adv. Drug Deliv. Rev.* **2009**, *61* (12), 1033–1042.

(57) Sridhar, R.; Sundarrajan, S.; Venugopal, J. R.; Ravichandran, R.; Ramakrishna, S. Electrospun Inorganic and Polymer Composite Nanofibers for Biomedical Applications. *J. Biomater. Sci. Polym. Ed.* **2013**, *24* (4), 365–385.

(58) Liao, S.; Li, B.; Ma, Z.; Wei, H.; Chan, C.; Ramakrishna, S. Biomimetic Electrospun Nanofibers for Tissue Regeneration. *Biomed. Mater.* **2006**, *1* (3), R45–R53.

(59) Hong, K. H.; Oh, K. W.; Kang, T. J. Preparation of Conducting Nylon-6 Electrospun Fiber Webs by Thein Situ Polymerization of Polyaniline. *J. Appl. Polym. Sci.* **2005**, *96* (4), 983–991.

(60) Correa, D. S.; Medeiros, E. S.; Oliveira, J. E.; Paterno, L. G.; Mattoso, L. H. C. Nanostructured Conjugated Polymers in Chemical Sensors: Synthesis, Properties and Applications. *J. Nanosci. Nanotechnol.* **2014**, *14* (9), 6509–6527.

(61) Roque, A. P.; Mercante, L. a.; Scagion, V. P.; Oliveira, J. E.; Mattoso, L. H. C.; De Boni, L.; Mendonca, C. R.; Correa, D. S. Fluorescent PMMA/MEH-PPV Electrospun Nanofibers: Investigation of Morphology, Solvent, and Surfactant Effect. *J. Polym. Sci. Part B Polym. Phys.* **2014**, *52* (21), 1388–1394.

(62) Raut, B. T.; Godse, P. R.; Pawar, S. G.; Chougule, M. A.; Bandgar, D. K.; Sen, S.; Patil, V. B. New Process for Fabrication of polyaniline–CdS Nanocomposites: Structural, Morphological and Optoelectronic Investigations. *J. Phys. Chem. Solids* **2013**, *74* (2), 236–244.

(63) Decher, G. Fuzzy Nanoassemblies: Toward Layered Polymeric Multicomposites. *Science (80-.).* **1997**, *277* (5330), 1232–1237.

(64) Blodgett, K. B. Films Built by Depositing Successive Monomolecular Layers on a

Solid Surface. *J. Am. Chem. Soc.* **1935**, *57* (6), 1007–1022.

(65) Srivastava, S.; Kotov, N. A. Composite Layer-by-Layer (LBL) Assembly with Inorganic Nanoparticles and Nanowires. *Acc. Chem. Res.* **2008**, *41* (12), 1831–1841.

(66) Carastan, D. J.; Demarquette, N. R. Microstructure of Nanocomposites of Styrenic Polymers. *Macromol. Symp.* **2006**, *233* (1), 152–160.

(67) Chen, D.; Miao, Y.-E.; Liu, T. Electrically Conductive Polyaniline/Polyimide Nanofiber Membranes Prepared via a Combination of Electrospinning and Subsequent In Situ Polymerization Growth. *ACS Appl. Mater. Interfaces* **2013**, *5* (4), 1206–1212.

(68) Nazarenko, S.; Meneghetti, P.; Julmon, P.; Olson, B. G.; Qutubuddin, S. Gas Barrier of Polystyrene Montmorillonite Clay Nanocomposites: Effect of Mineral Layer Aggregation. *J. Polym. Sci. Part B Polym. Phys.* **2007**, *45* (13), 1733–1753.

(69) Liu, R. Hybrid Organic/Inorganic Nanocomposites for Photovoltaic Cells. *Materials (Basel).* **2014**, *7* (4), 2747–2771.

(70) Sommers, A.; Wang, Q.; Han, X.; T'Joen, C.; Park, Y.; Jacobi, A. Ceramics and Ceramic Matrix Composites for Heat Exchangers in Advanced Thermal systems—A Review. *Appl. Therm. Eng.* **2010**, *30* (11–12), 1277–1291.

(71) Yano, H.; Sugiyama, J.; Nakagaito, A. N.; Nogi, M.; Matsuura, T.; Hikita, M.; Handa, K. Optically Transparent Composites Reinforced with Networks of Bacterial Nanofibers. *Adv. Mater.* **2005**, *17* (2), 153–155.

(72) Sahay, R.; Kumar, P. S.; Sridhar, R.; Sundaramurthy, J.; Venugopal, J.; Mhaisalkar, S. G.; Ramakrishna, S. Electrospun Composite Nanofibers and Their Multifaceted Applications. *J. Mater. Chem.* **2012**, *22* (26), 12953.

(73) Zhang, M.; Zhao, X.; Zhang, G.; Wei, G.; Su, Z. Electrospinning Design of Functional Nanostructures for Biosensor Applications. *J. Mater. Chem. B* **2017**.

(74) Narjinary, M.; Rana, P.; Sen, A.; Pal, M. Enhanced and Selective Acetone Sensing Properties of SnO2-MWCNT Nanocomposites: Promising Materials for Diabetes Sensor. *Mater. Des.* **2017**, *115*, 158–164.

(75) Wang, P.; Wang, D.; Zhang, M.; Zhu, Y.; Xu, Y.; Ma, X.; Wang, X. ZnO Nanosheets/graphene Oxide Nanocomposites for Highly Effective Acetone Vapor Detection. *Sensors Actuators B Chem.* **2016**, *230*, 477–484.

(76) Lu, X.; Wang, C.; Wei, Y. One-Dimensional Composite Nanomaterials: Synthesis by Electrospinning and Their Applications. *Small* **2009**, *5* (21), 2349–2370.

(77) Miller, D. R.; Akbar, S. A.; Morris, P. A. Nanoscale Metal Oxide-Based Heterojunctions for Gas Sensing: A Review. *Sensors Actuators B Chem.* **2014**, *204*, 250–272.

(78) Mirzaei, A.; Janghorban, K.; Hashemi, B.; Bonyani, M.; Leonardi, S. G.; Neri, G. A Novel Gas Sensor Based on Ag/Fe2O3 Core-Shell Nanocomposites. *Ceram. Int.* **2016**, *42* (16), 18974–18982.

(79) Wang;, Y.; Ding;, Y.; La;, A.; Lei;, Y. PREPARATION, CHARACTERIZATION AND GAS SENSING APPLICATION OF NOVEL CONDUCTING POLYPYRROLE COMPOSITE NANOFIBERS. In *Polypyrrole: Properties, Performance and Applications*; Mason, E. C., Weber, A. P., Eds.; Nova Science Publishers, Inc., 2011; p 17.

(80) Chaudhary, V.; Kaur, A. Enhanced and Selective Ammonia Sensing Behaviour of Poly(aniline Co-Pyrrole) Nanospheres Chemically Oxidative Polymerized at Low Temperature. *J. Ind. Eng. Chem.* **2015**, *26*, 143–148.

(81) Song, M.; Liu, F.; Ma, X. Study on Preparation and Gas Sensing Property of PANI. *Int. J. Control Autom.* **2015**, *8* (4), 267–274.

(82) Miller, D. R.; Akbar, S. A.; Morris, P. A. Nanoscale Metal Oxide-Based Heterojunctions for Gas Sensing: A Review. *Sensors Actuators B Chem.* **2014**, *204*, 250–272.

(83) Korotcenkov, G. Metal Oxides for Solid-State Gas Sensors: What Determines Our Choice? *Mater. Sci. Eng. B* **2007**, *139* (1), 1–23.

(84) Sze, S. M.; Kwok, K. N. *Physics of Semiconductor Devices*; 2007.

(85) Vuong, N. M.; Kim, D.; Kim, H. Surface Gas Sensing Kinetics of a WO3 Nanowire Sensor: Part 1—oxidizing Gases. *Sensors Actuators B Chem.* **2015**, *220*, 932–941.

(86) Vuong, N. M.; Kim, D.; Kim, H. Surface Gas Sensing Kinetics of a WO3 Nanowire Sensor: Part 2—Reducing Gases. *Sensors Actuators B Chem.* **2016**, *224*, 425–433.

(87) Walker, J. M.; Philip, S.; Martin, R. V.; Seinfeld, J. H. Simulation of Nitrate, Sulfate, and Ammonium Aerosols over the United States. *Atmos. Chem. Phys.* **2012**, *12* (22), 11213–11227.

(88) Corkery, G.; Ward, S.; Colum Kenny; Hemmingway, P. Title Monitoring Environmental Parameters in Poultry Production Facilities Author (S) Publication Date Publication Information Computer Aided Process Engineering , CAPE Forum 2013 , Graz University of Technology , Austria , 7-10 April 2013 Institute for. *Inst. Process Part. Eng. Graz Univ. Technol.* **2013**.

(89) Polat, H. E. EFFECTS OF POULTRY BUILDING DESIGN ON INDOOR AIR QUALITY IN HUMID CLIMATES. *J. Anim. Plant Sci.* **2015**, *25* (5), 1264–1272.

(90) Zhao, Y.; Xin, H.; Shepherd, T. Thermal Environment, Ammonia Concentrations, and Ammonia Emissions of Aviary Houses with White Laying Hens. *Trans. ASABE* **2013**, *56* (3), 1145–1156.

(91) Guštin, S.; Marinšek-Logar, R. Effect of pH, Temperature and Air Flow Rate on the Continuous Ammonia Stripping of the Anaerobic Digestion Effluent. *Process Saf. Environ. Prot.* **2011**, *89* (1), 61–66.

(92) Dunlop, M. W.; Blackall, P. J.; Stuetz, R. M. Odour Emissions from Poultry Litter – A Review Litter Properties, Odour Formation and Odorant Emissions from Porous Materials. *J. Environ. Manage.* **2016**, *177*, 306–319.

(93) Zhao, Y.; Shepherd, T. A.; Li, H.; Xin, H. Environmental Assessment of Three Egg Production Systems– Part I: Monitoring System and Indoor Air Quality. *Poult. Sci.* **2015**, *94* (3), 518–533.

(94) Loyon, L.; Burton, C. H.; Misselbrook, T.; Webb, J.; Philippe, F. X.; Aguilar, M.; Doreau, M.; Hassouna, M.; Veldkamp, T.; Dourmad, J. Y.; Bonmati, A.; Grimm, E.; Sommer, S. G. Best Available Technology for European Livestock Farms: Availability, Effectiveness and Uptake. *J. Environ. Manage.* **2016**, *166*, 1–11.

(95) Wagner, S.; Angenendt, E.; Beletskaya, O.; Zeddies, J. Costs and Benefits of Ammonia and Particulate Matter Abatement in German Agriculture Including

Interactions with Greenhouse Gas Emissions. *Agric. Syst.* **2015**, *141*, 58–68.

(96) Griffiths, R. F.; Megson, L. C. The Effect of Uncertainties in Human Toxic Response on Hazard Range Estimation for Ammonia and Chlorine. *Atmos. Environ.* **1984**, *18* (6), 1195–1206.

(97) Chang, C. W.; Chung, H.; Huang, C. F.; Su, H. J. Exposure Assessment to Airborne Endotoxin, Dust, Ammonia, Hydrogen Sulfide and Carbon Dioxide in Open Style Swine Houses. *Ann. Occup. Hyg.* **2001**, *45* (6), 457–465.

(98) Nicole, L.; Laberty-Robert, C.; Rozes, L.; Sanchez, C. Hybrid Materials Science: A Promised Land for the Integrative Design of Multifunctional Materials. *Nanoscale* **2014**, *6* (12), 6267–6292.

(99) Sharp, K. G. Inorganic/Organic Hybrid Materials. *Adv. Mater.* **1998**, *10* (15), 1243–1248.

(100) Convertino, A.; Leo, G.; Striccoli, M.; Di Marco, G.; Curri, M. L. Effect of Shape and Surface Chemistry of TiO2 Colloidal Nanocrystals on the Organic Vapor Absorption Capacity of TiO2/PMMA Composite. *Polymer (Guildf).* **2008**, *49* (25), 5526–5532.

(101) Scocioreanu, M.; Baibarac, M.; Baltog, I.; Pasuk, I.; Velula, T. Photoluminescence and Raman Evidence for Mechanico-Chemical Interaction of Polyaniline-Emeraldine Base with ZnS in Cubic and Hexagonal Phase. *J. Solid State Chem.* **2012**, *186*, 217–223.

(102) Gianotti, E.; Diaz, U.; Coluccia, S.; Corma, A. Hybrid Organic–inorganic Catalytic Mesoporous Materials with Proton Sponges as Building Blocks. *Phys. Chem. Chem. Phys.* **2011**, *13* (24), 11702.

(103) Kim, E.; Lee, Y.; Bang, J.; Kim, K.; Choe, S. Synthesis and Electrical Resistivity of the Monodisperse PMMA/Ag Hybrid Particles. *Mater. Chem. Phys.* **2012**, *134* (2–3), 814–820.

(104) Manzoli, A.; Shimizu, F. M.; Mercante, L. a.; Paris, E. C.; Oliveira, O. N.; Correa, D. S.; Mattoso, L. H. C. Layer-by-Layer Fabrication of AgCl–PANI Hybrid Nanocomposite Films for Electronic Tongues. *Phys. Chem. Chem. Phys.* **2014**, *16* (44), 24275–24281.

(105) Sanchez, C.; Belleville, P.; Popall, M.; Nicole, L. Applications of Advanced Hybrid Organic–inorganic Nanomaterials: From Laboratory to Market. *Chem. Soc. Rev.* **2011**, *40* (2), 696.

(106) Ding, B.; Wang, M.; Yu, J.; Sun, G. Gas Sensors Based on Electrospun Nanofibers. *Sensors (Basel).* **2009**, *9* (3), 1609–1624.

(107) Mercante, L. A.; Pavinatto, A.; Iwaki, L. E. O.; Scagion, V. P.; Zucolotto, V.; Oliveira, O. N.; Mattoso, L. H. C.; Correa, D. S. Electrospun Polyamide 6/Poly(allylamine Hydrochloride) Nanofibers Functionalized with Carbon Nanotubes for Electrochemical Detection of Dopamine. *ACS Appl. Mater. Interfaces* **2015**, *7* (8), 4784–4790.

(108) Oliveira, J. E.; Scagion, V. P.; Grassi, V.; Correa, D. S.; Mattoso, L. H. C. Modification of Electrospun Nylon Nanofibers Using Layer-by-Layer Films for Application in Flow Injection Electronic Tongue: Detection of Paraoxon Pesticide in Corn Crop. *Sensors Actuators B Chem.* **2012**, *171–172*, 249–255.

(109) Lv, Y.; Zhang, Y.; Du, Y.; Xu, J.; Wang, J. A Novel Porphyrin-Containing

Polyimide Nanofibrous Membrane for Colorimetric and Fluorometric Detection of Pyridine Vapor. *Sensors* **2013**, *13* (11), 15758–15769.

(110) Nguyen, L. T. H.; Chen, S.; Elumalai, N. K.; Prabhakaran, M. P.; Zong, Y.; Vijila, C.; Allakhverdiev, S. I.; Ramakrishna, S. Biological, Chemical, and Electronic Applications of Nanofibers. *Macromol. Mater. Eng.* **2013**, *298* (8), 822–867.

(111) Huang, Y.; Miao, Y.-E.; Ji, S.; Tjiu, W. W.; Liu, T. Electrospun Carbon Nanofibers Decorated with Ag–Pt Bimetallic Nanoparticles for Selective Detection of Dopamine. *ACS Appl. Mater. Interfaces* **2014**, *6* (15), 12449–12456.

(112) Wu, J.; Yin, F. Studies on the Electrocatalytic Oxidation of Dopamine at Phosphotungstic acid–ZnO Spun Fiber-Modified Electrode. *Sensors Actuators B Chem.* **2013**, *185*, 651–657.

(113) Jagtap, S.; Priolkar, K. R. Evaluation of ZnO Nanoparticles and Study of ZnO–TiO2 Composites for Lead Free Humidity Sensors. *Sensors Actuators B Chem.* **2013**, *183*, 411–418.

(114) Park, S.; An, S.; Ko, H.; Jin, C.; Lee, C. Synthesis of Nanograined ZnO Nanowires and Their Enhanced Gas Sensing Properties. *ACS Appl. Mater. Interfaces* **2012**, *4* (7), 3650–3656.

(115) Fang, L.; Huang, K.; Zhang, B.; Liu, B.; Liu, Y.; Zhang, Q. Nanosheet-Based 3D Hierarchical ZnO Structure Decorated with Au Nanoparticles for Enhanced Electrochemical Detection of Dopamine. *RSC Adv.* **2014**, *4* (90), 48986–48993.

(116) Baruah, S.; Dutta, J. Hydrothermal Growth of ZnO Nanostructures. *Sci. Technol. Adv. Mater.* **2009**, *10* (1), 13001.

(117) Guo, W.; Liu, T.; Zhang, H.; Sun, R.; Chen, Y.; Zeng, W.; Wang, Z. Gas-Sensing Performance Enhancement in ZnO Nanostructures by Hierarchical Morphology. *Sensors Actuators B Chem.* **2012**, *166–167*, 492–499.

(118) Li, Z.; Xiong, Y.; Xie, Y. Selected-Control Synthesis of ZnO Nanowires and Nanorods via a PEG-Assisted Route. *Inorg. Chem.* **2003**, *42* (24), 8105–8109.

(119) Xiao, J.; Qi, L. Surfactant-Assisted, Shape-Controlled Synthesis of Gold Nanocrystals. *Nanoscale* **2011**, *3* (4), 1383.

(120) Norris, S. A.; Watson, S. J. Geometric Simulation and Surface Statistics of Coarsening Faceted Surfaces. *Acta Mater.* **2007**, *55* (19), 6444–6452.

(121) Lin, M.; Fu, Z. Y.; Tan, H. R.; Tan, J. P. Y.; Ng, S. C.; Teo, E. Hydrothermal Synthesis of CeO 2 Nanocrystals: Ostwald Ripening or Oriented Attachment? *Cryst. Growth Des.* **2012**, *12* (6), 3296–3303.

(122) Privman, V.; Goia, D. V; Park, J.; Matijević, E. Mechanism of Formation of Monodispersed Colloids by Aggregation of Nanosize Precursors. *J. Colloid Interface Sci.* **1999**, *213* (1), 36–45.

(123) Georgiou, P.; Kolokotronis, K.; Simitzis, J. Synthesis of ZnO Nanostructures by Hydrothermal Method. *J. Nano Res.* **2009**, *6*, 157–168.

(124) Sudha, M.; Senthilkumar, S.; Hariharan, R.; Suganthi, A.; Rajarajan, M. Synthesis, Characterization and Study of Photocatalytic Activity of Surface Modified ZnO Nanoparticles by PEG Capping. *J. Sol-Gel Sci. Technol.* **2013**, *65* (3), 301–310.

(125) Andre, R. S.; Pavinatto, A.; Mercante, L. A.; Paris, E. C.; Mattoso, L. H. C.;

Correa, D. S. Improving the Electrochemical Properties of Polyamide 6/polyaniline Electrospun Nanofibers by Surface Modification with ZnO Nanoparticles. *RSC Adv.* **2015**, *5* (90), 73875–73881.

(126) Zhang, C.-L.; Yu, S.-H. Nanoparticles Meet Electrospinning: Recent Advances and Future Prospects. *Chem. Soc. Rev.* **2014**, *43* (13), 4423.

(127) McCarthy, P. A.; Huang, J.; Yang, S.-C.; Wang, H.-L. Synthesis and Characterization of Water-Soluble Chiral Conducting Polymer Nanocomposites. *Langmuir* **2002**, *18* (1), 259–263.

(128) Hu, H.; Cadenas, J. L.; Saniger, J. M.; Nair, P. K. Electrically Conducting Polyaniline-Poly(acrylic Acid) Blends. *Polym. Int.* **1998**, *45* (3), 262–270.

(129) Wei, A.; Pan, L.; Huang, W. Recent Progress in the ZnO Nanostructure-Based Sensors. *Mater. Sci. Eng. B* **2011**, *176* (18), 1409–1421.

(130) Anusha, J. R.; Kim, H.-J.; Fleming, A. T.; Das, S. J.; Yu, K.-H.; Kim, B. C.; Raj, C. J. Simple Fabrication of ZnO/Pt/chitosan Electrode for Enzymatic Glucose Biosensor. *Sensors Actuators B Chem.* **2014**, *202*, 827–833.

(131) Janegitz, B. C.; dos Santos, F. A.; Faria, R. C.; Zucolotto, V. Electrochemical Determination of Estradiol Using a Thin Film Containing Reduced Graphene Oxide and Dihexadecylphosphate. *Mater. Sci. Eng. C* **2014**, *37* (1), 14–19.

(132) Ding, J.; Zhu, S.; Zhu, T.; Sun, W.; Li, Q.; Wei, G.; Su, Z. Hydrothermal Synthesis of Zinc Oxide-Reduced Graphene Oxide Nanocomposites for an Electrochemical Hydrazine Sensor. *RSC Adv.* **2015**, *5* (29), 22935–22942.

(133) Su, P.-G. G.; Yang, L.-Y. Y. NH3 Gas Sensor Based on Pd/SnO2/RGO Ternary Composite Operated at Room-Temperature. *Sensors Actuators B Chem.* **2016**, *223*, 202–208.

(134) Hasan, M.; Ansari, M. O.; Cho, M. H.; Lee, M. Electrical Conductivity, Optical Property and Ammonia Sensing Studies on HCl Doped Au@polyaniline Nanocomposites. *Electron. Mater. Lett.* **2015**, *11* (1), 1–6.

(135) Cui, S.; Mao, S.; Wen, Z.; Chang, J.; Zhang, Y.; Chen, J. Controllable Synthesis of Silver Nanoparticle-Decorated Reduced Graphene Oxide Hybrids for Ammonia Detection. *Analyst* **2013**, *138* (10), 2877–2882.

(136) Bandgar, D. K.; Navale, S. T.; Mane, a. T.; Gupta, S. K.; Aswal, D. K.; Patil, V. B. Ammonia Sensing Properties of Polyaniline/α-Fe2O3 Hybrid Nanocomposites. *Synth. Met.* **2015**, *204*, 1–9.

(137) McQuilling, A. M.; Adams, P. J. Semi-Empirical Process-Based Models for Ammonia Emissions from Beef, Swine, and Poultry Operations in the United States. *Atmos. Environ.* **2015**, *120*, 127–136.

(138) Bittman, S.; Jones, K.; Vingarzan, R.; Hunt, D. E.; Sheppard, S. C.; Tait, J.; So, R.; Zhao, J. Weekly Agricultural Emissions and Ambient Concentrations of Ammonia: Validation of an Emission Inventory. *Atmos. Environ.* **2015**, *113*, 108–117.

(139) Ta, S.; Zhao, Y.; Li, H.; Jp, S.; Xin, H.; Shepherd, T. A.; Zhao, Y.; Li, H.; Stinn, J. P.; Hayes, M. D.; Xin, H. Environmental Assessment of Three Egg Production Systems — Part II. Ammonia, Greenhouse Gas, and Particulate Matter Emissions. *Poult. Sci.* **2015**, *94* (3), 534–543.

(140) Kondawar, S. B.; Patil, P. T.; Agrawal, S. P. Chemical Vapour Sensing Properties

of Electrospun Nanofibers of Polyaniline / ZnO Nanocomposites. *Adv. Mater. Lett.* **2014**, *5* (7), 389–395.

(141) Navarchian, A. H.; Hasanzadeh, Z.; Joulazadeh, M. Effect of Polymerization Conditions on Reaction Yield, Conductivity, and Ammonia Sensing of Polyaniline. *Adv. Polym. Technol.* **2013**, *32* (3), 5–9.

(142) Guia Trabalista. NR 15 - Atividades E Operações Insalubres. Copyright © 2003-2016 Portal Tributário Editora 2003.

(143) Bendahan, M.; Lauque, P.; Lambert-Mauriat, C.; Carchano, H.; Seguin, J. L. Sputtered Thin Films of CuBr for Ammonia Microsensors: Morphology, Composition and Ageing. *Sensors Actuators, B Chem.* **2002**, *84* (1), 6–11.

(144) Ponnusamy, D.; Madanagurusamy, S. Porous Anatase TiO2 Thin Films for NH3 Vapour Sensing. *J. Electron. Mater.* **2015**, *44* (12), 4726–4733.

(145) Jia, Y.; Yan, C.; Yu, H.; Chen, L.; Dong, F. One-Step Fabrication of Ammonia Sensor by Electrospinning PS- B -PMA Nanofibers on Quartz Crystal Microbalance. *Sensors Actuators B. Chem.* **2014**, *203*, 459–464.

(146) Abdulla, S.; Mathew, T. L.; Pullithadathil, B. Highly Sensitive, Room Temperature Gas Sensor Based on Polyaniline-Multiwalled Carbon Nanotubes (PANI/MWCNTs) Nanocomposite for Trace-Level Ammonia Detection. *Sensors Actuators B Chem.* **2015**, *221* (2), 1523–1534.

(147) Timmer, B.; Olthuis, W.; Berg, A. Van Den. Ammonia Sensors and Their Applications—a Review. *Sensors Actuators B Chem.* **2005**, *107* (2), 666–677.

(148) Liu, X.; Cheng, S.; Liu, H.; Hu, S.; Zhang, D.; Ning, H. A Survey on Gas Sensing Technology. *Sensors* **2012**, *12* (12), 9635–9665.

(149) Wu, Z.; Chen, X.; Zhu, S.; Zhou, Z.; Yao, Y.; Quan, W.; Liu, B. Enhanced Sensitivity of Ammonia Sensor Using Graphene/polyaniline Nanocomposite. *Sensors Actuators B Chem.* **2013**, *178*, 485–493.

(150) Li, Y.; Pathak, B.; Nisar, J.; Qian, Z.; Ahuja, R. Metal-Decorated Graphene Oxide for Ammonia Adsorption. *EPL (Europhysics Lett.* **2013**, *103* (2), 28007.

(151) Talwar, V.; Singh, O.; Singh, R. C. ZnO Assisted Polyaniline Nanofibers and Its Application as Ammonia Gas Sensor. *Sensors Actuators B Chem.* **2014**, *191*, 276–282.

(152) Pawar, S. G.; Chougule, M. a.; Patil, S. L.; Raut, B. T.; Godse, P. R.; Sen, S.; Patil, V. B. Room Temperature Ammonia Gas Sensor Based on Polyaniline-TiO2 Nanocomposite. *IEEE Sens. J.* **2011**, *11* (12), 3417–3423.

(153) Patil, U. V.; Ramgir, N. S.; Karmakar, N.; Bhogale, A.; Debnath, A. K.; Aswal, D. K.; Gupta, S. K.; Kothari, D. C. Room Temperature Ammonia Sensor Based on Copper Nanoparticle Intercalated Polyaniline Nanocomposite Thin Films. *Appl. Surf. Sci.* **2015**, *339*, 69–74.

(154) Crespilho, F. N.; Zucolotto, V.; Oliveira, O. N.; Nart, F. C. Electrochemistry of Layer-by-Layer Films: A Review. *Int. J. Electrochem. Sci.* **2006**, *1* (5), 194–214.

(155) Lvov, Y.; Haas, H.; Decher, G.; Moehwald, H.; Kalachev, A. Assembly of Polyelectrolyte Molecular Films onto Plasma-Treated Glass. *J. Phys. Chem.* **1993**, *97* (49), 12835–12841.

(156) Decher, G.; Hong, J.-D. Buildup of Ultrathin Multilayer Films by a Self-Assembly

Process, 1 Consecutive Adsorption of Anionic and Cationic Bipolar Amphiphiles on Charged Surfaces. *Makromol. Chemie. Macromol. Symp.* **1991**, *46* (1), 321–327.

(157) Chen, J.; Yang, J.; Yan, X.; Xue, Q. NH3 and HCl Sensing Characteristics of Polyaniline Nanofibers Deposited on Commercial Ceramic Substrates Using Interfacial Polymerization. *Synth. Met.* **2010**, *160* (23–24), 2452–2458.

(158) Prabhakaran, M. P.; Ghasemi-Mobarakeh, L.; Jin, G.; Ramakrishna, S. Electrospun Conducting Polymer Nanofibers and Electrical Stimulation of Nerve Stem Cells. *J. Biosci. Bioeng.* **2011**, *112* (5), 501–507.

(159) Valiavalappil, S.; Harinipriya, S. Electrically Conducting Nylon 6,6–polyaniline Short Composite Fibres Synthesised by the Solvent Coagulation Method. *Synth. Met.* **2012**, *162* (23), 2027–2032.

(160) Tuan, C. Van; Tuan, M. A.; Hieu, N. Van; Trung, T. Electrochemical Synthesis of Polyaniline Nanowires on Pt Interdigitated Microelectrode for Room Temperature NH3 Gas Sensor Application. *Curr. Appl. Phys.* **2012**, *12* (4), 1011–1016.

(161) de Barros, A.; Ferreira, M.; Constantino, C. J. L.; Ferreira, M. Nanocomposites Based on LbL Films of Polyaniline and Sodium Montmorillonite Clay. *Synth. Met.* **2014**, *197*, 119–125.

(162) Steffens, C.; Manzoli, A.; Oliveira, J. E.; Leite, F. L.; Correa, D. S.; Herrmann, P. S. P. Bio-Inspired Sensor for Insect Pheromone Analysis Based on Polyaniline Functionalized AFM Cantilever Sensor. *Sensors Actuators B Chem.* **2014**, *191*, 643–649.

(163) Li, C.-F.; Hsu, C.-Y.; Li, Y.-Y. NH3 Sensing Properties of ZnO Thin Films Prepared via Sol–gel Method. *J. Alloys Compd.* **2014**, *606*, 27–31.

(164) Khairy, M. Polyaniline–Zn0.2Mn0.8 Fe2O4 Ferrite Core–shell Composite: Preparation, Characterization and Properties. *J. Alloys Compd.* **2014**, *608*, 283–291.

(165) Sharma, M.; Jeevanandam, P. Synthesis , Characterization and Studies on Optical Properties of Indium Doped ZnO Nanoparticles. **2014**, *53* (May), 561–565.

(166) Anton, S. R.; Sodano, H. a. A Review of Power Harvesting Using Piezoelectric Materials (2003–2006). *Smart Mater. Struct.* **2007**, *16* (3), R1–R21.

(167) Varghese, S. S.; Lonkar, S.; Singh, K. K.; Swaminathan, S.; Abdala, A. Recent Advances in Graphene Based Gas Sensors. *Sensors Actuators B Chem.* **2015**, *218*, 160–183.

(168) Gayathri, S.; Jayabal, P.; Kottaisamy, M.; Ramakrishnan, V. Synthesis of ZnO Decorated Graphene Nanocomposite for Enhanced Photocatalytic Properties. *J. Appl. Phys.* **2014**, *115* (17), 173504.

(169) He, X.; Wu, L. -l.; Wang, J. -j.; Zhang, T.; Sun, H.; Shuai, N. Layer-by-Layer Assembly Deposition of Graphene Oxide on Poly(lactic Acid) Films to Improve the Barrier Properties. *High Perform. Polym.* **2015**, *27* (3), 318–325.

(170) William S. Hummers, J.; Offeman, R. E. Preparation of Graphitic Oxide. *J. Am. Chem. Soc* **1958**, *80* (1937), 1339.

(171) Kovtyukhova, N. I.; Ollivier, P. J.; Martin, B. R.; Mallouk, T. E.; Chizhik, S. a.; Buzaneva, E. V.; Gorchinskiy, A. D. Layer-by-Layer Assembly of Ultrathin Composite Films from Micron-Sized Graphite Oxide Sheets and Polycations.

Chem. Mater. **1999**, *11* (3), 771–778.

(172) Andre, R. S.; Shimizu, F. M.; Miyazaki, C. M.; Riul, A.; Manzani, D.; Ribeiro, S. J. L.; Oliveira, O. N.; Mattoso, L. H. C.; Correa, D. S. Hybrid Layer-by-Layer (LbL) Films of Polyaniline, Graphene Oxide and Zinc Oxide to Detect Ammonia. *Sensors Actuators B Chem.* **2017**, *238*, 795–801.

(173) Huang, X.; Hu, N.; Gao, R.; Yu, Y.; Wang, Y.; Yang, Z.; Siu-Wai Kong, E.; Wei, H.; Zhang, Y. Reduced Graphene Oxide–polyaniline Hybrid: Preparation, Characterization and Its Applications for Ammonia Gas Sensing. *J. Mater. Chem.* **2012**, *22* (42), 22488.

(174) Milekhin, A. G.; Yeryukov, N. A.; Sveshnikova, L. L.; Duda, T. A.; Zenkevich, E. I.; Kosolobov, S. S.; Latyshev, A. V.; Himcinski, C.; Surovtsev, N. V.; Adichtchev, S. V.; Feng, Z. C.; Wu, C. C.; Wuu, D. S.; Zahn, D. R. T. Surface Enhanced Raman Scattering of Light by ZnO Nanostructures. *J. Exp. Theor. Phys.* **2011**, *113* (6), 983–991.

(175) Barbosa Filho, J. A. D.; Queiroz, M. L. V.; Brasil, D. de F.; Vieira, F. M. C.; Silva, I. J. O. Transport of Broilers: Load Microclimate during Brazilian Summer. *Eng. Agrícola* **2014**, *34* (3), 405–412.

(176) Wang, C.; Yin, L.; Zhang, L.; Xiang, D.; Gao, R. Metal Oxide Gas Sensors: Sensitivity and Influencing Factors. *Sensors* **2010**, *10* (3), 2088–2106.

(177) Fine, G. F.; Cavanagh, L. M.; Afonja, A.; Binions, R. Metal Oxide Semi-Conductor Gas Sensors in Environmental Monitoring. *Sensors* **2010**, *10* (6), 5469–5502.

(178) Korotcenkov, G.; Han, S. H.; Cho, B. K. Material Design for Metal Oxide Chemiresistive Gas Sensors. *J. Sens. Sci. Technol.* **2013**, *22* (1), 1–17.

(179) Chen, T.-Y.; Chen, H.-I.; Hsu, C.-S.; Huang, C.-C.; Wu, J.-S.; Chou, P.-C.; Liu, W.-C. Characteristics of ZnO Nanorods-Based Ammonia Gas Sensors with a Cross-Linked Configuration. *Sensors Actuators B Chem.* **2015**, *221*, 491–498.

(180) Yoo, S.; Li, X.; Wu, Y.; Liu, W.; Wang, X.; Yi, W. Ammonia Gas Detection by Tannic Acid Functionalized and Reduced Graphene Oxide at Room Temperature. *J. Nanomater.* **2014**, *2014*, 1–6.

(181) Oliveira Jr, O. N.; Neves, T. A. T.; Paulovich, F. V; de Oliveira, M. C. F. Where Chemical Sensors May Assist in Clinical Diagnosis Exploring “Big Data.” *Chem. Lett.* **2014**, *43* (11), 1672–1679.

(182) Paulovich, F. V; Moraes, M. L.; Maki, R. M.; Ferreira, M.; Oliveira, O. N.; de Oliveira, M. C. F. Information Visualization Techniques for Sensing and Biosensing. *Analyst* **2011**, *136* (7), 1344–1350.

(183) Moraes, M. L.; Petri, L.; Oliveira, V.; Olivati, C. a.; De Oliveira, M. C. F.; Paulovich, F. V.; Oliveira, O. N.; Ferreira, M. Detection of Glucose and Triglycerides Using Information Visualization Methods to Process Impedance Spectroscopy Data. *Sensors Actuators, B Chem.* **2012**, *166–167*, 231–238.

(184) Xiang, C.; Jiang, D.; Zou, Y.; Chu, H.; Qiu, S.; Zhang, H.; Xu, F.; Sun, L.; Zheng, L. Ammonia Sensor Based on Polypyrrole–graphene Nanocomposite Decorated with Titania Nanoparticles. *Ceram. Int.* **2015**, *41* (5), 6432–6438.

(185) Bandgar, D. K.; Navale, S. T.; Naushad, M.; Mane, R. S.; Stadler, F. J.; Patil, V. B. Ultra-Sensitive Polyaniline–iron Oxide Nanocomposite Room Temperature Flexible Ammonia Sensor. *RSC Adv.* **2015**, *5* (84), 68964–68971.

(186) Li, Y.; Ban, H.; Yang, M. Highly Sensitive NH3 Gas Sensors Based on Novel Polypyrrole-Coated SnO2 Nanosheet Nanocomposites. *Sensors Actuators B Chem.* **2015**, *224*, 449–457.

(187) Bai, S.; Tian, Y. Y. Y. Y.; Cui, M.; Sun, J.; Tian, Y. Y. Y. Y.; Luo, R.; Chen, A.; Li, D. Polyaniline@SnO2 Heterojunction Loading on Flexible PET Thin Film for Detection of NH3 at Room Temperature. *Sensors Actuators B Chem.* **2016**, *226*, 540–547.

(188) Ji, S.; Li, Y.; Yang, M. Gas Sensing Properties of a Composite Composed of Electrospun Poly(methyl Methacrylate) Nanofibers and in Situ Polymerized Polyaniline. *Sensors Actuators B Chem.* **2008**, *133* (2), 644–649.

(189) Khuspe, G. D.; Navale, S. T.; Bandgar, D. K.; Sakhare, R. D.; Chougule, M. A.; Patil, V. B. SnO2nanoparticles-Modified Polyaniline Films as Highly Selective, Sensitive, Reproducible and Stable Ammonia Sensors. *Electron. Mater. Lett.* **2014**, *10* (1), 191–197.

(190) Yang, Y.; Yang, X.; Yang, W.; Li, S.; Xu, J.; Jiang, Y. Porous Conducting Polymer and Reduced Graphene Oxide Nanocomposites for Room Temperature Gas Detection. *RSC Adv.* **2014**, *4* (80), 42546–42553.

(191) Andre, R.; Kwak, D.; Dong, Q.; Zhong, W.; Correa, D.; Mattoso, L.; Lei, Y. Sensitive and Selective NH3 Monitoring at Room Temperature Using ZnO Ceramic Nanofibers Decorated with Poly(styrene Sulfonate). *Sensors* **2018**, *18* (4), 1058.

(192) Andre, R. S.; Chen, J.; Kwak, D.; Correa, D. S.; Mattoso, L. H. C.; Lei, Y. A Flexible and Disposable Poly(sodium 4-Styrenesulfonate)/polyaniline Coated Glass Microfiber Paper for Sensitive and Selective Detection of Ammonia at Room Temperature. *Synth. Met.* **2017**, *233*, 22–27.

(193) Di Natale, C.; Paolesse, R.; Martinelli, E.; Capuano, R. Solid-State Gas Sensors for Breath Analysis: A Review. *Anal. Chim. Acta* **2014**, *824*, 1–17.

(194) Liu, Y.; Sun, X.; Zhou, Z.; Lei, Y. Electrospun Ce–Ni–O Composite Nanofibers for Highly Selective Propane Detection at High Temperature Based on Its Rapid Reaction Kinetics. *J. Mater. Chem. A* **2014**, *2* (34), 14038.

(195) Arasaradnam, R. P.; Covington, J. A.; Harmston, C.; Nwokolo, C. U. Review Article: Next Generation Diagnostic Modalities in Gastroenterology - Gas Phase Volatile Compound Biomarker Detection. *Aliment. Pharmacol. Ther.* **2014**, *39* (8), 780–789.

(196) Zhou, Y.; Ding, C.; Qian, X.; An, X. Further Improvement of Flame Retardancy of Polyaniline-Deposited Paper Composite through Using Phytic Acid as Dopant or Co-Dopant. *Carbohydr. Polym.* **2015**, *115*, 670–676.

(197) Gmurek, M.; Bizukojc, M.; Mosinger, J.; Ledakowicz, S. Application of Photoactive Electrospun Nanofiber Materials with Immobilized Meso-Tetraphenylporphyrin for Parabens Photodegradation. *Catal. Today* **2015**, *240* (PA), 160–167.

(198) Cao, Y.; Liu, N.; Yang, P.; Shi, R.; Ma, Q.; Zhang, A.; Zhu, Y.; Wang, J.; Wang, J. High Luminescent Fibers with Hybrid SiO2-Coated CdTe Nanocrystals Fabricated by Electrospinning Technique. *Mater. Chem. Phys.* **2015**, *149–150*, 51–58.

(199) Cheng, B.; Tao, X.; Shi, L.; Yan, G.; Zhuang, X. Fabrication of ZrO2 Ceramic Fiber Mats by Solution Blowing Process. *Ceram. Int.* **2014**, *40* (9 PART B), 15013–15018.

(200) Leindecker, G. C.; Alves, A. K.; Bergmann, C. P. Synthesis of Niobium Oxide Fibers by Electrospinning and Characterization of Their Morphology and Optical Properties. *Ceram. Int.* **2014**, *40* (PB), 16195–16200.

(201) Sundarrajan, S.; Venkatesan, A.; Agarwal, S. R.; Shaik Anwar Ahamed, N. N.; Ramakrishna, S. Fabrication of NiO/zirconium Oxide Nanofibers by Electrospinning. *Mater. Sci. Eng. C* **2014**, *45*, 369–373.

(202) Zhang, Y.; Liu, Y.; Su, L.; Zhang, Z.; Huo, D.; Hou, C.; Lei, Y. CuO Nanowires Based Sensitive and Selective Non-Enzymatic Glucose Detection. *Sensors Actuators, B Chem.* **2014**, *191*, 86–93.

(203) Ding, Y.; Wang, Y.; Su, L.; Bellagamba, M.; Zhang, H.; Lei, Y. Electrospun Co3O4 Nanofibers for Sensitive and Selective Glucose Detection. *Biosens. Bioelectron.* **2010**, *26* (2), 542–548.

(204) Tang, W.; Wang, J. Mechanism for Toluene Detection of Flower-like ZnO Sensors Prepared by Hydrothermal Approach: Charge Transfer. *Sensors Actuators, B Chem.* **2014**, *207* (PA), 66–73.

(205) Mani, G. K.; Rayappan, J. B. B. A Highly Selective and Wide Range Ammonia sensor—Nanostructured ZnO:Co Thin Film. *Mater. Sci. Eng. B* **2015**, *191* (C), 41–50.

(206) Liu, Y.; Ding, Y.; Zhang, L.; Gao, P.-X.; Lei, Y. CeO2 Nanofibers for in Situ O2 and CO Sensing in Harsh Environments. *RSC Adv.* **2012**, *2* (12), 5193.

(207) Rahman, M. M.; Khan, S. B.; Marwani, H. M.; Asiri, A. M.; Alamry, K. A.; Rub, M. A.; Khan, A.; Khan, A. A. P.; Azum, N. Facile Synthesis of Doped ZnO-CdO Nanoblocks as Solid-Phase Adsorbent and Efficient Solar Photo-Catalyst Applications. *J. Ind. Eng. Chem.* **2014**, *20* (4), 2278–2286.

(208) Cai, X.; Hu, D.; Deng, S.; Han, B.; Wang, Y.; Wang, Y.; Wu, J. Isopropanol Sensing Properties of Coral-like ZnO-CdO Composites by Flash Preparation via Self-Sustained Decomposition of Metal-Organic Complexes. *Sensors Actuators, B Chem.* **2014**, *198*, 402–410.

(209) Park, S. Y.; Kim, S.; Yoo, J.; Lim, K.-H.; Lee, E.; Kim, K.; Kim, J.; Kim, Y. S. Aqueous Zinc Ammine Complex for Solution-Processed ZnO Semiconductors in Thin Film Transistors. *RSC Adv.* **2014**, *4* (22), 11295.

(210) Hsieh, P.-T.; Chen, Y.-C.; Kao, K.-S.; Wang, C.-M. Luminescence Mechanism of ZnO Thin Film Investigated by XPS Measurement. *Appl. Phys. A* **2007**, *90* (2), 317–321.

(211) Seekaew, Y.; Lokavee, S.; Phokharatkul, D.; Wisitsoraat, A.; Kerdcharoen, T.; Wongchoosuk, C. Low-Cost and Flexible Printed graphene–PEDOT:PSS Gas Sensor for Ammonia Detection. *Org. Electron.* **2014**, *15* (11), 2971–2981.

(212) Xu, S.; Kan, K.; Yang, Y.; Jiang, C.; Gao, J.; Jing, L.; Shen, P.; Li, L.; Shi, K. Enhanced NH3 Gas Sensing Performance Based on Electrospun Alkaline-Earth Metals Composited SnO2 Nanofibers. *J. Alloys Compd.* **2015**, *618*, 240–247.

(213) Dhivya Ponnusamy; Sridharan Madanagurusamy. Nanostructured ZnO Films for Room Temperature Ammonia Sensing. *J. Electron. Mater.* **2014**, *43* (9), 3211–3216.

(214) Aba, L.; Yusuf, Y.; Mitrayana, M.; Triyana, K. Selectivity Improvement of Gas Sensor Based on Poly(3,4-ethylenedioxythiophene):Poly(styrenesulfonate) Thin

Film by Using Imprinting Method. *J. Mod. Phys.* **2012**, *3* (7), 529–533.

(215) Qin, Y.; Pan, S.; Howlader, M. M. R.; Ghosh, R.; Hu, N.-X.; Deen, M. J. Paper-Based, Hand-Drawn Free Chlorine Sensor with Poly(3,4-ethylenedioxythiophene):Poly(styrenesulfonate). *Anal. Chem.* **2016**, *88* (21), 10384–10389.

(216) Massoumi, B.; Entezami, A. Controlled Release of Sulfosalicylic Acid during Electrochemical Switching of Conducting Polymer Bilayers. *Eur. Polym. J.* **2001**, *37* (5), 1015–1020.

(217) Jang, J.; Ha, J.; Cho, J. Fabrication of Water-Dispersible Polyaniline-Poly(4-Styrenesulfonate) Nanoparticles For Inkjet-Printed Chemical-Sensor Applications. *Adv. Mater.* **2007**, *19* (13), 1772–1775.

(218) Park, M.-K.; Onishi, K.; Locklin, J.; Caruso, F.; Advincula, R. C. Self-Assembly and Characterization of Polyaniline and Sulfonated Polystyrene Multilayer-Coated Colloidal Particles and Hollow Shells. *Langmuir* **2003**, *19* (20), 8550–8554.

(219) Liu, H.; Kameoka, J.; Czaplewski, D. A.; Craighead, H. G. Polymeric Nanowire Chemical Sensor. *Nano Lett.* **2004**, *4* (4), 671–675.

(220) Nair, S.; Hsiao, E.; Kim, S. H. Fabrication of Electrically-Conducting Nonwoven Porous Mats of Polystyrene–polypyrrole Core–shell Nanofibers via Electrospinning and Vapor Phase Polymerization. *J. Mater. Chem.* **2008**, *18* (42), 5155.

(221) Wang, Y.; Coti, K. K.; Wang, J.; Alam, M. M.; Shyue, J.-J.; Lu, W.; Padture, N. P.; Tseng, H.-R. Individually Addressable Crystalline Conducting Polymer Nanowires in a Microelectrode Sensor Array. *Nanotechnology* **2007**, *18* (42), 424021.

(222) Wang, Y.; Jia, W.; Strout, T.; Ding, Y.; Lei, Y. Preparation, Characterization and Sensitive Gas Sensing of Conductive Core-Sheath TiO2-PEDOT Nanocables. *Sensors* **2009**, *9* (9), 6752–6763.

(223) Wang, N.; Hu, C. G.; Xia, C. H.; Feng, B.; Zhang, Z. W.; Xi, Y.; Xiong, Y. F. Ultrasensitive Gas Sensitivity Property of BaMnO3 Nanorods. *Appl. Phys. Lett.* **2007**, *90* (16), 163111.

(224) Horrillo, M. .; Sayago, I.; Arés, L.; Rodrigo, J.; Gutiérrez, J.; Götz, A.; Gràcia, I.; Fonseca, L.; Cané, C.; Lora-Tamayo, E. Detection of Low NO2 Concentrations with Low Power Micromachined Tin Oxide Gas Sensors. *Sensors Actuators B Chem.* **1999**, *58* (1–3), 325–329.

(225) ROSSINYOL, E.; PRIM, A.; PELLICER, E.; RODRIGUEZ, J.; PEIRO, F.; CORNET, A.; MORANTE, J.; TIAN, B.; BO, T.; ZHAO, D. Mesostructured Pure and Copper-Catalyzed Tungsten Oxide for NO2 Detection. *Sensors Actuators B Chem.* **2007**, *126* (1), 18–23.

(226) Rout, C. S.; Ganesh, K.; Govindaraj, A.; Rao, C. N. R. Sensors for the Nitrogen Oxides, NO2, NO and N2O, Based on In2O3 and WO3 Nanowires. *Appl. Phys. A* **2006**, *85* (3), 241–246.

(227) Wang, Y.; Akhigbe, J.; Ding, Y.; Brückner, C.; Lei, Y. Meso-Tritolylcorrole-Functionalized Single-Walled Carbon Nanotube Donor□Acceptor Nanocomposites for NO2 Detection. *Electroanalysis* **2012**, *24* (6), 1348–1355.

Appendix A

Complementary data of Chapter IV

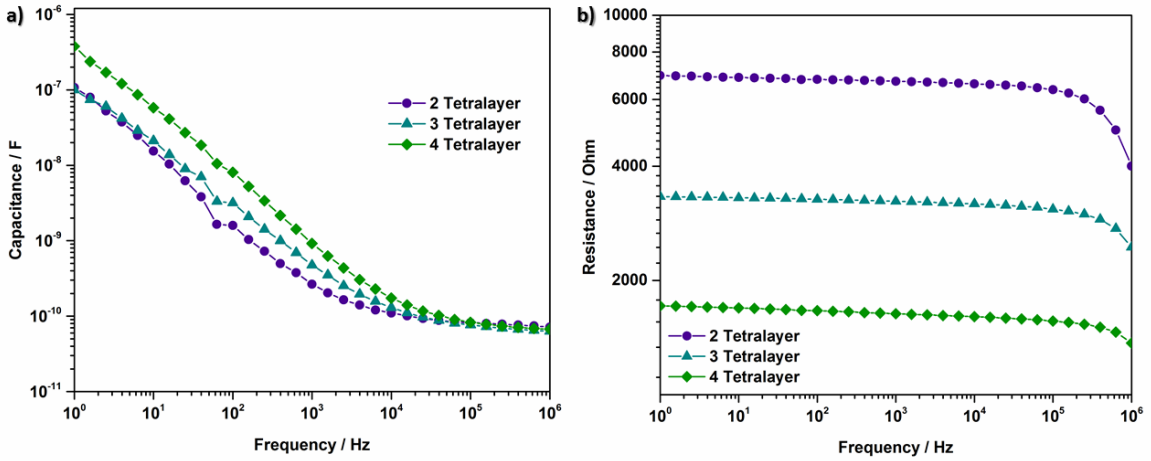

Figure A.1: a) Capacitance and b) Resistance variation versus frequency for all three platforms.

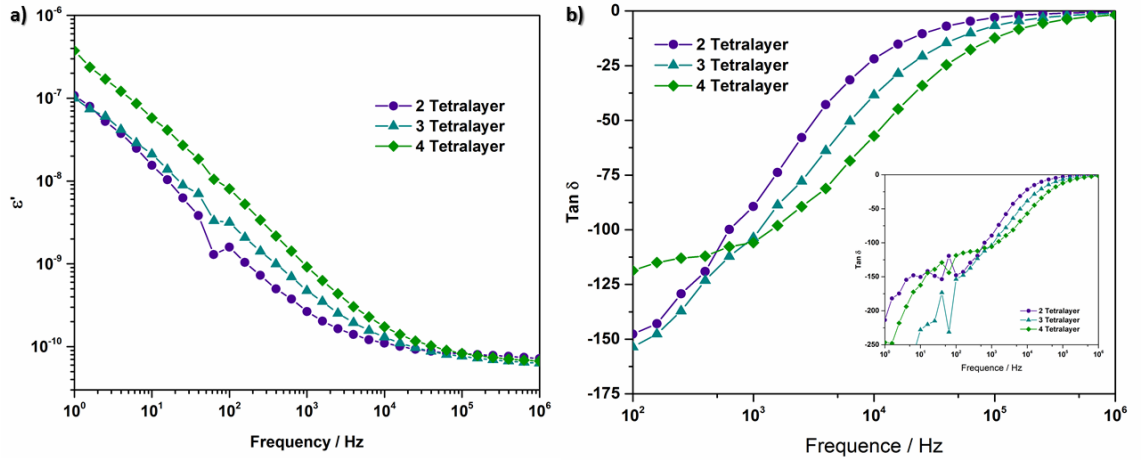

Figure A.2 a) Real part of dielectric properties and b) tangent loss for all three platforms.

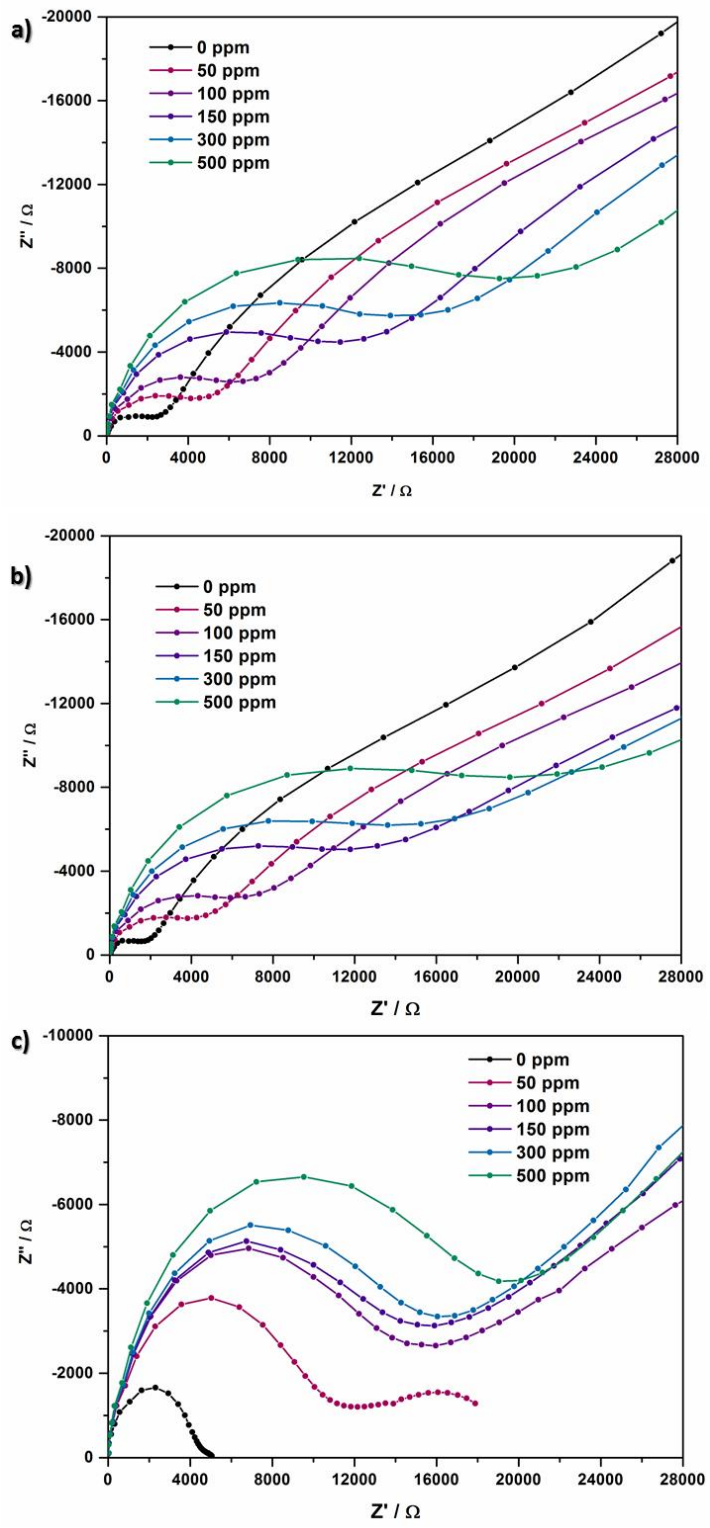

Figure A.3: Nyquist plots of a) PGPZ2T, b) PGPZ3T and PGPZ4T when exposed in several concentrations of NH_3.

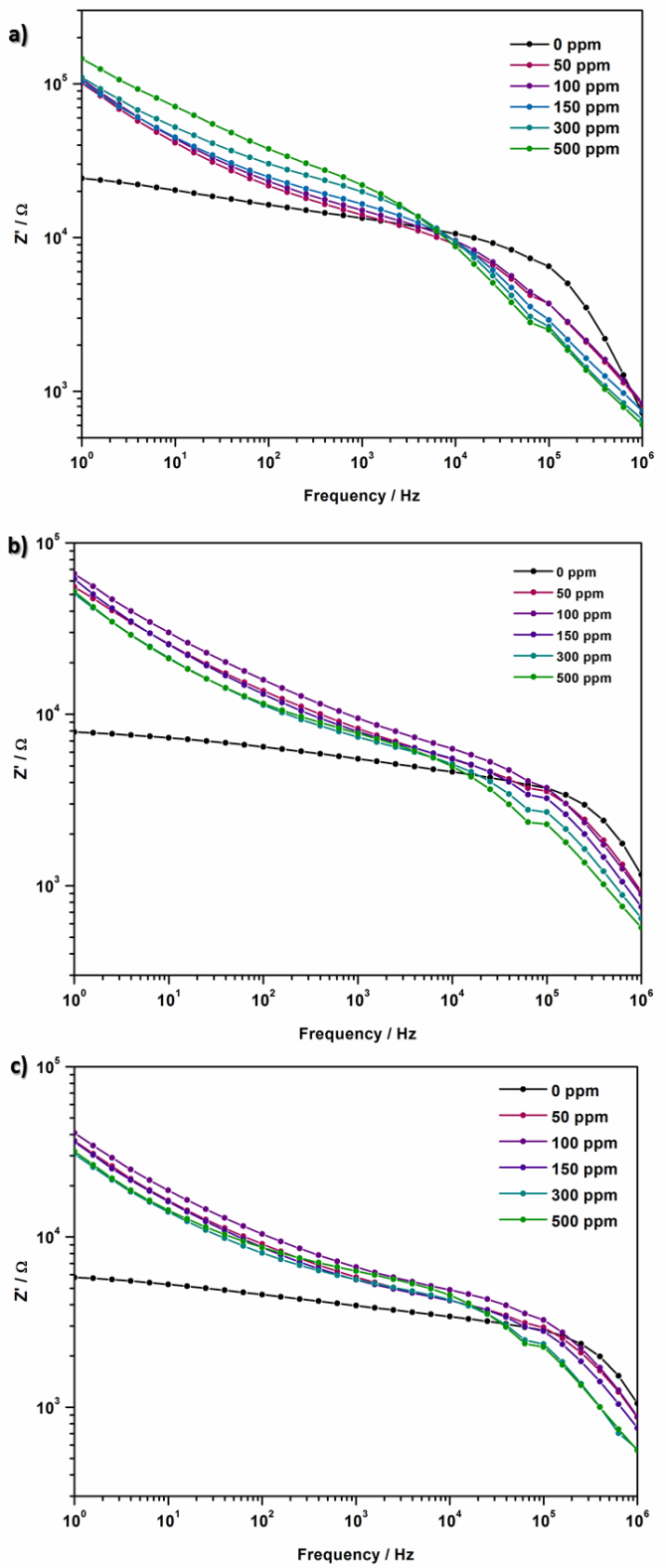

Figure A.4: Impedance spectra of a) PGPZ2T, b) PGPZ3T and c) PGPZ4T film when exposed in several concentrations of NH_3.

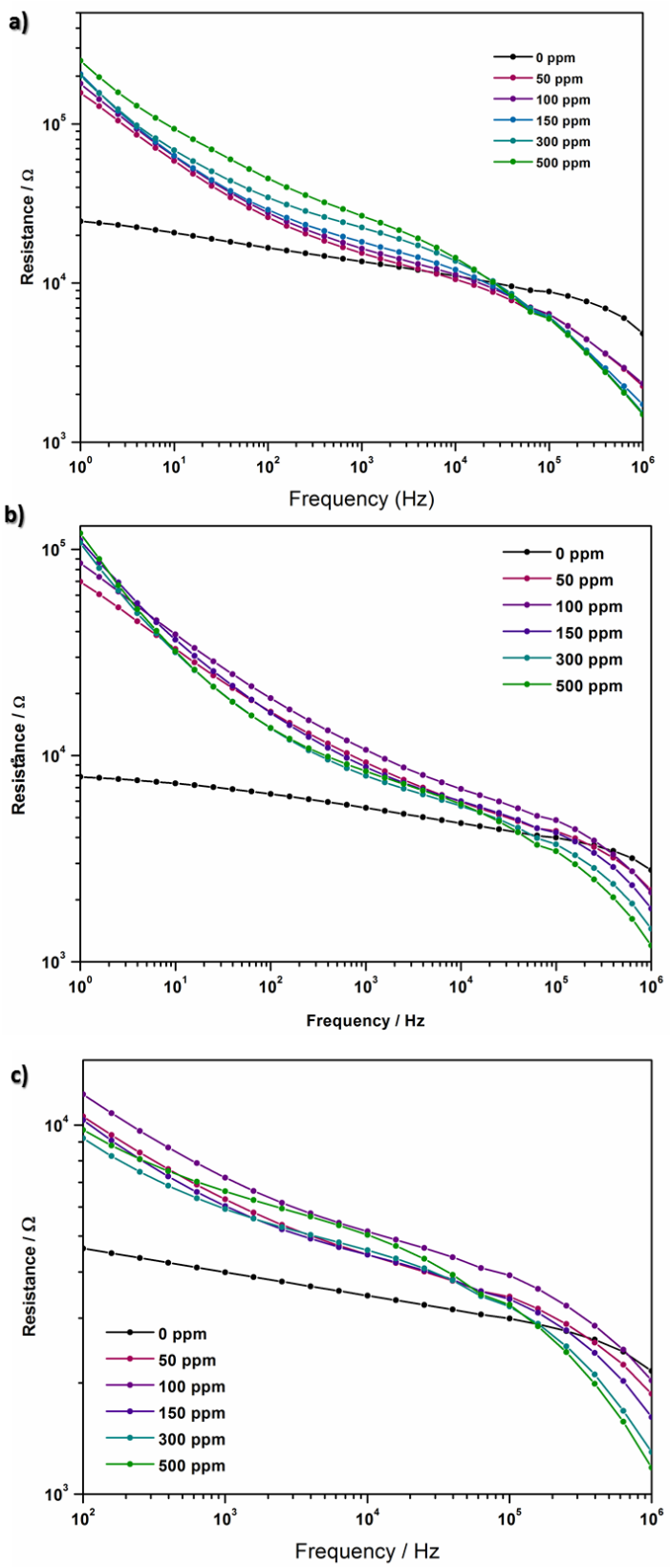

Figure A.5: Resistance variation of a) PGPZ2T, b) PGPZ3T and c) PGPZ4T film when exposed in several concentrations of NH_3.

Appendix B

Publication rights and permissions

Sensor and Actuators B – Elsevier rights and permissions

- Rafaela S. Andre, Flávio M. Shimizu, Celina M. Miyazaki, Antonio Riul Jr, Danilo Manzani, Sidney J.L. Ribeiro, Osvaldo N. Oliveira Jr, Luiz H.C. Mattoso and Daniel S. Correa, **Hybrid layer-by-layer (LbL) films of polyaniline, graphene oxide and zinc oxide to detect ammonia,** Sensors and Actuators B: Chemical, **2017**, 238, 795–801.

ELSEVIER LICENSE TERMS AND CONDITIONS

May 02, 2018

This Agreement between Rafaela S. Andre ("You") and Elsevier ("Elsevier") consists of your license details and the terms and conditions provided by Elsevier and Copyright Clearance Center.

License Number	4063800982213
License date	Mar 07, 2017
Licensed Content Publisher	Elsevier
Licensed Content Publication	Sensors and Actuators B: Chemical
Licensed Content Title	Hybrid layer-by-layer (LbL) films of polyaniline, graphene oxide and zinc oxide to detect ammonia
Licensed Content Author	Rafaela S. Andre,Flávio M. Shimizu,Celina M. Miyazaki,Antonio Riul,Danilo Manzani,Sidney J.L. Ribeiro,Osvaldo N. Oliveira,Luiz H.C. Mattoso,Daniel S. Correa
Licensed Content Date	Jan 1, 2017
Licensed Content Volume	238
Licensed Content Issue	n/a
Licensed Content Pages	7
Start Page	795
End Page	801
Type of Use	reuse in a thesis/dissertation
Portion	full article
Format	both print and electronic
Are you the author of this Elsevier article?	Yes
Will you be translating?	No
Title of your thesis/dissertation	Nanostructured composites based on conducting polymer/ceramic as a sensing platform for ammonia gas monitoring
Expected completion date	Apr 2017
Estimated size (number of pages)	120
Requestor Location	Rafaela S. Andre Rua XV deNovembro, 1452 São Carlos, SP 13560-970 Brazil Attn: Rafaela S. Andre
Total	**0.00 USD**
Terms and Conditions	

INTRODUCTION

1. The publisher for this copyrighted material is Elsevier. By clicking "accept" in connection with completing this licensing transaction, you agree that the following terms and conditions apply to this transaction (along with the Billing and Payment terms and conditions established by Copyright Clearance Center, Inc. ("CCC"), at the time that you opened your Rightslink account and that are available at any time at http://myaccount.copyright.com).

GENERAL TERMS

2. Elsevier hereby grants you permission to reproduce the aforementioned material subject to the terms and conditions indicated.
3. Acknowledgement: If any part of the material to be used (for example, figures) has appeared in our publication with credit or acknowledgement to another source, permission must also be sought from that source. If such permission is not obtained then that material may not be included in your publication/copies. Suitable acknowledgement to the source must be made, either as a footnote or in a reference list at the end of your publication, as follows:
"Reprinted from Publication title, Vol /edition number, Author(s), Title of article / title of chapter, Pages No., Copyright (Year), with permission from Elsevier [OR APPLICABLE SOCIETY COPYRIGHT OWNER]." Also Lancet special credit - "Reprinted from The

RSC Advances – The Royal Society of Chemistry rights and permissions

- R. S. Andre, A. Pavinatto, L. A. Mercante, Elaine C. Paris, Luiz H. C. Mattoso and Daniel S. Correa**, Improving the electrochemical properties of polyamide 6/polyaniline electrospun nanofibers by surface modification with ZnO nanoparticles,** RSC Advances Journal **2015**, *5* (90), 73875-73881.

Improving the electrochemical properties of polyamide 6/polyaniline electrospun nanofibers by surface modification with ZnO nanoparticles

R. S. Andre, A. Pavinatto, L. A. Mercante, E. C. Paris, L. H. C. Mattoso and D. S. Correa, *RSC Adv.*, 2015, **5**, 73875
DOI: 10.1039/C5RA15588F

Sensors – MDP rights and permissions

- Rafaela S. Andre, Dongwook Kwak, Qiuchen Dong, Wei Zhong, Daniel S. Correa, Luiz H. C. Mattoso and Yu Lei, **Sensitive and Selective NH_3 Monitoring at Room Temperature Using ZnO Ceramic Nanofibers Decorated with Poly(styrene sulfonate),** Sensors **2018**, 18(4), 1058. Open access journal.

-

Sensors **2018**, *18*(4), 1058; https://doi.org/10.3390/s18041058 Open Access Article

Sensitive and Selective NH_3 Monitoring at Room Temperature Using ZnO Ceramic Nanofibers Decorated with Poly(styrene sulfonate)

Rafaela S. Andre [1,2,3], Dongwook Kwak [4], Qiuchen Dong [5], Wei Zhong [6], Daniel S. Correa [2,3,*], Luiz H. C. Mattoso [2,3] and Yu Lei [1,*]

1 Department of Chemical and Biomolecular Engineering, University of Connecticut, 191 Auditorium Road, Storrs, CT 06269, USA
2 Nanotechnology National Laboratory for Agriculture (LNNA), Embrapa Instrumentação, São Carlos 13560-970, SP, Brazil
3 PPGQ, Department of Chemistry, Center for Exact Sciences and Technology, Federal University of São Carlos (UFSCar), São Carlos 13565-905, SP, Brazil
4 Department of Materials Science and Engineering, University of Connecticut, 97 North Eagleville Road, Storrs, CT 06269, USA
5 Department of Biomedical Engineering, University of Connecticut, 260 Glenbrook Road, Storrs, CT 06269, USA
6 Department of Chemistry, University of Connecticut, 55 North Eagleville Road, Storrs, CT 06269, USA

* Authors to whom correspondence should be addressed.

Received: 13 February 2018 / Revised: 22 March 2018 / Accepted: 30 March 2018 / Published: 1 April 2018

(This article belongs to the Section Chemical Sensors)

Synthetic Metals – Elsevier rights and permissions

- Rafaela S. Andre, Jun Chen, Dongwook Kwak, Daniel S. Correa, Luiz H.C. Mattoso, Yu Lei, **A flexible and disposable poly(sodium 4-styrenesulfonate)/polyaniline coated glass microfiber paper for sensitive and selective detection of ammonia at room temperature,** Synthetic Metals **2017**, 233, 22-27.

ELSEVIER LICENSE
TERMS AND CONDITIONS

Dec 18, 2017

This Agreement between Rafaela S. Andre ("You") and Elsevier ("Elsevier") consists of your license details and the terms and conditions provided by Elsevier and Copyright Clearance Center.

The publisher has provided special terms related to this request that can be found at the end of the Publisher's Terms and Conditions.

License Number	4227660888503
License date	Nov 14, 2017
Licensed Content Publisher	Elsevier
Licensed Content Publication	Synthetic Metals
Licensed Content Title	A flexible and disposable poly(sodium 4-styrenesulfonate)/polyaniline coated glass microfiber paper for sensitive and selective detection of ammonia at room temperature
Licensed Content Author	Rafaela S. Andre,Jun Chen,Dongwook Kwak,Daniel S. Correa,Luiz H.C. Mattoso,Yu Lei
Licensed Content Date	Nov 1, 2017
Licensed Content Volume	233
Licensed Content Issue	n/a
Licensed Content Pages	6
Start Page	22
End Page	27
Type of Use	reuse in a thesis/dissertation
Portion	full article
Format	both print and electronic
Are you the author of this Elsevier article?	Yes
Will you be translating?	No
Title of your thesis/dissertation	Nanostructured composites based on conducting polymer/ceramic as a sensing platform for ammonia gas monitoring
Expected completion date	Apr 2017
Estimated size (number of pages)	120
Requestor Location	Rafaela S. Andre Rua XV deNovembro, 1452 São Carlos, SP 13560-970 Brazil Attn: Rafaela S. Andre
Billing Type	Invoice
Billing Address	Rafaela S. Andre Rua XV deNovembro, 1452 São Carlos, Brazil 13560-970 Attn: Rafaela S. Andre